



Title	Studies on Characterization of Nanostructured Lipid Carrier and Its Applications to Encapsulation of Biomolecules
Author(s)	Izza, Ni'matul
Citation	大阪大学, 2022, 博士論文
Version Type	VoR
URL	https://doi.org/10.18910/89642
rights	
Note	

The University of Osaka Institutional Knowledge Archive : OUKA

<https://ir.library.osaka-u.ac.jp/>

The University of Osaka

**Studies on Characterization of
Nanostructured Lipid Carrier and Its Applications
to Encapsulation of Biomolecules**

NI'MATUL IZZA

SEPTEMBER 2022

**Studies on Characterization of
Nanostructured Lipid Carrier and Its Applications
to Encapsulation of Biomolecules**

A dissertation submitted to

**THE GRADUATE SCHOOL OF ENGINEERING SCIENCE OSAKA
UNIVERSITY**

in partial fulfillment of the requirements for the degree of

DOCTOR OF PHILOSOPHY IN ENGINEERING

BY

NI'MATUL IZZA

SEPTEMBER 2022

Abstract

Nanostructured Lipid Carrier (NLC) is one of the most promising lipid nanoparticles. The combination of solid and liquid lipids used as the core region results in some beneficial features that can overcome the disadvantages relating to the target drugs and its precursors, such as instability and insolubility. In this study, a comprehensive characterization of physicochemical properties and internal structure of the NLC was performed. Based on the characterized properties of the NLC, a method to encapsulate biomolecules (i.e., polyphenols and RNA) was established, focusing on their loading performance and behaviors. The findings obtained are expected to be applied in optimizing the design and formulation of NLC as a drug carrier.

In chapter 2, the self-assembly properties of NLC have been systematically characterized. A ternary diagram of the aqueous solution mixing three lipids (cetyl-palmitate (CP: solid), caprylic triglyceride (CaTG: liquid), and Tween 80(T80)) was clarified based on the properties to summarize the possible structures formed at different compositions of NLC, showing the formation of four possible NLC, such as micelle, O/W emulsion, solid-lipid nanoparticles, and their intermediate states. The formation of CP/CaTG/T80 assemblies is dominated by O/W emulsion-like characteristics, which were strongly affected by the presence of liquid lipid. Based on the ternary diagram, T80 was the most influential component in the NLC system. The above strategy to characterize the NLC self-assembly can provide us a fundamental and meaningful insight relating to the encapsulation of a target molecules, including biomolecules.

In chapter 3, a comprehensive characterization of the core region of the NLC was conducted, focusing on the molecular behaviors and their physicochemical properties. A modified method of conventional fluorescence-based analysis was newly developed to investigate the anisotropy of inner and outer cores of different NLCs. The obtained results show that NLC represented a unique core-shell structure with higher rigidity of the outer core than that of the inner core. Further internal characterizations revealed that NLC could have a polymorphism crystal lamellar structure depending on the lipid composition. The above findings improve the understanding of the microscopic structure and properties of NLC cores and could be applied to designing a specific NLC carrier for various products and administration.

The above studies clarify the dependence of lipid composition on the molecular and physicochemical properties of NLCs. Based on the characterized properties of NLC core, a method to encapsulate some biomolecules was proposed based on the loading performance with its appropriate quality, by selecting polyphenols and tRNA as case studies of small and large biomolecules.

In chapter 4, three different polyphenols with different lipophilicity were employed as targeted loading drugs in NLC. The results indicated that the hydrophobicity of polyphenols could be the most influential on the entrapment efficiency of each polyphenol and further on the actual antioxidant activity. Resveratrol, the most hydrophobic molecule in this study, demonstrated the highest entrapment efficiency; however, it has the lowest specific antioxidant activity compared to other polyphenols, especially quercetin, the least hydrophobic molecules. Additionally, NLCs have improved all the antioxidant activity per unit concentration of polyphenol (specific antioxidant activity) compared to the free polyphenols. It was found that the antioxidative activity was varied depending on the plausible location of polyphenols in NLC core and the antioxidative activity could be varied depending on the properties of the employed polyphenols.

In chapter 5, the evaluation of NLC performance in loading RNA-based products is conducted. tRNA was selected as a product model and 1,2-dioleoyl-3-trimethylammonium-propane (DOTAP) was employed as a supporting lipid to improve its loading in NLCs. The different lipid composition was used for the tRNA carrier; then, tRNA conformation was investigated by the circular dichroism (CD) spectroscopic analysis. A step-by-step evaluation was also conducted to understand the properties changing during fabrication process. According to the result, tRNA was denatured during the process, and it was found that the DOTAP-modified NLC with its appropriate characters could entrap the tRNA. Also, the composition of NLC can affects the final particle size and entrapment efficiency. The obtained result is expected to have a significant contribution in the development NLC-based platform for RNA-based therapy.

In chapter 6, the general conclusion of this study is summarized, and suggestions for clarifying the role of NLC as a potential drug delivery system and its wide application in many drug administrations are discussed as an extension of this thesis.

Preface

This dissertation work was conducted under the supervision of Professor Hiroshi Umakoshi at Division of Chemical Engineering, Graduate School of Engineering Science, Osaka University from 2019 to 2022.

The objective of this thesis is to comprehensively characterize the physico-chemical properties, morphology, and internal structure of the NLC. Based on the characterized properties of the NLC, a method to encapsulate biomolecules (*i.e.*, polyphenols and RNA) was established, focusing on their loading performance and behaviors.

The author hopes that this research would contribute to the design and development of lipid-based nanocarriers for various target materials and drug administration. Furthermore, the findings obtained are expected to be useful in optimizing the design and formulation of NLC as a nanocarrier platform.

Ni'matul Izza

Division of Chemical Engineering
Graduate School of Engineering Science
Osaka University
Toyonaka, Osaka, 560-8531, Japan

Contents

Abstract	i
Preface	iii
Contents	iv
Chapter 1	1
General Introduction	1
1. Lipid-based nanoparticles	1
1.1 Types of lipid-based nanoparticles	1
1.2 Prospective properties of LNPs	3
2. NLCs Overview	4
3. Nanostructured lipid carriers for DDSs application	6
4. NLC Structure and Properties	8
5. Overview of this study	10
Chapter 2	15
Self-Assembly State Characterization of CP/ CaTG /T80 Nanostructured Lipid Carriers in Aqueous Environment	15
1. Introduction	15
2. Materials and Methods	17
2.1 Materials	17
2.2 NLC Preparation	18
2.3 Dynamic Light Scattering Analysis	19
2.4 Membrane Fluidity Evaluation	19
2.5 Membrane Polarity Evaluation	19
3. Result and Discussion	20
3.1 Particle Size Distribution and Surface Potential of NLC	20
3.2 Effect of T80 Concentration on Membrane Fluidity	23
3.3 Effect of T80 Concentration on Membrane Polarity	25
3.4 Determination of Self-Assembly State based on Fluidity and Polarity Analysis	28
3.5 Ternary Diagram of CP/CaTG/T80 Self-Assembly Systems	31
4. Summary	33
Chapter 3	35
Dependence of Core-Shell Structure on Lipid Composition of Nanostructured Lipid Carriers	35
1. Introduction	35
2. Materials and Methods	36
2.1 Materials	36

2.2 NLC Preparation	36
2.3 Dynamic Light Scattering (DLS) Analysis	38
2.4 Fluorescence Anisotropy (Polarization)	38
2.5 Cryo-TEM Observation	39
2.6 Differential Scanning Calorimetry (DSC)	39
2.7 X-Ray Diffraction (XRD)	40
3. Results	40
3.1 Basic Nano-properties and Stability	40
3.2 Fluorescence anisotropy of DPH at NLC	43
3.3 Morphological Observations	45
3.4 Thermodynamic Behavior	47
3.5 Crystal Behavior	50
4. Discussion	52
4.1 Properties of Crystal	52
4.2 Effect of Lipid Composition	53
4.3 Structure of NLCs	54
4.4 Long-term Stability of NLC	56
5. Strategy of Designing NLCs	56
6. Summary	59
Chapter 4	61
Characterization of Entrapment Behaviour of Polyphenols in Nanostructured Lipid Carriers and Its Effect on Their Antioxidative Activity	61
1. Introduction	61
2. Materials and Methods	64
2.1 Materials	64
2.2 NLC Preparation	64
2.3 Drug Loading Performance	65
2.4 Antioxidant Activity	67
2.5 Dynamic Light Scattering	68
3. Results and Discussion	68
3.1 Particle size distribution and stability	68
3.2 Drug Loading Performance	70
3.3 Antioxidant Activity	74
4. Conclusion	76
Chapter 5	79
Investigation of tRNA Conformation During NLCs Fabrication	79
1. Introduction	79
2. Material and Methods	80
2.1 Materials	80
2.2 DOTAP-modified NLC Preparation	80

2.3 Particle Size, PDI and Zeta Potential	81
2.4 Circular Dichroism (CD) Analysis	82
2.5 Entrapment Efficiency	82
3. Result and Discussion	82
3.1 Basic Nano-properties of NLC-DOTAP-tRNA	82
3.2 Step-by-step Evaluation of NLC-DOTAP-tRNA in Their Formulation Process	84
3.3 tRNA conformation during NLC-DOTAP-tRNA fabrication	85
3.4 Entrapment Efficiency	87
3.5 Plausible structure formation of NLC-DOTAP-tRNA during preparation	88
4. Summary	90
Chapter 6	91
General Conclusion	91
Suggestion for Future Works	94
Nomenclatures	96
List of Abbreviations	97
References	98
List of Publications	111
Acknowledgement	113

Chapter 1

General Introduction

1. Lipid-based nanoparticles

Lipid-based nanoparticles (LNPs) are a colloidal system that has been widely used as carriers in drug delivery system. Their characteristics and ability to improve bioavailability and stability of drugs has gained attention in many studies (Aburai et al., 2020; Terada et al., 2021). The applications of LNPs have also been developed in other application fields, such as cosmetics, functional food, nutrition, agriculture, and medical imaging. It has also been reported that LNPs can improve administrative routes and biodistribution of drugs with minimum side effects.

1.1 Types of lipid-based nanoparticles

A variety of drug carriers are employed for drug delivery systems (DDSs), and they consist of different lipid components with different advantages and disadvantages. In general, LNPs have spherical shape comprising of a lipid bilayer that surrounding aqueous/ liquid/ amorphous phase and they include various self-assemblies, such as liposomes, lipid nanoparticles (LNPs), and emulsions (**Figure 1-1**) (Kumar, 2018; Shah et al., 2021). The LNPs have different structure which can determine their function.

Liposomes, composed of one or more phospholipid bilayers, can be categorized as the most-common LNP. Based on its function as nanocarrier, this type of LNPs is extremely versatile because it can cargo both of hydrophilic and hydrophobic targeted molecules, including small drug molecules, protein, and nucleic acids. A few liposomal drug formulations have been successfully proceeded from concept to clinical application and applied to medical practitioners (Tenchov et al., 2021).

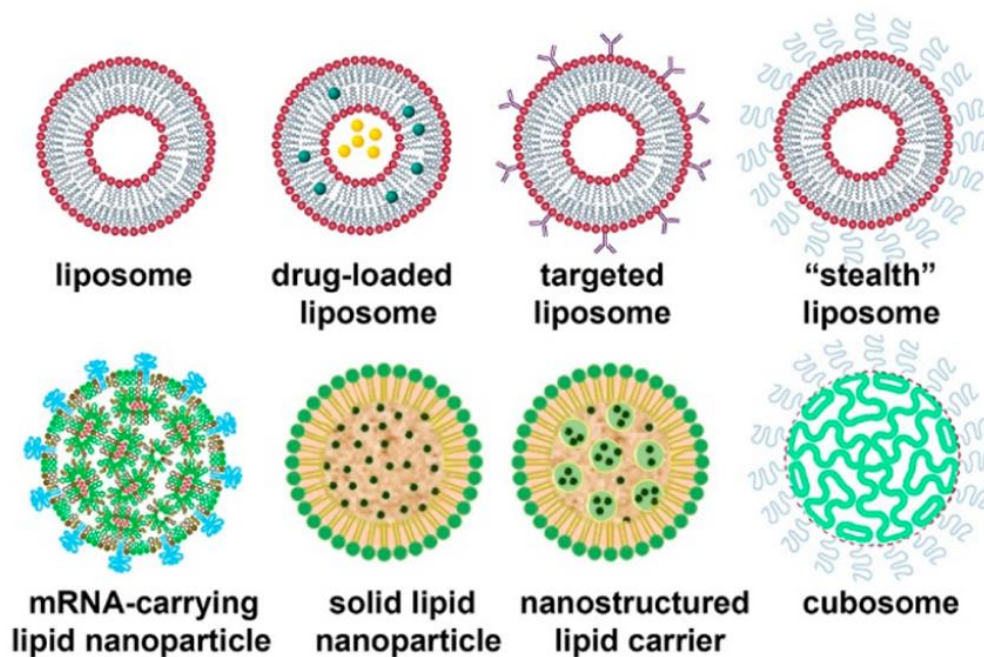


Figure 1- 1 Types of Lipid Nanoparticles (Tenchov et al., 2021).

Another generation of LNPs is solid lipid nanoparticles (SLNs). This carrier can be fabricated by triglycerides, complex glycerides, and waxes (Üner & Yener, 2007), or other lipids that have a solid phase in room temperature. The drug is dissolved in the lipid core component that is formed by the homogeneous solid solutions. SLN has excellent advantages: e.g., increasing the performance of products such as improving stability (Salminen et al., 2016), enhancing the activity and drug solubility (Gaur et al., 2014; Schlupp et al., 2011), and enhancing skin penetration for topical delivery systems (Schlupp et al., 2011). However, the highly ordered core limits drug loading capacity and causes drug expulsion during storage (Alsaad et al., 2020; Naseri et al., 2015).

Nanostructured lipid carriers (NLCs) were fabricated to accomplish the structure and function of SLNs (Müller et al., 2002b). The liquid oil is mixed into the solid lipid to modify the lipid matrix of the lipid core, resulted in a new internal structure and properties (**Figure 1-2**). The improve structure and properties make more flexible conditions of the lipid matrix resulted in higher drug capacity and prevents drug expulsion. A general aspect of NLCs is overviewed as follows based on the previous findings, focusing on application, preparation and characterization, structure, and properties of the NLCs.

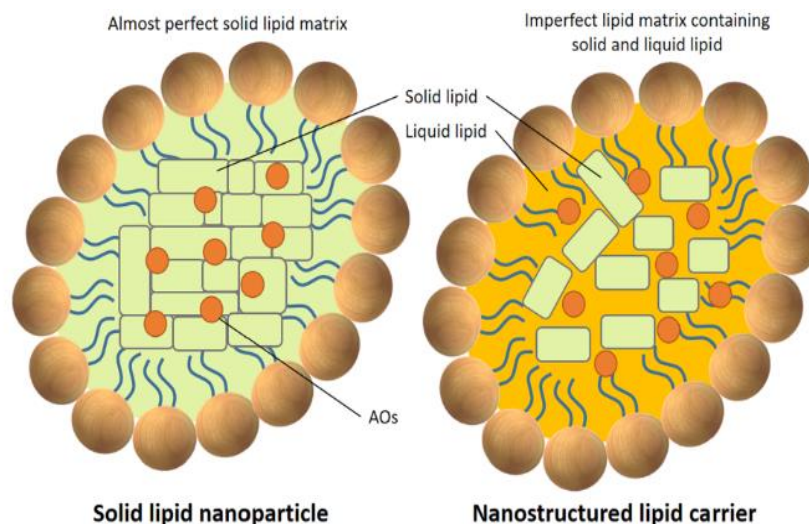


Figure 1- 2 SLN and NLC structure (van Tran et al., 2019)

1.2 Prospective properties of LNPs

In order to design an appropriate LNPs, the following properties may be worth to be considered: micro viscosity or fluidity, phase state and phase transition temperature, size, electric charge, biocompatibility, toxicity, circulation time and uptake, cargo release, and entrapment efficiency and stability. A brief explanation of each property is provided as follows:

- *Micro viscosity or fluidity* of the internal environment is an essential property in drug delivery system. This property has been reported to have a significant impact on the LNPs performance as a carrier. Bompard *et al.* reported that the selective targeting of cancer cell can be achieved by modulating the fluidity of the core region of LNPs from various lipid composition in liposomal drug delivery system (Bompard et al., 2020). Lipid nanocarriers such as SLNs, nano emulsions, and NLCs with different matrix fluidity may contribute to the activity depending on the incorporated drugs. For example, in the skin application, the matrix fluidity is reported to have ability to regulates the occlusive effect, film forming capacity, release, and wound healing (Liakopoulou et al., 2021). In liposomal drug delivery system, cholesterol is widely used to modulate the fluidity of bilayer to be more solid or fluid.

- *Phase state* contributes to their particle stability and encapsulation efficiency. It can also affect the interaction with membrane cells and drug release. The phase state transition temperature should also be considered while designing LNPs. The stability of the loading can be estimated from phase transition temperature against environmental temperature. In general, the longer acyl chain lipids and the higher saturation degrees, the higher melting/ transition temperature.
- *Particle size* can affect the LNPs circulation time and drug uptake. Also, this property is important the administration process of the loaded materials. The particle size of LNPs is tightly related to the preparation methods, such as ultrasonication, extrusion, or microfluidic method, which have been most of the utilized to fabricate LNPs and control the particle size (Tenchov et al., 2021).
- *Surface electric charge*, expressed as zeta potential, is also essential parameter of LNP. This affect to the electric stability of particles, drug release rate, blood circulation time, and fusion into biomembrane. In particular uses, such as RNA-based delivery system, the positive-charged lipid (cationic lipid) is useful for supported lipid that can interact with negatively charged of RNA phosphate.
- *Stability and release property* required to be balance for an effective LNPs. The carriers need to be stable enough to carry the loaded drugs safely to the targeted site. At the same time, it is expected to have capability of releasing the target delivery at the specific target location. To facilitate the drug release, external stimuli can be applied. For instance, the use of ionizable lipid to facilitate the drug release in the specific target location that has different pH.

The other parameters such as biocompatibility, *toxicity*, *circulation time* and *uptake*, are also crucial in regard of LNPs application and can be investigated with experimental in-vitro and in-vivo investigation.

2. NLCs Overview

In the past decades, NLCs gain attention in the pharmaceutical field and widely studied among researchers (**Figure 1-3 (A)**). The advantages of NLC in increasing biocompatibility, stability, and loading efficiencies have been primarily studied. Aditya *et al.* employed NLC (from glycerol monostearate (solid lipid), oleic acid (liquid lipid),

lecithin and Tween 80 (surfactant)) to increase the oral availability of curcumin and genistein and demonstrated its *in vitro* digestion and anti-prostate cancer activity in their study (Aditya et al., 2013). They suggested that the use of NLC could make curcumin and genistein more stable and dispersible in an aqueous solution. Ruiz *et al.* utilized NLC (from Precirol® ATO 5 (solid lipid), sunflower oil, and Tween 80 and poloxamer 407 as surfactant) to encapsulate astaxanthin to preserve its antioxidant activity (Rodriguez-Ruiz et al., 2018a): the lipid environment could maintain and stimulate the antioxidant capacity. Other studies discussed the application of NLC to deliver specific compounds for various functions, such as salinomycin for antiviral (Pindiprolu et al., 2020), halobetasol for topical treatment of inflammation (Carvajal-Vidal et al., 2020), hydrochlorothiazide for pediatric therapy (Cirri et al., 2018), and quercetin for anti-breast cancer (Sun et al., 2014a). As aforementioned, most of the studies report the application of NLCs for a particular disease, some others reported synthesis and the performance after loading an active compound as well as the preparation methods. The trend of NLCs research topics is summarized in the **Figure 1-3 (B)**. As can be seen, fundamental research of NLCs is still infrequent; therefore, one of highlighted studies in this thesis is about fundamental characterization and behavior of NLCs.

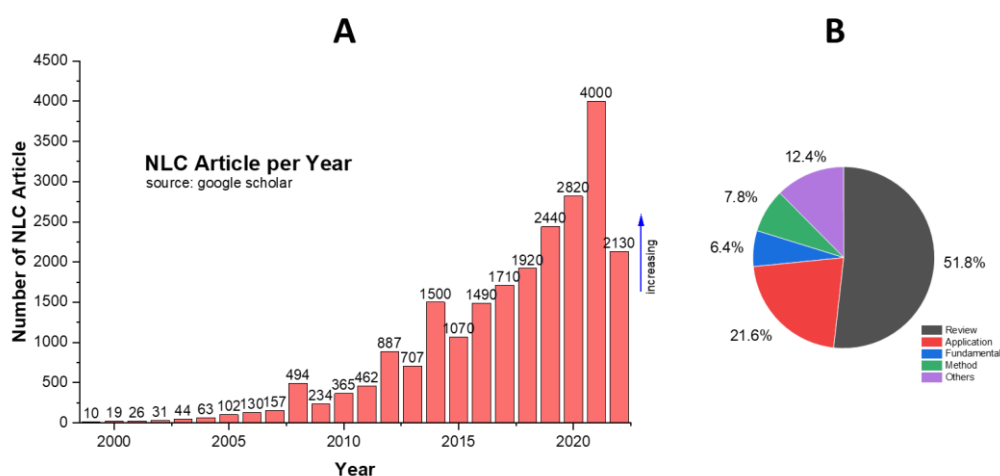


Figure 1- 3 Number of NLC articles per year (A), and trends in NLC research topics (B)

In the current study, cetyl palmitate (CP) (solid lipid) and caprylic triglyceride (CaTG) (liquid lipid) were herein employed as core lipid components, whereas Tween 80 (T80) was utilized as the surfactant. Guilherme *et al.* (2019) conducted preliminary research about the mixture of CP and CaTG and resulted that it demonstrated a high dissolution capacity for their hydrophobic drug molecules, naproxen (Guilherme et al.,

2019). These lipid components and surfactant are also well-known for cosmetics ingredient and have emollient properties and highly effective moisturizer (Moldovan *et al.*, 2021) (Nielsen *et al.*, 2016).

3. Nanostructured lipid carriers for DDSs application

NLCs as the new generation of LNPs consists of mixed solid and liquid lipid was presented towards the end of 1990s to conquer some of the limitations of SLNs, such as the low loading capacity and drug leakage during the storage time (Alsaad *et al.*, 2020; Naseri *et al.*, 2015). The core of SLNs starts to form a perfectly ordered crystal structure immediately after homogenization and during storage. Because of the perfect crystal nature of solid lipid, SLNs have limited space for the loaded drug. This downside could be avoided in the NLCs formulation. The presence of additional liquid oil leads to form imperfect crystal matrix and possibly amorphous in the core that allows greater drug loading and prevents leakage at the same time (Salvi & Pawar, 2019). Additionally, NLCs has been reported to have a better controlled drug release characteristic (Jores *et al.*, 2004; Müller *et al.*, 2002b). The improving drug loading capacity and decreasing sudden release are related to the existence of liquid lipid in NLC lipid matrix.

Numerous applications of NLCs in pharmaceutical field with a variety of administrations. Some of them are illustrated as **Figure 1-4**.

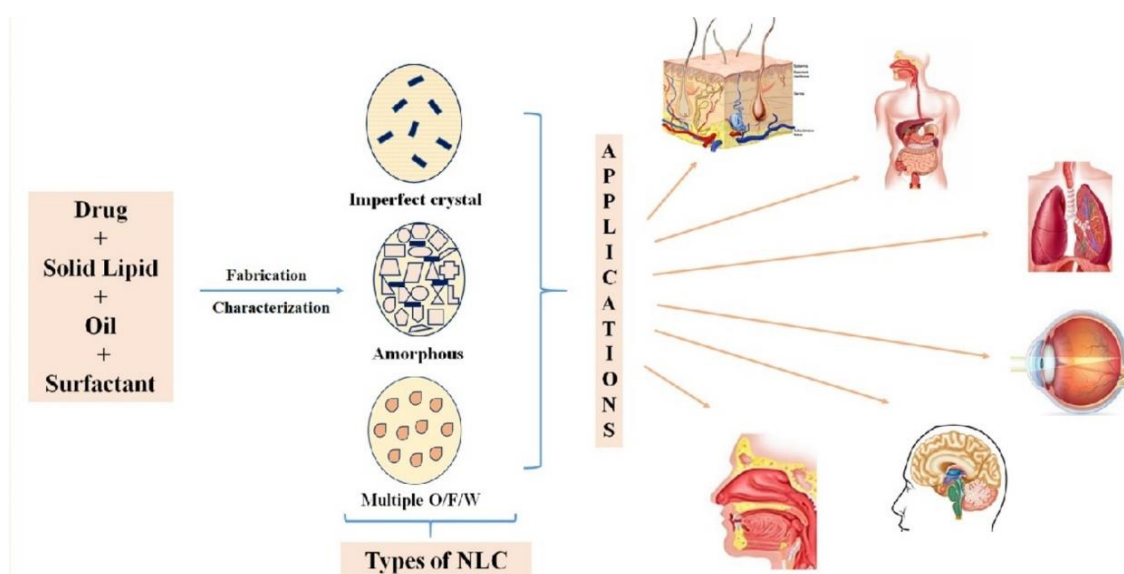


Figure 1- 4 Plausible administrations of NLCs (Khosa *et al.*, 2018)

The following are brief explanations of some plausible NLCs administrations:

[Oral administration]

Due to its ease, painless, and patient adaptability, oral administration is the simplest and favorable pathway in drug administration. However, some particular drugs have some solubility and bioavailability issues as a result of the process in gastrointestinal tract (GIT), which can be chemical, physical, and enzymatic barriers. NLCs application for oral administration have been studied in regard to increase the drug uptake and bioavailability. As the NLC lipid constituents are partially proceed to become free fatty acid (ex: diglycerides), the lipid carrier also subsequently prolong the time in the digestion system resulting in a higher drug absorption. Moreover, the surface region extensively increases owing to the nanoscale, which improves the interaction of NLC to the gut wall. Simultaneously, NLC triggers the release of bile that facilitates drug solubilization and enhancing drug absorption.

[Topical delivery]

Another preferred drug administration is topical delivery for skin applications. Compared to parenteral and oral administration, topical administration is more favorable in regard of the systemic side effects. It can maintain the drug at the targeted site for a longer time and deflect the pre-systemic metabolism. The most challenging of the success of topical administration is the low drug uptake because the stratum corneum in the skin layer inhibits the drug molecules as like inhibits the toxic molecules. NLCs have various recommended features over conventional topical delivery system such as cream and emulsion system. By the formation of less ordered lipid matrix, NLCs can incorporate large quantities of drugs. Also because of the solidifies lipid matrix, NLCs can provide controlled release and possible to prolong the drug release. NLCs have been reported to enhance efficacy of skin application, prolonged drug release, minimize irritation, and safe for various therapeutic targets, such as N- palmitoylethanolamide (Tronino et al., 2016), indomethacin, (Han et al., 2012), celecoxib (Joshi & Patravale, 2008), and podophyllotoxin for warts (J. Zhao et al., 2016).

[Brain targeting]

Blood-brain barrier (BBB) remains challenging and still being the major obstacles for successful delivery of therapeutic agents to brain. Studies about delivery performance of drug carrier and the efficacy of the therapeutic agents in brain related disease are conducted in recent years. Wu and co-workers studied about surface decorated NLC with transferrin receptor monoclonal antibody OX26 to deliver salvianolic acid B and baicalin to the brain. The result shows that surface decorated NLCs enhanced brain delivery of both drugs when compared to NLCs and solution (Y. Wu et al., 2019). Khan et al. conducted evaluation of anticonvulsant and anxiolytic effects of carbamazepine loaded NLCs as a brain delivery system (N. Khan et al., 2020). Zhao and co-worker introduced lactoferrin decorated NLCs to deliver nimodipine (neuro- protective agent) to brain tissue efficiently. The result of in vivo biodistribution assay using DiR (as a fluorescence probe) showed that lactoferrin decorated NLCs has the highest brain deposition (C. Zhao et al., 2018).

[Ocular drug delivery]

In the recent study, NLC has been reported to have ability to ocular delivery system. Not only safe, non-invasive, and patient compliant, NLCs also can increase permeation into cornea and increase the bioavailability. Also, the mucoadhesive behaviour of NLCs improve the interactions with the corneal membrane causes a longer residence time, improve bioavailability, and less systemic side effects. NLC formulation has been studied for various disorder related to eyes, such as glaucoma, infectious, and eyes inflammation (Sánchez-López et al., 2017).

4. NLC Structure and Properties

According to the variation in the composition of lipid and oil mixtures and the various preparation methods, NLC can be classified into three categories (**Figure 1-5**): (i) imperfect, (ii) multiple, and (iii) amorphous types (Chauhan et al., 2020; Tamjidi et al., 2013; van Tran et al., 2019). Imperfect type NLC highly involves disorder state of lipids such as glycerides, composed of several fatty acids, which resulted an imperfection in the crystal order. The drug loading can possibly be increased by increasing the crystal imperfection using various saturation and length of carbon chain of glycerides. Multiple

oil-in-fat-in-water (O/F/W) type NLC consists of nanosized liquid oil compartments distributed in the solid matrix. The drug loading can be increased because the solubility of drug is higher in the liquid compartments. The presence of the surrounding solid lipid crystals supports in prolonging drug release as well as stabilize the loaded drug. Lastly, amorphous type has lack of crystalline structure that originally from β -modification form. This structure can also inhibit the drug leakage during storage due to its amorphous matrix. The illustration of NLC variation types is provided in **Figure 1-5**.

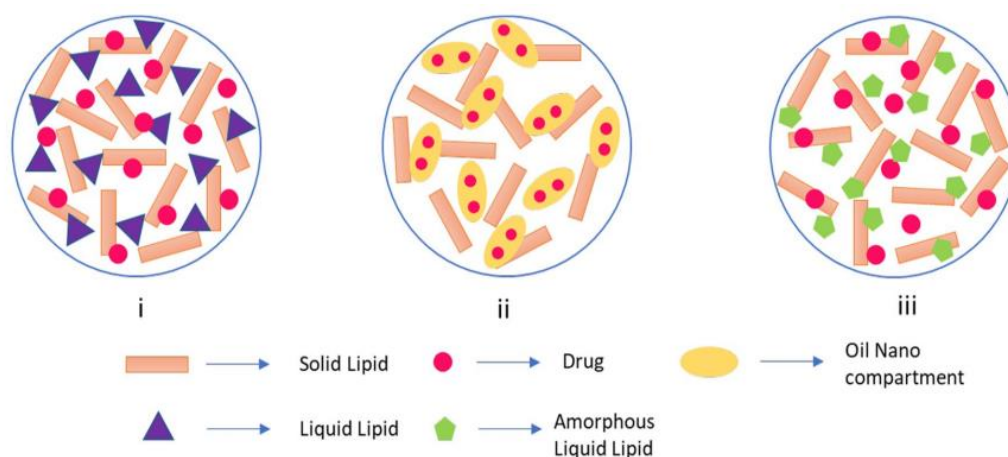


Figure 1- 5 NLC types based on the lipid composition (J. Garg et al., 2022)

Even though the variation of NLC structures have been introduced in some previous studies, the details of fundamental properties and internal structure that resulted by different lipid composition have not been comprehensively discussed. Some crucial parameters in drug delivery applications are closely related to the fundamental properties, such as stability of particle and loading materials and drug release profile. Understanding such behaviour and fundamental properties is important to design and formulate NLC for various desired properties for wider applications.

Based on the current situations of NLC studies, the design of NLC for DDS platform is still challenging. The presence of the solid lipids tends to generate crystallization in the lipid matrix during NLC production and storage. The crystal matrices have advantages in improving the stability and enhancing loading capacity; however, these crystallization process can also generate some drug leakage and instability. The crystallization process is complex and may have a strong dependent on the lipid composition. In addition, lipid composition may have effects on the fundamental properties, such as phase state and internal structure of NLC, which are essential

properties of nanocarrier. These properties can also affect the entrapment behavior of the loaded materials and resulted in a different activity in the application stage. Therefore, it is important to understand the properties, structure, and behavior of NLCs that are dependent of the lipid composition.

5. Overview of this study

The final purpose of this study is to comprehensively characterize the physicochemical properties and molecular/internal structure of NLCs. The information obtained are expected to be applied in designing and formulating a nanocarrier system with specific properties that could be useful for certain drug and administration. For understanding the effect of lipid composition in encapsulating some loaded materials; herein, the application of NLCs to entrap biomolecules are also studied. Some polyphenols as a small biomolecules model are employed to be entrapped into the NLCs, whereas tRNA was used as a macromolecules model. The obtained result could be a future projection of the wide applications of NLCs as nanocarrier.

In chapter 2, the self-assembly properties of NLC have been characterized. As a result, a ternary diagram was developed based on the properties to summarize the possible structures formed at different compositions of NLC. Four possible formations have occurred: micelle-like, O/W emulsion-like, SLN-like, and intermediate states. The formation of CP/CaTG/T80 assemblies is dominated by O/W emulsion-like characteristics, which were strongly affected by the presence of liquid lipid. Based on the ternary diagram, T80 was the most influential component in the NLC system. The findings in this study could be an essential reference in formulating a high-performance NLC system. The results also become provision for determining the formula in the following research.

In chapter 3, a comprehensive molecular and physicochemical characterization of the NLC core region was conducted. A modification of fluorescence-based analysis was applied to investigate the anisotropy of NLCs in the inner and outer core. Based on the result, NLCs represented a unique core-shell structure with higher rigidity of the outer core than that of the inner core. Further internal characterizations revealed that NLCs has a polymorphism crystal lamellar structure dependent on the lipid composition. The

findings improve understanding of the microscopic structure and properties of NLCs and could be applied for designing a specific NLC carrier for various products and administration.

The above studies discover the dependency of molecular and physicochemical properties of NLC on lipid composition. The behavior of internal structure as a result of the lipid composition was also discussed. Based on chapter 2 and 3, a schematic design of NLCs preparation was constructed. Furthermore, the following chapters are the case study investigating NLC loading performance to encapsulate some biomolecules: small molecules and large molecules.

In chapter 4, three different polyphenols with different lipophilicity were employed as targeted loading drugs in NLCs. The results indicated that the hydrophobicity of polyphenols could be the most influential on the entrapment efficiency of each polyphenol and further on the actual antioxidant activity. Resveratrol, the most hydrophobic molecule in this study, demonstrated the highest entrapment efficiency; however, it has the lowest specific antioxidant activity compared to other polyphenols, especially quercetin, the least hydrophobic molecules. Additionally, NLC composition also be considered to have effect on Kaempferol loading. Finally, NLCs have improved all the antioxidant activity per unit concentration of polyphenol (specific antioxidant activity) compared to the free polyphenols.

In chapter 5, the evaluation of NLC performance in encapsulating such RNA-based products is conducted. tRNA was selected as a product model, and the cationic lipid, 1,2-dioleoyl-3-trimethylammonium-propane (DOTAP) was employed as a supporting lipid. The conformation of tRNA was evaluated with circular-dichroism spectroscopy at step-by-step preparation. According to the result, tRNA was denatured during the process, and it was found that the DOTAP-modified NLC with its appropriate characters could entrap the tRNA. Also, the composition of NLC can affects the final particle size and entrapment efficiency.

In chapter 6, the general conclusion of this study is summarized, and suggestions for clarifying the role of NLC as a potential drug delivery system and its wide application in many drug administrations are discussed as an extension of this thesis.

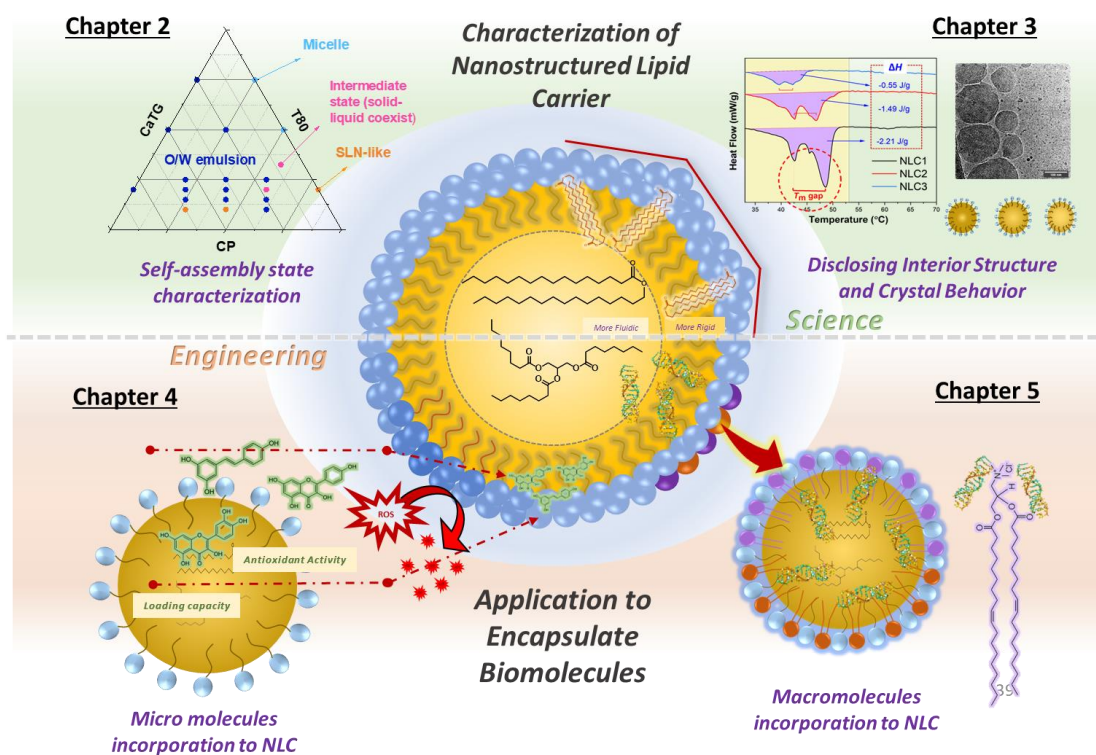


Figure 1- 6 Concept map of the present study

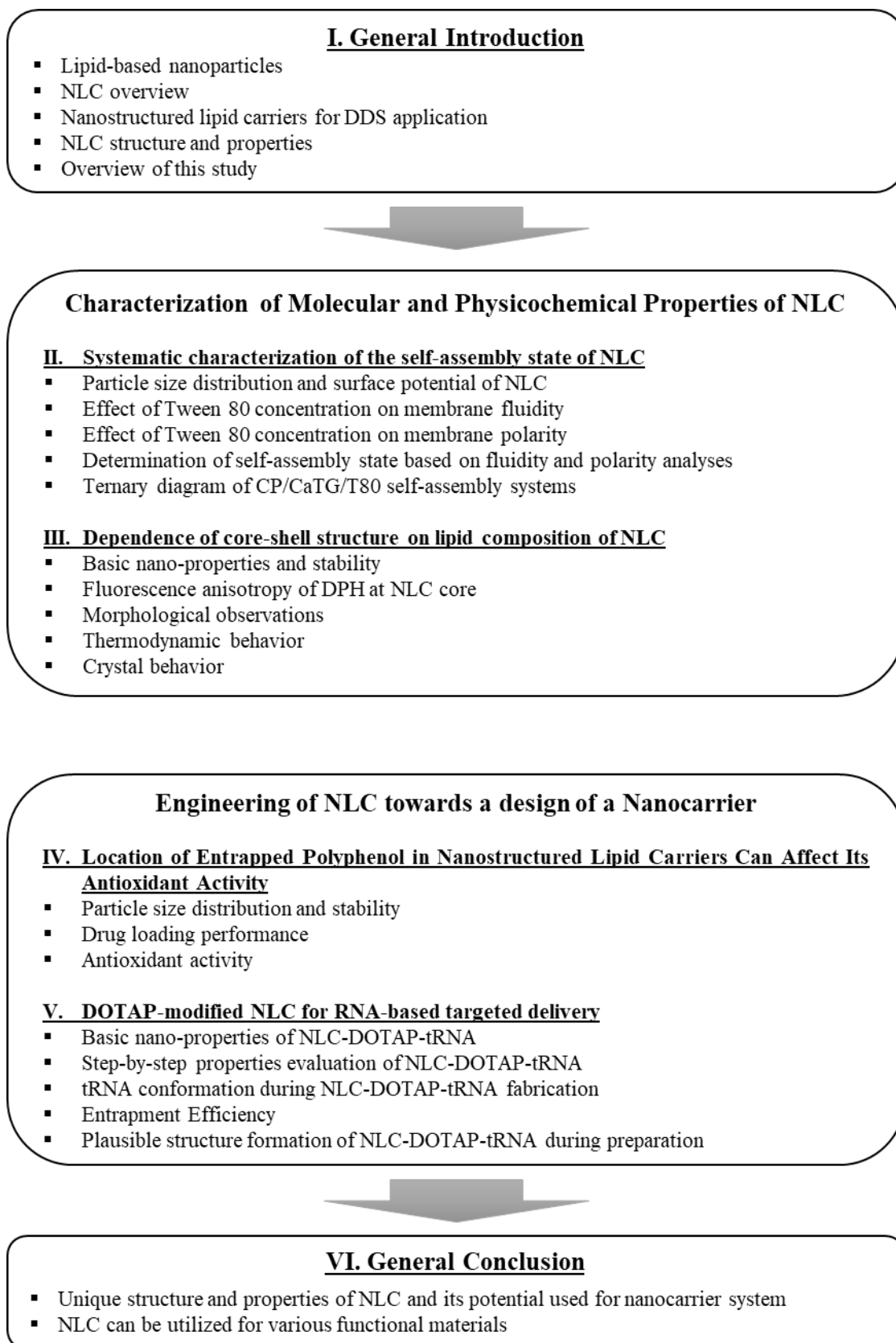


Figure 1- 7 Framework of The Present Study

Chapter 2

Self-Assembly State Characterization of CP/ CaTG /T80 Nanostructured Lipid Carriers in Aqueous Environment

1. Introduction

The fundamental characteristics of NLC, which can be altered depending on lipid composition, are necessary to be well-understood to attain better performance in the drug delivery system (DDS) applications. Preferentially, structural properties played an essential role in nanoparticle studies, and the shape and size distribution are characterized as the first classification of nanocarriers administration in DDS (Sen Gupta, 2016; Uebbing et al., 2020). A smaller NLC with low polydispersity index (PDI) is preferred in DDS. For lipid-based carriers such as phospholipid liposome, niosome, and NLC, the physicochemical properties of the self-assembly, such as phase state, surface charge, membrane fluidity and polarity, are also necessary to maintain the function of the drug carrier (Bnyan et al., 2018; Bompard et al., 2020). In general, a specific surface area of particles increases with a decrease in particle size. At the particle surface, the molecular packing would be decreased by downsizing due to tight curvature. To investigate the microscopic environment of the self-assembly in water, fluorescence-based analysis, such as 1,6-diphenyl-1,3,5-hexatriene (DPH, for membrane fluidity) and 6-dodecanoyl-2-dimethylaminophthalene (Laurdan, for membrane polarity) are commonly used (Nyholm et al., 2011; Suga et al., 2018b; Suga & Umakoshi, 2013). These probes are powerful tools to investigate the microscopic environment of the self-assembly system (Suga et al., 2014; Suga & Umakoshi, 2013). The systematic fluorescence-based analysis of membrane properties, based on membrane fluidity and polarity, has successfully provided insights into the phase behaviors and phase transition due to external stimuli. This method has been applied for lipid mixture systems such as phospholipid/sterol (Bui, Suga, and Umakoshi, 2019), fatty acid dispersions (Ma et al., 2018), gel-phase dispersion of oleic acid/1-oleoylglycerol (Suga et al., 2018a), bicelle characterization (Sen Gupta, 2016; Suga et al., 2020; Taguchi et al., 2018), and non-ionic surfactant assemblies (niosome) (Hayashi et al., 2011). Although fluorescence analysis sometimes has little disadvantages

of the fluorescent probe localization in water environment; the results will be valuable to imagine the physical assembly state and molecular behavior of lipids in NLC.

The majority of NLC studies report the synthesis and the performance after loading an active compound, such as entrapment efficiency, stability, and bioactivity. Many researchers have investigated the effect of "lipid (or surfactant) compositions" on the property and performance of NLC (Nahak et al., 2016; Saedi et al., 2018; Zhao et al., 2014; Zheng et al., 2013). A lipid mixture of solid lipid/liquid oil/surfactant is employed for NLC composition, wherein the possible roles of solid lipid, liquid oil, and surfactant seem to form core matrix, decrease the rigidity, and stabilize the particle. However, the essential role of each component on the physicochemical properties has not been discussed in-depth yet. Also, the understanding of how the detailed structure and self-assembly of the NLC corresponds to each constituent has not been studied yet. Therefore, a systematic characterization, focusing on both the structure and the physicochemical property, is necessary to investigate the fundamental roles of lipid components and develop functional NLC. Aforementioned characterization methods (Suga et al., 2014; Suga & Umakoshi, 2013) can assess the microscopic environment of self-assembling nanostructured lipid systems in aqueous medium.

In this chapter, a systematic characterization was conducted to compare the fundamental properties of NLC, SLN, nanoemulsion (O/W emulsion), and surfactant micelle, and the influence of each lipid component was evaluated. Cetyl Palmitate (solid lipid) and Caprylic Triglyceride (liquid lipid) were herein employed as core lipid components. The combination of the two lipids has been reported to produce an excellent physical property of NLC (Guilherme et al., 2019; Pornputtapitak et al., 2019). Polysorbate 80 (Tween 80 (T80)) was selected as a particle stabilizer (surfactant) to reduce the particle size and increase the stability (Aditya et al., 2013; Eh Suk et al., 2020; Nahak et al., 2016; Saedi et al., 2018). The lipid mixtures used in this study are presented in **Table 1**. Based on the fluorescent probe technique, the membrane fluidity and polarity of ternary mixture systems of CP/CaTG/T80 were analyzed. Then, for the first time, the self-assembly state of NLC in different ratios was attempted to be determined by comparing those of well-investigated self-assemblies (SLN, O/W emulsion, micelle). Consequently, a ternary diagram of NLC structure and physicochemical properties was investigated based on the resulting NLC properties. In brief, by utilizing the different

ratios of NLC components, the various structures and the ternary diagram could be constructed, which is an important reference for developing high-performance NLC.

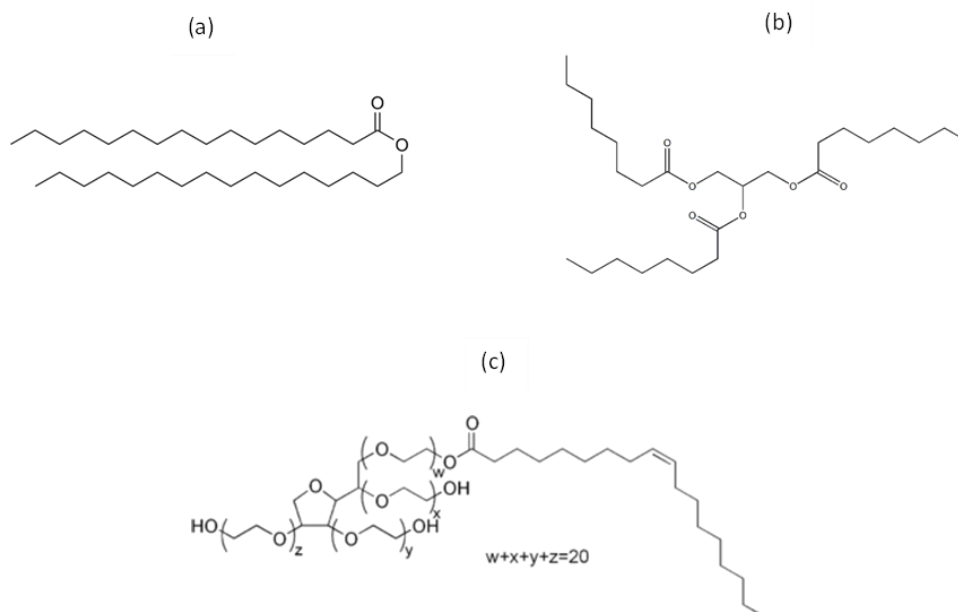
Table 2- 1. Lipid compositions used in this work

Sample	Lipid composition		
	CP [mol%]	CaTG [mol%]	T80 [mol%]
1	62.5	27.5	10
2	60	25	15
3	57.5	22.5	20
4	55	20	25
5	45	45	10
6	42.5	42.5	15
7	40	40	20
8	37.5	37.5	25
9	27.5	62.5	10
10	25	60	15
11	22.5	57.5	20
12	20	55	25
13	57.5	10	32.5
14	25	25	50
15	80	0	20
16	0	50	50
17	0	80	20
18	25	0	75
19	0	25	75
20	50	0	50

2. Materials and Methods

2.1 Materials

CP and CaTG were purchased from Sigma-Aldrich (St. Louis, MO), polysorbate 80 from plant (T80) was purchased from Fujifilm Wako Pure Chemical Industry (Osaka, Japan). Molecular structures and physical properties of CP, CaTG, and T80 are shown in **Fig. 2-1**. 1,6-diphenyl-1,3,5-hexatriene (DPH) and 6-dodecanoyl-2-dimethyl-aminophthalene (Laurdan) were purchased from Sigma-Aldrich (St. Louis, MO). All chemicals were used without further purification. Ultrapure water was prepared using Direct-Q® UV3 (Merck Millipore Co., Tokyo, Japan).



	T_m [°C]	M_w [g/mol]	Density [g/cm ³]	1/ <i>P</i> [-]	<i>GP</i> ₃₄₀ [-]	Log <i>P</i>
CP	53	481	0.4 (solid)	3.8	-0.3	13.06
CaTG	9	470	0.9 (liquid)	13.2	0.7	9.39
T80	-25	1310	1.10 (liquid)	9.3	-0.25	4.8

Fig 2- 1 Molecular structures and properties of NLC constituent at 25 °C. Cetyl Palmitate (CP) (a), Caprylic Triglyceride (CaTG) (b), and Tween 80 (T80) (c).

2.2 NLC Preparation

NLC were prepared by a modified hot homogenization-sonication method (Guilherme et al., 2019). Briefly, the lipid mixture was prepared by mixing an aliquot amount of CP and CaTG and was then agitated and heated at 65 °C (above the melting temperature (T_m) of CP: 53 °C). The aqueous suspension of T80 was separately prepared by dispersing T80 with 2 ml of ultrapure water and heated at 65 °C. The suspension was added dropwise to the melted lipid under agitation for 15 minutes. The obtained coarse emulsion was then sonicated immediately for 3 minutes with a probe sonicator (TOMY Ultrasonic Disruptor UD-200). Power output ultrasound was set by tuning the output dial (we use no. 4 this experiment). The total concentration of lipid ([CP] + [CaTG] + [T80]) was 100 mM. The obtained suspension was subsequently cooled at room temperature for 24 hours and stored at 4 °C for further analysis.

2.3 Dynamic Light Scattering Analysis

Particle size, PDI, and zeta potential (ζ -potential) were measured by Dynamic Light Scattering (DLS) using a Malvern Zetasizer Nano series (Malvern, UK). The measurement was conducted at 25 °C using a disposable cuvette, and the sample was diluted in ultrapure water before evaluated.

2.4 Membrane Fluidity Evaluation

The membrane fluidity of the NLC were evaluated using the fluorescence polarization method as a previous study with a slight modification of the lipid/DPH ratio (Bui, Suga, & Umakoshi, 2019; J. Han et al., 2017; Suga et al., 2018b, 2020; Suga & Umakoshi, 2013; Taguchi et al., 2018). Four microliters of DPH solution (10 μ M in ethanol) were added to the diluted NLC suspension in a molar ratio of lipid/DPH=12500/1. The total concentration of lipid ([CP] + [CaTG] + [T80]) and DPH was 5 mM and 0.4 μ M, respectively. The samples were then incubated for at least 2 hours at 37 °C. The fluorescence polarization was measured using fluorescence spectrophotometer FP-8500 (JASCO, Tokyo, Japan). The samples were excited with vertically polarized light (360 nm), and emission intensities both perpendicular (I_{\perp}) (0°, 90°) and parallel (I_{\parallel}) (0°, 0°) to the exciting light that were recorded at 430 nm. The polarization (P) of DPH at 25 °C was then calculated using the following equations (Eqs. 2-1 and 2-2), and fluidity ($1/P$) was defined as reciprocal of polarization:

$$P = \frac{I_{\parallel} - GI_{\perp}}{I_{\parallel} + GI_{\perp}} \quad \text{Eq. 2-1}$$

$$G = \frac{i_{\perp}}{i_{\parallel}} \quad \text{Eq. 2-2}$$

where i_{\perp} and i_{\parallel} are emission intensities perpendicular to the horizontally (90°, 0°) and parallel (90°, 90°) to horizontally polarized excitation light, respectively, and G is the correction factor.

2.5 Membrane Polarity Evaluation.

The membrane polarity of the NLC were measured using Laurdan as a polarity-sensitive fluorescence probe (Harris et al., 2002; Ma et al., 2018; Watanabe et al., 2019b). The samples were prepared in a similar way as in the fluidity measurement. Ten microliters of Laurdan solution (100 μ M in ethanol) were added to the diluted NLC

suspension with molar ratio of lipid/ Laurdan=100/1. The suspensions were then incubated for at least 2 hours at 37 °C. The fluorescence spectrum of Laurdan was recorded with an excitation wavelength of 340 nm at emission wavelengths from 400 to 600 nm (Bui, Suga, Kuhl, et al., 2019; J. Han et al., 2017; Suga et al., 2016a, 2018b; Suga & Umakoshi, 2013; Taguchi et al., 2018). According to the previous studies, the membrane polarity (GP_{340}) at 25 °C was calculated using **Eq. 2-3**:

$$GP_{340} = \frac{(I_{440} - I_{490})}{(I_{440} + I_{490})} \quad \text{Eq. 2-3}$$

where I_{440} and I_{490} are emission intensities at 440 and 490 nm, respectively.

3. Result and Discussion

3.1. Particle Size Distribution and Surface Potential of NLC.

Particle size, PDI, and ζ -potential are the main characteristics of colloidal materials in dispersion, describing their structural property and stability. The hydrodynamic diameter (particle size) of NLC ranged from 215-404 nm (**Fig 2-2 (a)**), and the sizes decreased with the increase of surfactant (T80) concentration. The particle size of the samples with the concentration of CP > CaTG (No. 1, 2, 3, 4) gradually decreased, while those with CP = CaTG (No. 5, 6, 7, 8) and CP < CaTG (No. 9, 10, 11, 12) slightly decreased. The surfactant controlled the particle growth by adsorbing on the surface of NLC; therefore, the surface energy of NLC decreased and prevented aggregation (Chauhan et al., 2020; Teeranachaideekul et al., 2007). An adequate surfactant that could be sufficient to cover all the available NLC resulted in complete dispersion. However, in the samples enriched with liquid lipid component, CP < CaTG (No. 9, 10, 11, 12), the particle size increase with the increase of T80 concentration from 10 % to 15 %. At these low concentrations, the particles were unstable and easy to aggregate. This condition might influence the average size distribution of the resultant particles. Regarding the lipid compositions, the higher concentration of CaTG leads to the formation of more hydrophobic particles; thus, the particles need more surfactant to stabilize.

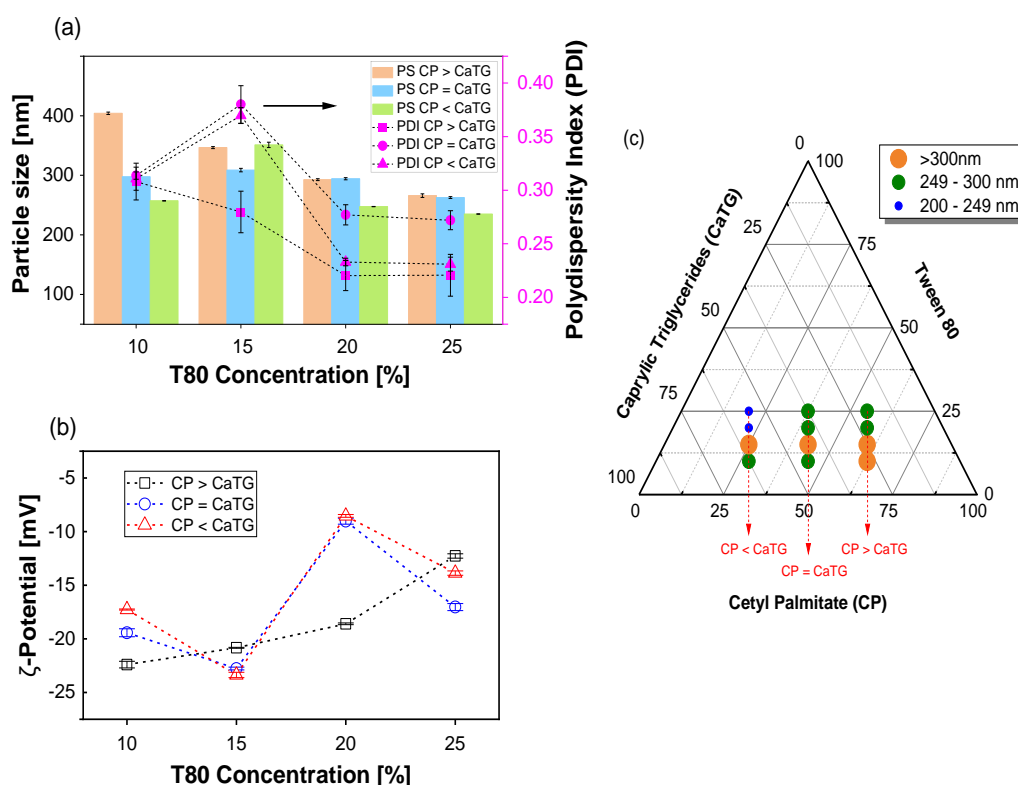


Fig 2- 2 The influence of T80 concentration and lipid composition on particle size and PDI (a), and ζ -potential (b); The particle size of NLC in ternary diagram (c). The measurement was conducted using DLS apparatus at 25 °C. Values: mean \pm SD ($n = 3$).

The PDI is an index that used to define the particle size distribution and how homogenous the particles are. For instance, a PDI value below 0.3 indicates a well-dispersed and homogeneous particle and also acceptable for drug delivery applications (Badran, 2014). The PDI values of NLCs ranged from 0.12 to 0.38 (**Fig. 2-2 (a)**), which confirmed that most samples were fairly monodispersed. Showing a similar trend with that of particle size, the PDI value was also influenced by the T80 concentration. For example, PDI values gradually decreased with the increase of surfactant concentration. However, the PDI increased at T80 concentrations (10-15 %) in samples where CP = CaTG and CP < CaTG. This result indicated that the ratio of liquid component is not responsible for the mono-dispersity; therefore, the addition of the surfactant was needed. In summary, the high PDI values indicate heterogeneity caused by an insufficient surfactant in the dispersion leading to the formation of aggregations among particles.

ζ -potential is one of the indicators for the stability of a colloidal system. The high potential generally indicates high stability and high prevention of aggregation, as a result of the strong repulsion force among particles (Honary & Zahir, 2013; Houacine et al., 2020). Theoretically, absolute ζ -potential values above 30 mV contribute to good stability, about 20 mV provide only short-term stability, and about 5 mV causes a fast aggregation (Honary & Zahir, 2013). In the present study, the ζ -potential value ranged from -8 to -24 mV (**Fig. 2-2 (b)**). The negative value of ζ -potential could be caused by the dissociation of fatty acid, carboxylic, or carbonyl functional group (Ginés et al., 2017; Nahak et al., 2016). In an aqueous solution, the CaTG could react with water and produce fatty acid, contributing to the negative value of ζ -potential together with the carbonyl group of CP and CaTG. According to the mentioned theory, some of the observed NLC samples had short-time stability, and other samples with ζ -potential below absolute 20 mV had a lack of stability. However, T80, as a nonionic surfactant, was reported to provide steric stability instead of electric stability; therefore, ζ -potential of absolute 20 mV or much lower could provide adequate stabilization (Hoeller et al., 2009; Honary & Zahir, 2013). Also, the neutral surface charge that was formed by non-ionic T80 causes the decrease of the lipid negativity; therefore, ζ -potential of the sample approaches zero by the addition of surfactant. In **Fig. 2-2 (b)**, the saturated lipid-enriched samples (No. 1, 2, 3, 4) showed a decrease in the negative ζ -potential values, indicating that the electric stability of NLC gradually decreased with the addition of T80. The ζ -potential values for the samples with CP = CaTG (No. 5, 6, 7, 8) and with CP < CaTG (No. 9, 10, 11, 12) fluctuated and also decreased. The use liquid-state lipid (CaTG) promoted more fluidic particle, and furthermore affect the zeta potential due to electric repulsion among particles.

To better understand the influence of lipid composition on the particle size, a ternary diagram of the NLC was developed (**Fig. 2-2 (c)**). T80, as a surfactant, had strong influence on the particle size; higher surfactant concentration showed a tendency to result smaller particles. However, at a lower T80 concentration ($10\% \leq \text{T80} \leq 15\%$) or at a higher CaTG concentration ($\text{CaTG} \geq 50\%$), the size of the sample became larger with increasing surfactant concentration. The low amount of surfactant (T80) and the high amount of liquid lipid (CaTG) might cause the particle to be unstable, which indicates that the particle size increased due to aggregation. Otherwise, as the concentration of T80 increased (more than 15 %), the particle size was again decreased due to the dispersing

effect of surfactant. The ternary diagram provided systematic knowledge about the effect of the lipid and surfactant composition on particle size. Overall, T80 at 20 and 25 % (No. 3, 4, 7, 8, 11, 12) resulted in monodispersed assemblies with a smaller size (< 300 nm).

3.2 Effect of T80 Concentration on Membrane Fluidity.

DPH, a fluorescence probe, has been widely applied for evaluating membrane fluidity for various kinds of self-assemblies (Bui et al., 2019a; Han et al., 2017; Mach et al., 2020; Poojari et al., 2019; Suga et al., 2016b). DPH is located at the hydrocarbon chain part (hydrophobic core) of the self-assembly in water, and $1/P$ value is reciprocal of polarization obtained by the DPH fluorescence analysis and reflects the membrane fluidity. Firstly, the unary CP, CaTG, and T80 were characterized by DPH (**Fig. 2-1**). Although the dispersions of pure CP and pure CaTG were not stable after long storage, their membrane properties were obtained just after preparation. For pure CP assembly, the $1/P$ was 3.8, much lower than that of pure CaTG ($1/P = 13.1$) or pure T80 ($1/P = 9.2$). A lower $1/P$ value indicates an ordered state: $1/P = 2.8-2.9$ for gel phase of 1,2-dipalmitoyl-*sn*-glycero-3-phosphocholine (DPPC) systems. (Bui, Suga, Kuhl, et al., 2019; Suga & Umakoshi, 2013) Because the T_m of CP is $53\text{ }^{\circ}\text{C}$, it is expected that CP molecules are in solid state at $37\text{ }^{\circ}\text{C}$ (incubation temperature) and $25\text{ }^{\circ}\text{C}$ (analysis temperature). Thus, a lower $1/P$ value of pure CP assembly revealed the solid state. In contrast, pure CaTG and pure T80 assemblies showed higher fluidity ($1/P > 6$) (Bui, Suga, & Umakoshi, 2019; Suga & Umakoshi, 2013) suggesting fluid state (disordered state). In previous studies, such higher fluidities are observed in oleic acid O/W emulsion ($1/P = 13.9 \pm 0.8$) (Suga et al., 2016a) or sodium bis(2-ethylhexyl) sulfosuccinate (AOT) micelle ($1/P = 13.3 \pm 1.8$) (Iwasaki et al., 2017). In brief, the membrane fluidity analysis could reveal the state of lipids in each assembly: CP as solid, CaTG and T80 as fluid.

Fig 2-3 (a) shows the $1/P$ values of CP/80 and CaTG/T80 binary mixture systems. Both pure CaTG and pure T80 assemblies displayed a higher fluidity, and the CaTG/T80 mixtures also showed higher $1/P$ values, which could be categorized as a disordered state. In contrast, CP/T80 = 80/20 showed a lower $1/P$ value similar to pure CP assembly, suggesting a solid state. CP/T80 = 50/50 could be an intermediate (heterogeneous) state, wherein solid and liquid states coexist with each other in the assembly. It was reported that the insertion of unsaturated fatty acid (oleic acid, *etc.*) could disturb the solid-ordered

phase of DPPC bilayer (Onuki et al., 2006). Due to the kink structure in oleoyl group, T80 could disturb tightly packed saturated hydrocarbon chains of CP at the T80 molar fraction >0.2.

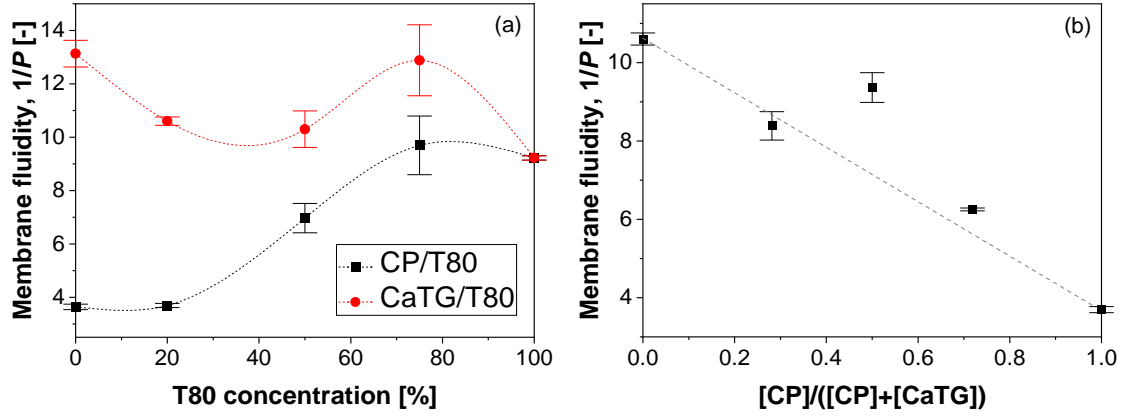


Fig 2- 3 Membrane fluidity ($1/P$) evaluation of binary systems (a), and ternary systems at T80 = 20 % (b) by using the fluorescent probe DPH. Samples were measured at 25 °C. The dashed line in Figure 2 (b) means a reference line for the ideal condition. Values: mean \pm SD ($n = 3$).

At the T80 molar ratio of 0.2 (20 mol%), the $1/P$ values of CP/CaTG/T80 ternary mixture systems were investigated (**Fig. 2-3 (b)**). As investigated above, the $1/P_{[CP/T80 = 80/20]}$ and $1/P_{[CaTG/T80 = 80/20]}$ were 3.7 and 10.6, respectively. Given that the membrane rigidity of CP/CaTG/T80 ternary system is altered depending on the molar fraction of CP, the fluidity ($= 1/P_{[ideal]}$), estimated as follows, would be gradually shifted. Herein, $1/P_{[ideal]}$ is estimated as **Eqs. 2-4 and 2-5**:

$$1/P_{ideal} = x * 1/P_{[CP/T80=80/20]} + (1 - x) * 1/P_{[CaTG/T80=80/20]} \quad \text{Eq. 2- 4}$$

$$x = \frac{[CP]}{[CP]+[CaTG]} \quad \text{Eq. 2- 5}$$

In **Fig. 2-3 (b)**, the trend of the fluidity of the ternary mixture at T80 = 20mol% is following the ideal $1/P$. Nonetheless, the $1/P$ value of CP/CaTG/T80 = 40/40/20 (No. 7) was higher than the expected value. This result suggests that these lipids were miscible at this composition, and the NLC could be considered as a more disordered state (liquid). The increase of T80 molar fraction tends to increase $1/P$ values (**Fig. 2-4**), and most NLC displayed higher fluidity as well as O/W emulsion or micelle. At the low concentration of T80 (T80 = 10 mol%), the samples CP/CaTG/T80 = 27.5/62.5/10 (No. 9) and CP/CaTG/T80 = 45/45/10 (No. 5) showed lower fluidity values similar to pure CP, suggesting that their state could be categorized as SLN. Hence, it is assumed that the variation of T80 concentration does not significantly affect fluidity in this concentration.

Based on the membrane fluidity analysis, no significant changes were found unless the composition requires $CP > CaTG$. In this case, most of CP molecules (saturated lipid) were influenced by the coexisting CaTG and T80, wherein the NLC matrix could be in a highly disordered state.

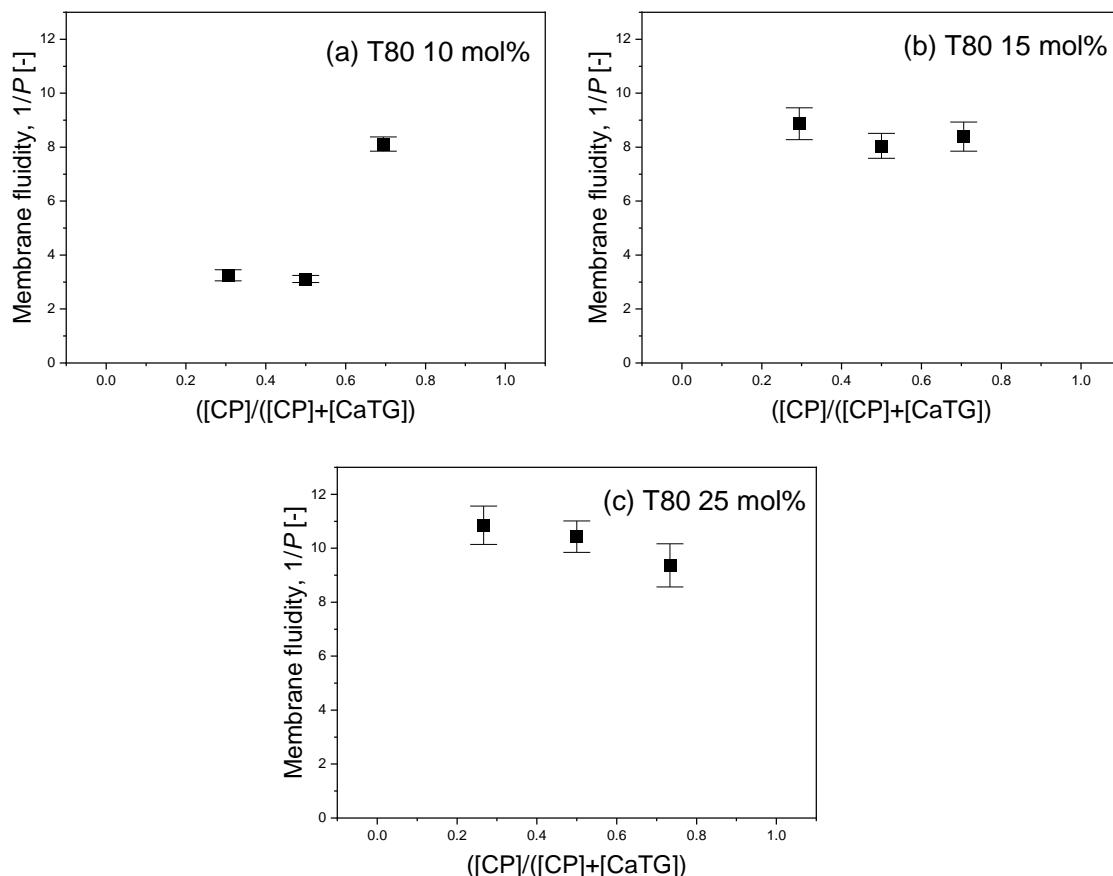


Fig 2- 4 Membrane fluidity ($1/P$) of binary systems (other T80 concentrations). Values: mean \pm SD ($n = 3$).

3.3 Effect of T80 Concentration on Membrane Polarity.

Laurdan is a polar sensitive probe whose emission peak position reflects the surrounding polarity of Laurdan at self-assembly surface. It is reported that a hydrated membrane, such as the fluid phase of liposome or micelle, resulted in the red-shifted emission peak (at around 490 nm), while the solid-ordered phase (gel phase) of liposome resulted in the blue-shifted emission peak (440 nm) (Parasassi & Gratton, 1995; Watanabe, Goto, et al., 2019a). The Laurdan in O/W emulsion resulted in the emission peak at 420-430 nm (Suga et al., 2016a, 2018a). A GP_{340} analysis is well employed to compare the polar environment of membrane, wherein $GP_{340} > 0$ indicates a hydrophobic environment

(less hydrated membrane) and $GP_{340} < 0$ indicates a hydrated membrane. The emission spectra shift shows the polarity changes around the Laurdan (**Fig. 2-5**).

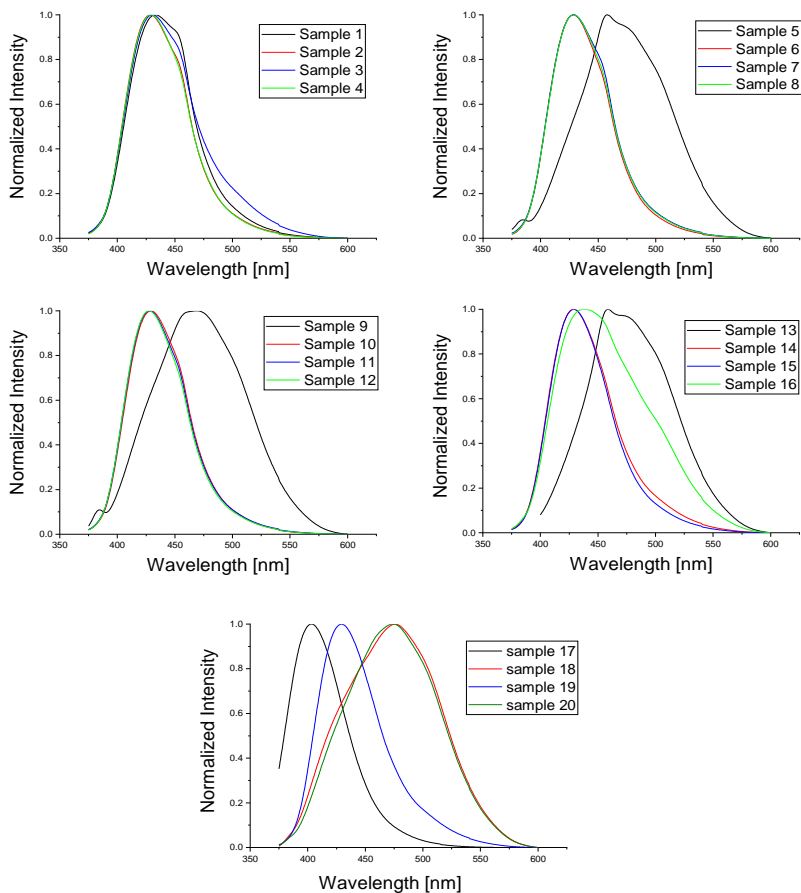


Fig 2- 5 Laurdan spectra of all samples. See Table 1 for each composition.

Similar to that of DPH fluorescence analysis, the GP_{340} values of unary systems of CP, CaTG, and T80 were characterized (**Fig. 2-1**). Pure CP assembly had GP_{340} value of -0.3 , which was not significantly different from T80 ($GP_{340} \sim -0.25$). This result is surprisingly indicating that CP is hydrophilic instead of hydrophobic. Originally, CP is derived from palmitic acid, a wax reported as a highly hydrophobic property (Saji, 2020). However, when a layer of wax is eroded, it may absorb water molecules and result in polar environment, and measured as hydrophilic surroundings (Barthlott et al., 2016, 2017). In this study, the pure CP assembly was prepared with the same method as the NLC preparation, including stirring and sonicating. These treatments were possibly eroding the wax structure of CP, then caused water molecules to be absorbed and resulting

in a polar environment (hydrophilic environment). On the other hand, pure CaTG assembly showed a much higher GP_{340} value ($GP_{340} \sim 0.7$), suggesting the hydrophobic environment. This behavior is similar to that of oleic acid (OA) assemblies and O/W emulsion in the previous study, which has a highly liquid-disordered state and hydrophobic environment (Suga et al., 2016a).

The GP_{340} values of CP/T80 and CaTG/T80 binary systems are displayed in **Fig 2-6 (a)**. Both pure CP and T80 showed lower GP_{340} value, as well as CP/T80 binary system, which could be identified as hydrophilic environment. The addition of T80 to the aqueous CP did not significantly affect the GP_{340} value because its original GP_{340} is similar. The CP/T80 binary system showed a slightly higher GP_{340} than its original constituents, indicating the interaction between CP and T80 could make the environment less hydrated. On the other hand, CaTG/T80 binary systems showed a higher polarity similar to pure CaTG, indicating that the addition of T80 did not significantly affect the polar environment of CaTG.

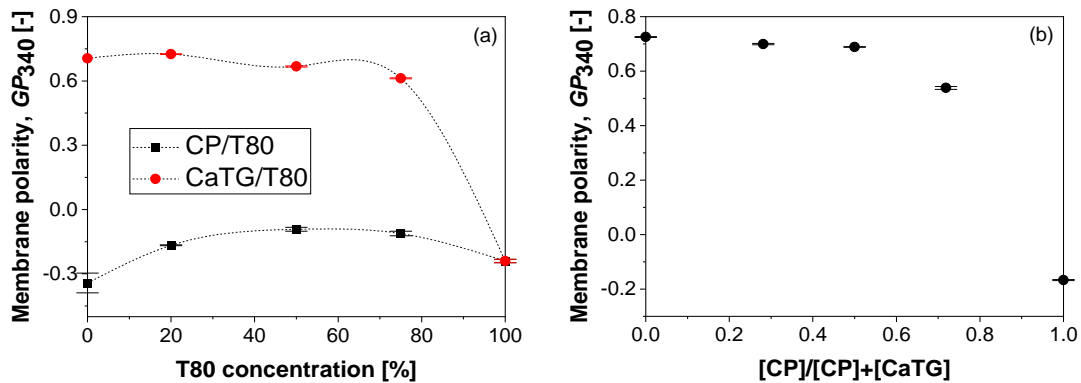


Fig 2- 6 Membrane polarity (GP_{340}) evaluation of binary systems (a), and ternary systems at T80 = 20 % (b) by using the fluorescent probe Laurdan. Samples were measured at 25 °C. Values: mean \pm SD ($n = 3$).

Similar to membrane fluidity investigation, the membrane polarity of ternary systems was investigated at the T80 molar ratio of 0.2 (20 mol%). As investigated in **Fig. 2-6 (b)**, the GP_{340} values of CP/T80 = 80/20 (No. 15) and CaTG/T80 = 80/20 (No. 17) were -0.17 and 0.72 , respectively. This result suggests that the membrane polarity of CP/CaTG/T80 ternary system can be varied depending on molar fraction of lipid. However, the data shows similar behavior to the binary system of CaTG/T80 instead of linear form, which is no significant GP_{340} value change and indicates a strong hydrophobic property of CaTG. Notably, the GP_{340} value of CP/CaTG/T80 =

57.5/22.5/20 (No. 3) decreased as compared to that of CP/T80 = 80/20 (No. 15), indicating that the higher amount of CP could slightly lower the hydrophobicity. Other T80 molar fractions give a similar GP_{340} value (**Fig. 2-7**), and most of NLC showed a high GP_{340} similar to O/W emulsion. At a low concentration of T80 (T80 = 10 mol%), the samples CP/CaTG/T80 = 27.5/62.5/10 (No. 9) and CP/CaTG/T80 = 45/45/10 (No. 5) exhibited a negative GP_{340} value similar to that of pure CP and T80. This result strengthens the hypothesis that their state could be categorized as SLN. Based on membrane polarity analysis, no significant changes existed with the different composition of lipid components.

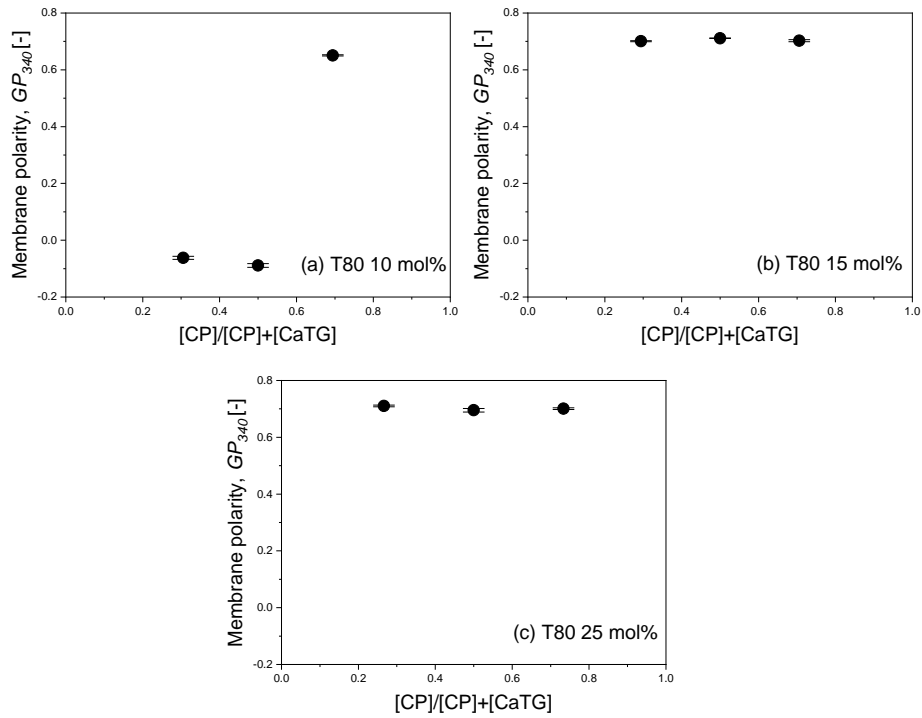


Fig 2- 7 Membrane polarity (GP_{340}) evaluation of binary systems (other T80 concentrations). Values: mean \pm SD ($n = 3$).

3.4 Determination of Self-Assembly State based on Fluidity and Polarity Analysis.

Cartesian diagram, based on membrane fluidity ($1/P$) and polarity (GP_{340}), was employed for a systematic analysis of the state of ternary lipid mixture systems. Similar to the previous studies (Suga et al., 2018a; Suga & Umakoshi, 2013), the data of membrane fluidity ($1/P$, in x -axis) and membrane polarity (GP_{340} , in y -axis) are plotted (**Fig. 2-8**). In this study, the assembly state was categorized into three types: a liquid state-assembly like O/W emulsion (disordered, e.g., pure CaTG); a micelle state-assembly

(disordered, e.g., pure T80); and a solid state-assembly (ordered, e.g., pure CP) (**Fig. 2-9**). Because the T_m of CP is 53 °C, pure CP assembly is SLN-like structure, and the property of SLN is comparable to others.

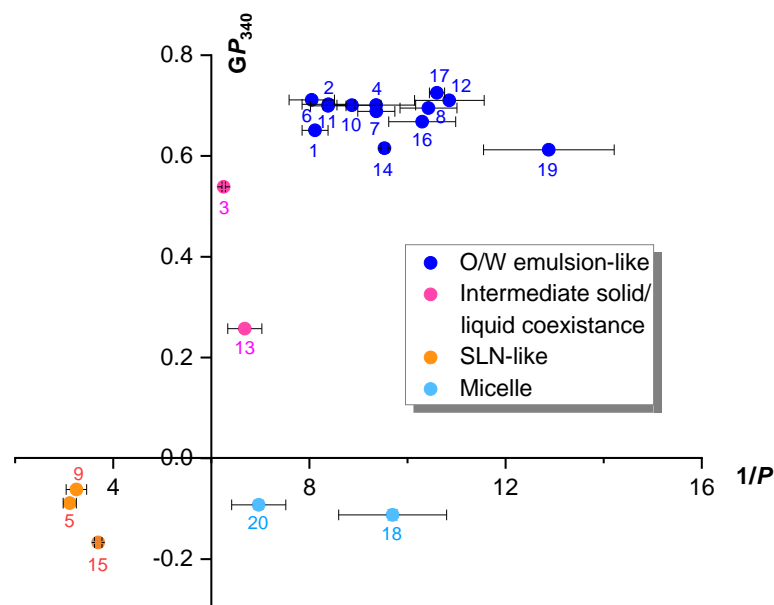


Fig 2- 8 Summary of membrane properties in the Cartesian diagram. The total lipid and surfactant were 100 mM. The sample compositions are shown in Table 1. Values: mean \pm SD ($n = 3$).

The state of each self-assembly was distinguished based on the membrane property, which is differently plotted in the Cartesian diagram (**Fig. 2-8**). The observed samples are located in three different states. In more detail, SLN state could be obtained when T80 = 10 mol% (No. 5 and 9) and T80 = 20 mol% without any CaTG (liquid component) (No. 15), while micelle state could be obtained when the sample has no CaTG (liquid component) (No. 18 and 20). This condition suggests that liquid lipid component has a significant influence on the self-assembly formation, and it causes the rest of the samples to be categorized as O/W emulsion. However, samples No. 3 and 13 demonstrated an exciting behavior, located in the intermediate of the three different states. This suggests the coexistence of solid and liquid states that might be suited to the criteria of NLC. Considering the purpose of making more liquified structure, the heterogeneous state and the particular samples of O/W emulsion-like might suitable for a drug carrier. Describing from the fluidity and polarity, $1/P$ value of 6–10 is necessary, as well as GP_{340} of 0.5–0.7. Nonetheless, the desirable membrane properties for a model drug are tightly related to the administration routes of the drug release; for example, more fluidic and

more hydrophilic properties are applicable for injection administration, while less fluidity and more hydrophobic are suitable for topical administration (Zhai et al., 2019).

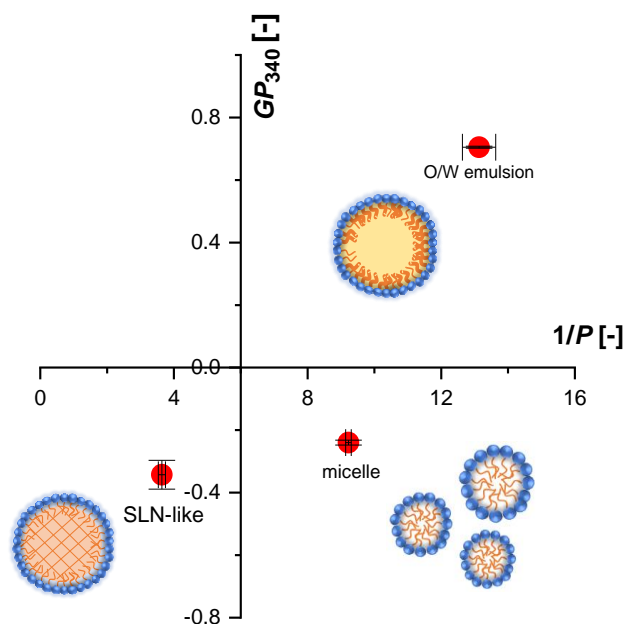


Fig 2- 9 Membrane property comparison of unary systems at 25 °C. Pure CP assembly as SLN, pure CaTG as O/W emulsion, and pure T80 assembly as micelle. Values: mean \pm SD ($n = 3$).

Based on the summary of membrane properties in the Cartesian diagram, the observed samples have unique characteristics. Compared to the previous study of liposome (Shaker et al., 2017). CP/CaTG/T80 ternary system has a reverse behavior. For further details, the solid-state assembly (SLN) was obtained when both fluidity and polarity were low, and the liquid state was obtained when both fluidity and polarity were high; while the ordered phase of liposomes was taken when fluidity was low and polarity was high, and the disordered phase was the reverse; fluidity was high and polarity was low. Generally, the highly packed membrane is categorized as ordered phase; then, the membrane is less hydrated by a water molecule and is considered more hydrophobic (Bui, Suga, & Umakoshi, 2019; J. Han et al., 2017). In the case of NLC, the membrane properties can be varied depending on the ration of solid-state component (CP) and liquid-state one (CaTG). As already mentioned, pure CP assembly had a much lower GP_{340} value, while pure CaTG assembly showed a much higher GP_{340} value similar to O/W emulsion of oleic acid.

3.5 Ternary Diagram of CP/CaTG/T80 Self-Assembly Systems.

Constructed by the investigated assembly state in the Cartesian diagram analysis, the ternary diagram of the CP/CaTG/T80 (Total: 100 mM) was developed to understand the self-assembly behavior affected by the constituents. As shown in **Fig. 2-10**, the four colors described the self-assembly state of the observed system. The dark, blue-colored points (disordered state, O/W emulsion-like) are the most abundant: they could be characterized as NLC. This behavior supports the hypothesis about the strong influence of CaTG components on the assembly formation of NLC system. In addition, a micelle might not be formed if CaTG existed; while a certain fraction of CP and T80 could require to form other self-assembly structure, solid-state (typical SLN), or solid and liquid coexistence (NLC-like).

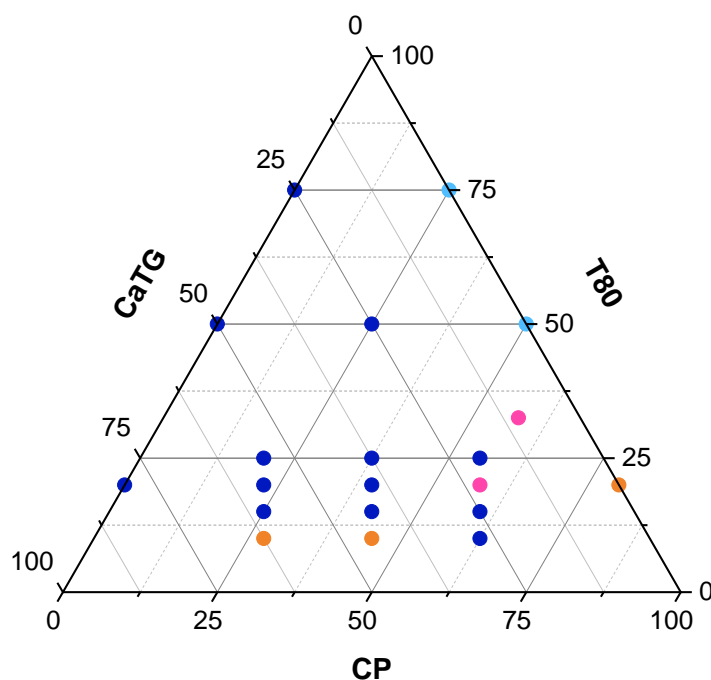


Fig 2- 10 Ternary diagram of CP/CaTG/T80 self-assemblies. *Dark blue*: Liquid state (emulsion-like, NLC), *orange*: solid state (SLN-like), *light blue*: micelle, and *pink*: intermediate (heterogeneous state).

Evaluated from the bottom to the upper of the diagram, T80 has an essential role in forming a self-assembly structure. The concentration of T80 at 12.5–40 mol% is required to form other self-assemblies in the aqueous solution, instead of only micelle. Above those concentrations, the assemblies formed O/W emulsion or micelle depending on the CaTG concentration. In the lipid nanoparticle studies, the role of the T80 is

originally for surface-active agents (Bashiri et al., 2020; Eh Suk et al., 2020); consequently, to stabilize the particle, the concentration should be adequate to cover the particle surface. Regarding this property, the samples with high CP (saturated lipid), CP/CaTG/T80 = 62.5/10/27.5 (No. 1) and CP/CaTG/T80 = 60/15/25 (No. 2) tended to form O/W emulsion because the solid component was rapidly aggregated, and the small amount of T80 interacts with CaTG to form emulsion instead of SLN structure. On the other hand, the lack of surfactant (T80) in the system with a high amount of liquid lipid (CaTG) might cause nanoparticle instability. CaTG has high hydrophobicity and fluidity that could generate the NLC easily affected by adding the surfactant.

Based on the diagram, 12.5-50 mol% of T80 and 50-75 mol% of CP are needed to form the assembly of solid and liquid coexistence, while the required liquid component is only 10–30 mol%. Even though it needs further investigation, these compositions (pink color in **Fig. 2-10**) could be categorized as NLC because they are suitable with the NLC definition, consisting of solid lipid component with partially disorganized state due to the incorporation of liquid lipid. NLC with a high condensed matrix tends to cause a low drug loading due to the inflexible lipid matrix. Thus, although it showed an average particle size, the heterogeneous state could be useful for NLC. For liposome-based drug loading studies, 10% of resveratrol and 8% of quercetin significantly altered the properties of the membranes, especially in heterogeneous phase state (De Granada-Flor et al., 2019; J. Han et al., 2017). Thus, ordered or heterogeneous phase state of the membrane could be interactive with hydrophobic drugs such as polyphenol. Considering the type of the drug payload, the defined NLC might be applicable to encapsulate a hydrophobic drug due to its highly hydrophobic core.

Compared to liposomes, NLCs have attractive behavior regarding the particle size and assembly state relationship. In the case of liposomes, ordered phase liposomes generally resulted in smaller particles, and the disordered phase resulted in larger particles (Shaker et al., 2017). The membrane packing could be responsible for this phenomenon. Interestingly, NLCs have a converse behavior; the liquid state-assembly such as O/W emulsion (disordered phase) tended to form a smaller particle size, and those with solid state-assembly (ordered phase) tended to form a bigger particle size. This anomaly might correspond to the presence of the surfactant in the NLC constituent as it played a vital role in controlling the particle size (Eh Suk et al., 2020; How et al., 2011).

4. Summary

The structural and physicochemical properties of NLCs have been characterized. The T80 concentration at 20 mol% and 25 mol% resulted in monodispersed assemblies with particle size < 300 nm, which could be applied for drug delivery. In addition, a systematic characterization of self-assembly properties of the CP/CaTG/T80 ternary mixtures was also successfully performed using fluorescence-based analysis. This chapter demonstrated that the self-assembly state constructed by CP/CaTG/T80 varies depending on the lipids and surfactant composition. Four possible formations have occurred: micelle-like, O/W emulsion-like, SLN-like, and intermediate state (solid-liquid coexistence). The formation of CP/CaTG/T80 assemblies are dominated by O/W emulsion-like characteristics, which was strongly affected by the presence of CaTG. Based on the ternary diagram, T80 was the most influential component in NLC system. Even though further morphological investigations are needed, this is the first report of self-assembly characterization of NLC, and it could be a meaningful insight related to the future drug delivery applications.

Chapter 3

Dependence of Core-Shell Structure on Lipid Composition of Nanostructured Lipid Carriers

1. Introduction

The fundamental properties and structure of a carrier are crucial for the success of a delivery system because drug release and the sustained/controlled release through a particular route are closely related to the carrier properties. For instance, more fluidic and hydrophilic properties are desirable for the injection route, whereas more viscous and lipophilic properties are appropriate for the topical route (Zhai et al., 2019). In transdermal DDS, understanding the physicochemical properties, such as particle size, fluidity/ rigidity, and carrier morphology, is important to determine the possibility of skin penetration. It has been reported that rigid liposomes can prolong transdermal delivery as they deposit on the skin surface; whereas fluid vesicles can be considered for transdermal diffusion.(Richard et al., 2020) Understanding of these basic properties and behavior will be crucial in optimizing the design of a carrier for a particular purpose.

According to previous studies, the plausible structure of NLC can be classified into three categories: (i) imperfect type (consisting of imperfect crystals and a mixture of solid and liquid lipids are in a highly disordered state), (ii) amorphous type (a lack of crystalline structure), and (iii) multiple types (containing nano-compartments inside the particle) (Chauhan et al., 2020; Tamjidi et al., 2013; van Tran et al., 2019). Although, the variety of NLC structures has been introduced, none of the studies have comprehensively elucidated the internal structure of NLC. In addition, the influence of lipid composition on NLC internal structure has not yet been elaborated.

The design of NLC for DDS applications is still challenging. The presence of solid lipid in the lipid matrix generates crystallization process during the production and storage of NLC. This process can have advantages as was mentioned to improve the stability and enhancing loading capacity; however, at the same time, it can also cause drug leakage and instability. The crystallization process is complex phenomena and may strongly be dependent on the lipid composition. Also, lipid composition may have effects

on the fundamental properties, such as phase state and internal structure of NLC, which are essential properties of nanocarrier. These properties can also affect the entrapment behavior of the loaded materials and resulted in a different activity in the application stage. Therefore, it is important to understand the properties, structure and behavior of NLCs that are dependent of the lipid composition.

In this chapter, some physicochemical characterizations of NLC were performed including dynamic light scattering (DLS) for measuring the hydrodynamic diameter and size distribution, fluorescence-based analysis using diphenylhexatriene (DPH) as a fluorescence probe for evaluating the rigidity of the core part of NLCs, cryo-transmission electron microscopy (cryo-TEM) for morphological study, differential scanning calorimetry (DSC) to observe the thermal behavior of NLC, and X-ray diffraction (XRD) to confirm the crystalline structure and behavior. Such comprehensive characterizations would provide well-defined fundamental properties of NLC and ultimately help in optimization of the DDS carrier design. These findings related to the internal structure of NLC and its relationship with the lipid composition provide new insights and significant contribution to the design of highly effective drug carrier.

2. Materials and Methods

2.1 Materials

CP and CaTG, $\geq 99\%$ of purity, were purchased from Sigma-Aldrich (St. Louis, MO), and plant-based polysorbate 80 (T80) ($\geq 97\%$ purity) was purchased from Fujifilm Wako Pure Chemical Industry (Osaka, Japan). The molecular structure and physical properties of CP, CaTG, and T80 are shown in **Figure 2-1 (Chapter 2)**. 1,6-Diphenyl-1,3,5-hexatriene (DPH) ($\geq 99\%$ purity) was purchased from Sigma-Aldrich (St. Louis, MO). All chemicals were used without further purification. Ultrapure water was prepared using Direct-Q® UV3 (Merck Millipore Co., Tokyo, Japan).

2.2 NLC Preparation

NLC were prepared using a combination of hot homogenization and ultrasonication methods, as reported previously (Guilherme et al., 2019; Izza et al., 2021). A schematic of the NLC preparation process is shown in **Figure 3-1**. First, both lipid

components, solid lipid (CP) and liquid lipid (CaTG), were stirred and preheated at 65 °C (above the melting point of CP) using a water bath heater. Surfactant (T80) was prepared separately in an aqueous solution and preheated at the same temperature (65 °C). After solid lipid components were melted completely and mixed well with liquid lipid, T80 solution was added dropwise to the lipid mixture. The stirred-tank heating process was then continued for 15 min, followed by sonication (Probe sonicator-TOMY Ultrasonic Disruptor UD-200) for 3 min. Power output ultrasound was set by tuning the output dial (no. 4 for this experiment). The sample dispersion was then left for 24 h at room temperature (25 °C) to stabilize the structure and then stored at 4 °C. Before analysis, the samples were kept for some time at room temperature. The total concentration of lipids and surfactant was 100 mM, and different compositions of NLC are shown in **Table 3-1**. The same surfactant concentration (25 mol%) was chosen considering the consistency in stability according to a previous study (Izza et al., 2021), whereas NLC with three different compositions were prepared to investigate the influence of lipid composition on the properties and internal structure of NLC.

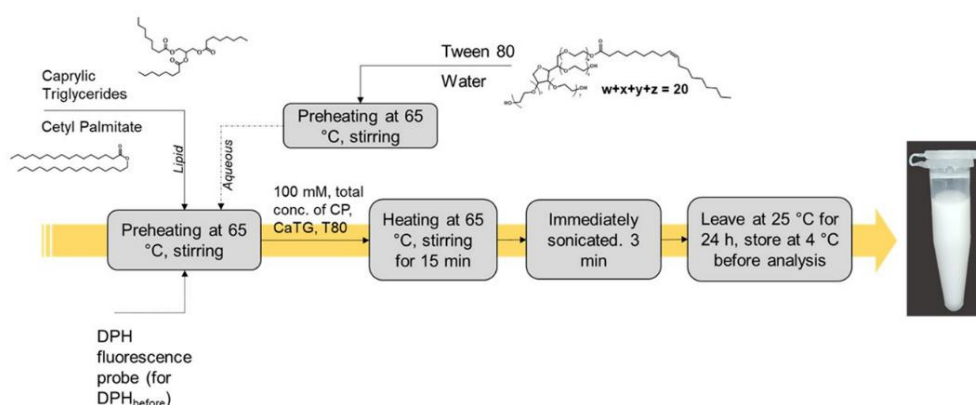


Figure 3- 1. A schematic of NLC preparation process

Table 3-1. NLC compositions used in this study

Sample	Lipid composition (100 mM in total)		
	CP [mol%] (Solid Lipid)	CaTG [mol%] (Liquid Lipid)	T80 [mol%] (Surfactant)
NLC 1 [S]/ [L] > 1	55	20	25
NLC 2 [S]/ [L] = 1	37.5	37.5	25
NLC 3 [S]/ [L] < 1	20	55	25

*[S]/ [L] = ratio of solid lipid to liquid lipid concentration

2.3 Dynamic Light Scattering (DLS) Analysis

Particle size (z-average) and polydispersity index (PDI) were analyzed using Malvern Zetasizer Nano series (Malvern, UK) by DLS technique. According to the DLS theory, each parameter was calculated as the average of at least three measurements, and each measurement was obtained from the mean of at least 10 readings for each sample. Measurements were performed at 25 °C. Before analysis, NLC samples were diluted to 1 mM in ultrapure water and placed in disposable cuvette.

Measurement of the binary mixture of NLC constituents was performed as additional supporting data. The binary mixtures (CP-CaTG) and (CP-T80) were prepared using the same method as for the NLC samples. However, considering the instability of particles without a surfactant, DLS analysis of the CP-CaTG binary mixture was performed immediately after sample preparation without keeping at room temperature.

2.4 Fluorescence Anisotropy (Polarization)

The fluorescence polarization method using DPH as the fluorescence probe was employed to measure the internal rigidity of NLC. DPH solution (10 μM) was prepared in ethanol and added to the diluted NLC samples. The molar ratio of lipid/DPH = 12,500/1 with a total concentration of lipid and DPH was 0.5 mM and 0.04 μM, respectively. Before analysis, the samples were incubated for 2 h at 37 °C. The fluorescence spectrophotometer FP-8500 (JASCO, Tokyo, Japan) was used to measure fluorescence polarization. The samples were excited with vertically polarized light (360 nm), and emission intensities, both perpendicular (I_{VH}) (0°, 90°) and parallel (I_{VV}) (0°, 0°) to the excitation light, were recorded at 430 nm. The anisotropy (r) of DPH at 25 °C was then calculated using the following equations (Eqs. 3-1 and 3-2):

$$r = \frac{I_{VV} - GI_{VH}}{I_{VV} + 2GI_{VH}} \quad \text{Eq. 3-1}$$

$$G = \frac{i_{HV}}{i_{HH}} \quad \text{Eq. 3-2}$$

where i_{HV} and i_{HH} are the emission intensities perpendicular (90°, 0°), and parallel (90°, 90°) to the horizontally polarized excitation light, respectively, and G is the correction factor.

In this study, two different measurement modes were applied. First, the conventional method (DPH_{after}), in which DPH was added after NLC was completely fabricated as previously described in chapter 2. Other than that, DPH was added during the fabrication process along with the lipid mixture (DPH_{before}). Using this method, DPH is expected to distribute the deeper NLC interior.

2.5 Cryo-TEM Observation

NLC samples were prepared at a concentration of 100 mM using the same protocol and method as described in a previous study, with slight modification.(Cizmar & Yuana, 2017) The samples were added to a standard electron microscope holey carbon grid (Quantifoil Micro Tools GmbH, Jena, Germany). The excess sample solution was removed from the grid by blotting procedures utilizing a Vitrobot system (Thermo Fisher Scientific, MA USA), and the grid was rapidly frozen using liquid ethane. Images were captured under cryogenic conditions (~88 K) at a magnification of 59,000× operating a Titan Krios (Thermo Fisher Scientific, MA USA) at 300 kV using Falcon2 CMOS camera. The image processing was carried out using the *Image-J 1.53k* software (*Java*).

Fast Fourier transform (FFT) analysis was performed as additional image processing to measure the lattice distance of the multilamellar structure using the *Image-J* feature. First, a multilamellar image was selected from the cryo-TEM images. Starting from the signal processing FFT, a pattern with spots, expressing the high frequency of the signal, was provided. By selecting the spot, an inverse FFT image can be generated, and the lattice distance can be calculated from the plot profile.

2.6 Differential Scanning Calorimetry (DSC)

DSC analysis of NLC was conducted using DSC-60 apparatus (Shimadzu, Kyoto, Japan). Three microliters of the sample and pure water were placed into different aluminum pans under a dry nitrogen environment. The heating process was performed at a rate of 2 °C/min between 25 and 70 °C. The melting point (T_m) and enthalpy of the transition process were determined using additional peak analyzer tools in Origin-Pro 2021 software. DSC analysis was performed for pure CP, binary mixtures, and NLC samples. For the analysis of pure CP, an empty (air) reference pan was used, whereas for binary mixtures and NLC samples, the reference pan was filled with ultrapure water (which was also used to prepare sample solution). The binary mixtures (CP-CaTG) and

(CP-T80) were prepared using the same method as for the NLC samples. The crystallinity index (*CI*) was calculated as described in a previous study.(Li et al., 2022)

2.7 X-Ray Diffraction (XRD)

XRD experiments were performed using Rigaku Smart Lab X-ray diffractometer (Rigaku, Tokyo, Japan), with monochromatic Cu K α radiation (λ) 0.1542 nm at 40 kV, and 30 mA graded elliptic multilayer optics. The NLC samples (100 μ L) were transferred to the bottom of the glass plate. The diffraction pattern was recorded with an imaging plate and was carried out at 25 °C for 38 min. Crystallinity was calculated based on the resulting peaks using **Eq. 3-3**. The crystalline and amorphous areas were calculated using a peak analyzer in the Origin software.

$$\text{Crystallinity (\%)} = \frac{\text{Crystal area}}{\text{Crystal area} + \text{Amorph area}} * 100 \quad \text{Eq. 3- 3}$$

3. Results

3.1 Basic Nano-properties and Stability

CP, CaTG, and T80 were used as the solid lipid, liquid lipid, and surfactant, respectively. These three components were dispersed in an aqueous environment to form NLC structure. Because T80 has a large hydrophilic head group, it is located at the interface and stably disperses the particle.(Nahak et al., 2016b; Rabe et al., 2020) In addition, T80 has an octanol-water partition coefficient ($\text{Log}P = 4.8$) lower than that of the other components (**Figure 2-1, table**), implying that T80 is mainly distributed in the region close to aqueous phase. Our previous study identified the dependence of self-assembly behavior on NLC composition, including surfactant concentration.(Izza et al., 2021) Considering that the surfactant concentration affects particle stability, samples with the same concentration of surfactant and different lipid compositions (NLC 1, NLC 2, and NLC 3) were chosen for the current study (**Figure 3-2**).

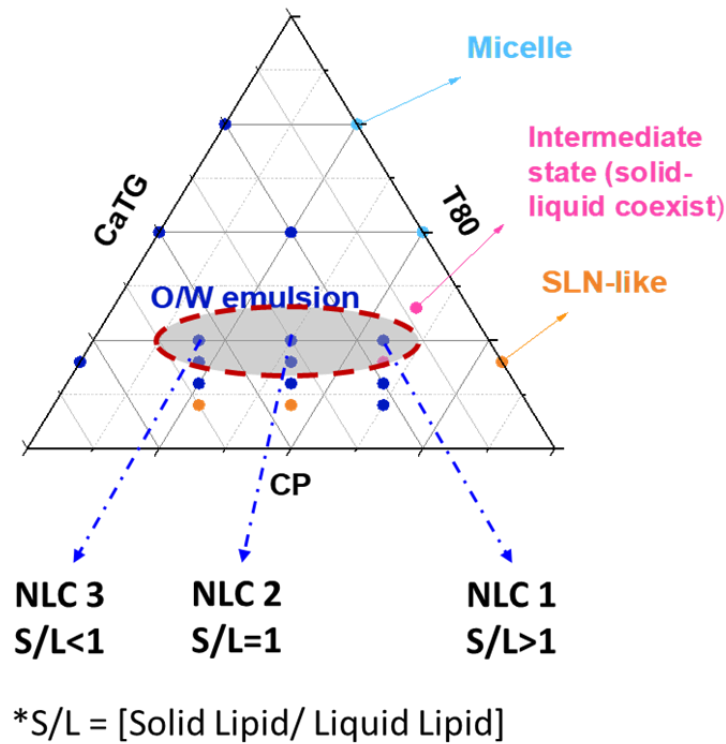


Figure 3- 2 NLC Composition chosen in this chapter based on the chapter 2 result.

As confirmed by DLS, NLC were successfully manufactured with a particle size of 169.5-225.9 nm as shown in **Figure 3-3 (a)**. According to the results, the sample enriched with solid lipid (NLC 1) had a larger particle size. This is presumably because the solid lipid CP has nearly double the volume per unit weight compared to the liquid lipid CaTG (**Figure 2-1, table**). Contrarily, another study reported increase in particle size in the presence of liquid lipid.(Li et al., 2022) This might be due to the presence of a different lipid constituent, particularly the solid lipid, which was glycerol tristearin (GTS) having similar volume per unit weight to the liquid lipid medium-chain triglycerides (MCT), and liquid lipid had a greater influence on the diameter of NLC. Hence, the findings of previous study and our study implies that distinct values of volume per unit weight of solid lipids may have different effects on particle size. Furthermore, it is likely that owing to the solid property of CP, an irregular lipid matrix might be formed in the entire NLC core structure, resulting in a larger average particle size. This result agreed with those of other NLC precursor studies; the particle size was decreased with the addition of liquid lipid. NLC had smaller particle size than that of SLN because of the dispersion effect of liquid lipids.(Sakellari et al., 2021; K. W. Wu et al., 2021)

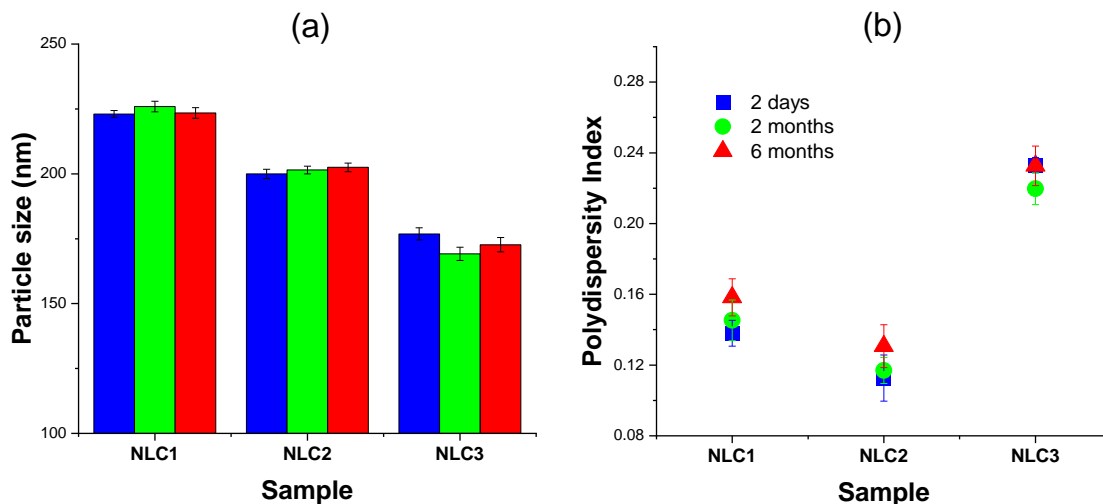


Figure 3- 3 Particle size (a) and PDI (b) of NLC during storage. Blue: 2 days, green: 2 months, red: 6 months. Error bar represents the standard deviations ($n=3$). All sample were measure at T = 25 °C.

The polydispersity index (PDI) was used to determine particle size distribution. A value below 0.3 denotes a well-dispersed and homogeneous particle, a prerequisite for its application as a DDS carrier (Badran, 2014). All NLC samples had PDI of less than 0.25 (**Figure 3-3 (b)**), indicating that all samples were monodispersed. Furthermore, the distribution curve demonstrated a unimodal distribution (**Figure 3-4**), suggesting the NLC did not aggregate or coalesce. These results indicate that different lipid composition did not significantly alter the PDI; however, the sample with a high concentration of CaTG (NLC 3) showed the highest PDI value among the three NLCs, indicating that a broader particle size distribution can be obtained with the contribution of high amounts of liquid lipids.

To ensure the NLC stability, the long-term stability of the particles was observed, and the results are shown in **Figures 3-3 (a) & (b)**. All the samples were stored at 4 °C, and the particle size and PDI were again measured after two months and six months. All the observed NLC (NLC 1, NLC 2, and NLC 3) demonstrated high particle stability, as indicated by the stable particle size and PDI, even after storage for six months. This result is agreed with the previous study resulted that the performance of NLC in terms of particle stability was longer and preferable than that of SLN (Kelidari et al., 2017). The particle size of NLC remain stable even after being stored under room temperature for 6 months.

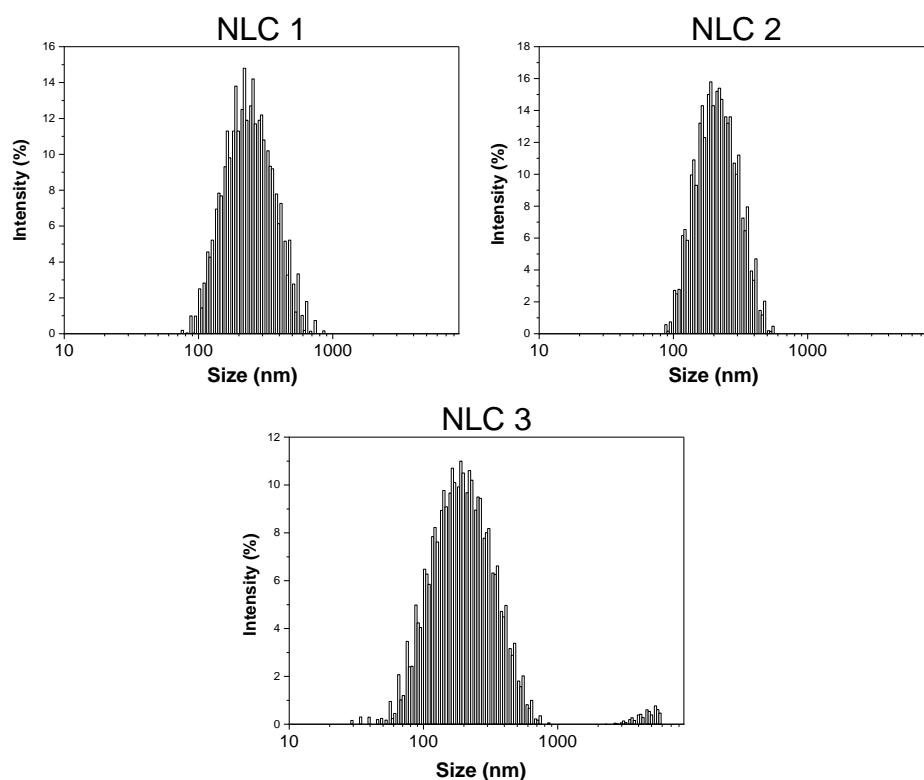


Figure 3- 4 Size distribution curve

3.2 Fluorescence anisotropy of DPH at NLC

Fluorescence-based analysis using DPH as the fluorescence probe was performed to measure the fluorescence anisotropy (r). Higher anisotropy represents lower rigidity of the surrounding fluorophore. This methodology has been widely used to measure the membrane fluidity of multiform self-assembly structures (Poojari et al., 2019b; Stott et al., 2008; Watanabe, Goto, et al., 2019b). The present study followed a modified procedure, as mentioned in the experimental section. The anisotropy of the NLC samples is shown in **Figure 3-5**. The fluorescence spectra of both DPH_{before} and DPH_{after} samples were evaluated before analysis to ensure that the emitted light intensity represents only the difference of DPH-surrounding structures, which is demonstrated by the same spectral shape (**Figure 3-6**). According to the results, the anisotropy decreased with increase in the concentration of liquid lipid, which fluidity increased, demonstrating the nature of liquid lipids.

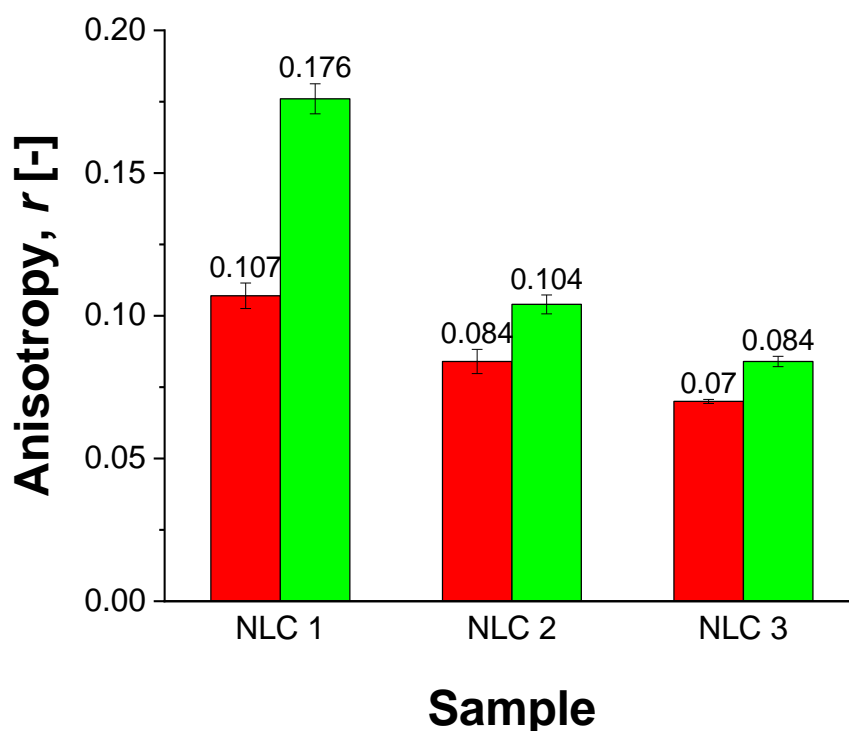


Figure 3- 5 Anisotropy (r) of NLC based on DPH-fluorescence analysis. Error bar represents the standard deviations ($n=3$). Red: DPH_{before}, green: DPH_{after}

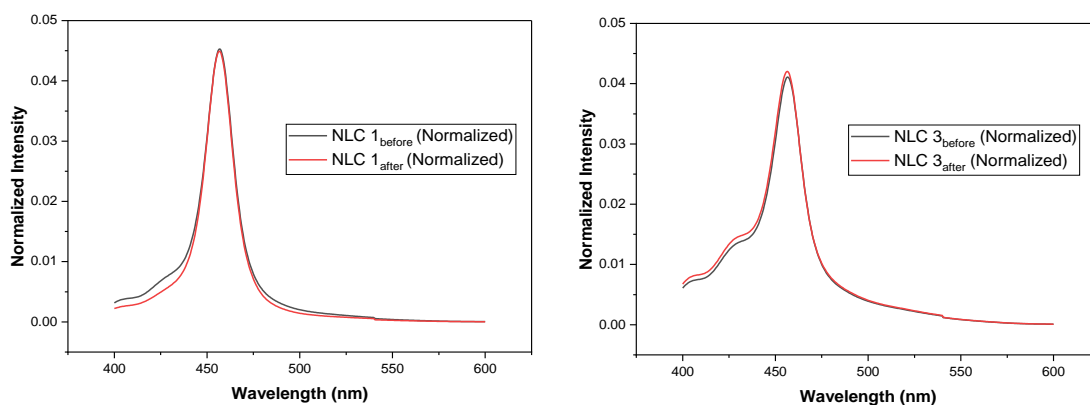


Figure 3- 6 Normalized fluorescence intensity of DPH_{before} and DPH_{after}.

As a general trend, a marked difference in the anisotropy between DPH_{before} and DPH_{after} was revealed for all NLC. This difference indicates heterogeneity of NLC related to the location of DPH. Furthermore, the sample DPH_{after} has a higher anisotropy, which implies to the higher rigidity than that of DPH_{before}. In the sample DPH_{before}, DPH might preferably be located in the inner core since it was preliminarily mixed with the lipids and has hydrophobic nature. In the case of DPH_{after}, the DPH might locate at the shallower

position (surface region) of the matured NLC particles. The particles of the sample DPH_{before} might have a more rigid outer shell core and a less rigid inner core considering the deeper location of DPH. This different rigidity indicates that NLCs have a core-shell structure, as is illustrated in **Figure 3-7**.

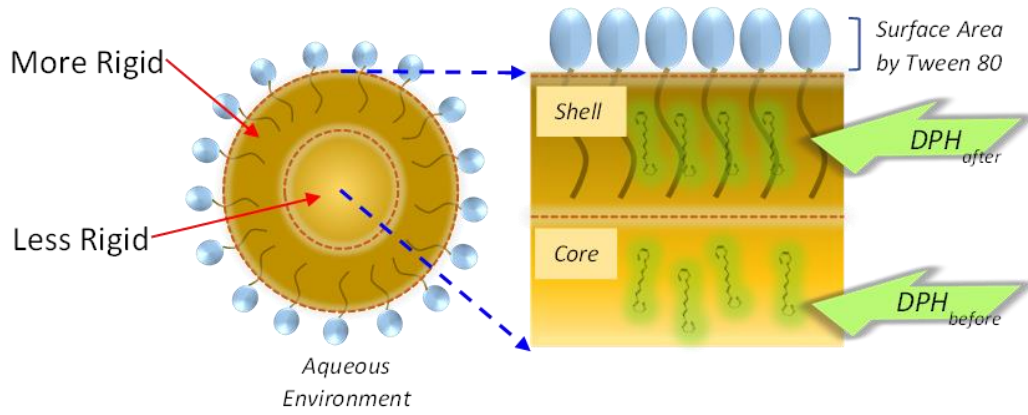


Figure 3- 7 Illustration of NLC core-shell structure

3.3 Morphological Observations

Cryo-TEM was used to observe the morphological appearance of NLC. Cryo-TEM images of the NLC samples are presented in **Figure 3-8**. A spherical shape was observed, and the particle size was almost in agreement with the DLS results. Interestingly, a crystal-like structure was found in most NLC particles, particularly in the solid lipid CP-enriched samples. The higher the concentration of CP, the more the number of crystals that appeared. Notably, a multi-lamellar structure was frequently observed in the sample enriched with CP (NLC 1), as shown in **Figure 3-8 (a)**. As the solid lipid CP indicates the lipid rigidity, this phenomenon of multi-lamellar structure is in line with a previous study reporting that multi-lamellarity may occur simultaneously with membrane rigidity.(Eygeris et al., 2020)

FFT analysis was performed to analyze the distance between the lamellar structures on a selected multi-lamellar area. The results of signal processing are displayed in **Figure 3-9 (b)**. The spots correspond to the high frequency of the repeated signal, and then by inverting the FFT of the selected spot, the inverse FFT image was generated (**Figure 3-8 (c)**). This image makes the distance calculation much easier, particularly because the distance can be calculated using the plot profile, as shown in **Figure 3-8 (d)**.

(b)

The average distance between the multi-lamellar planes was approximately 4.375 nm. This length was most likely correlated with the size of two CP molecules that formed the multi-lamellar structure.

On the other hand, NLC 2 and NLC 3 samples with a lower CP concentration displayed a faceted surface, demonstrating a two-dimensional crystal structure (**Figure 3-8 (b) & (c)**). Owing to the high concentration of liquid lipids in NLC 2 and NLC 3, the crystals could move freely and disturb the spherical structure of NLC and resulting in a faceted structure.

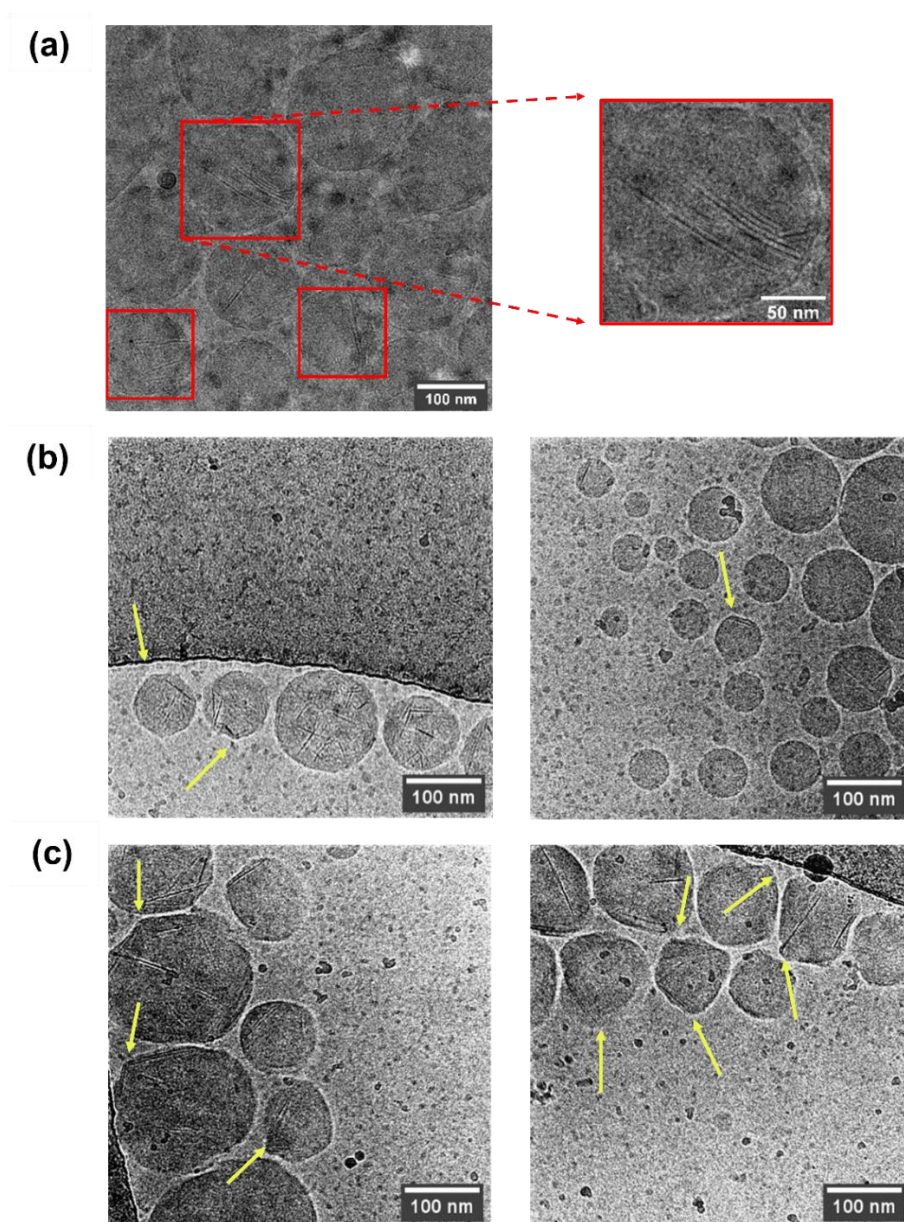


Figure 3- 8 Cryo-TEM image of NLC 1 (a), NLC 2 (b), NLC 3 (c). The sample concentration was 100 mM. *Yellow arrows* indicate the faceted structure of NLC.

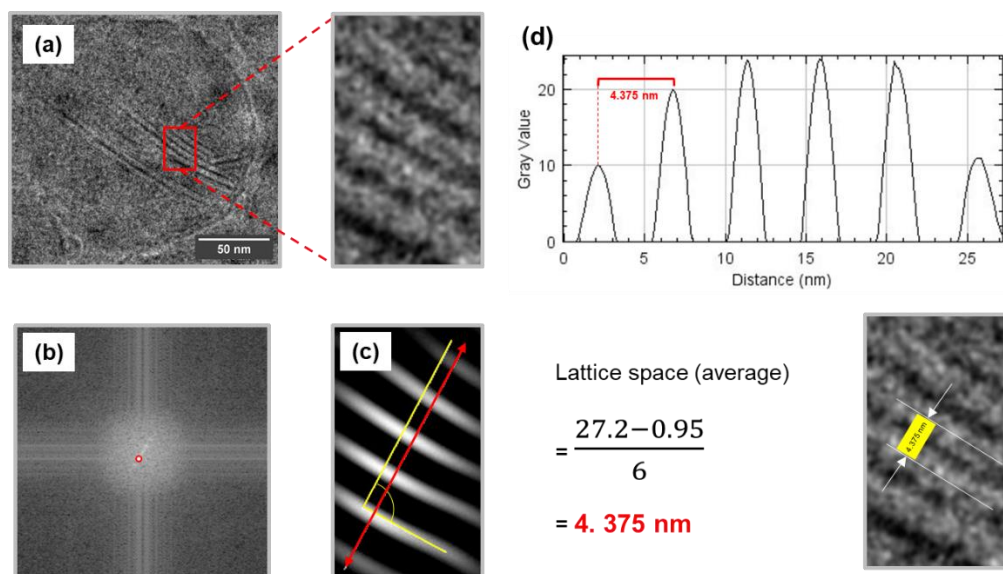


Figure 3- 9 Fast Fourier Transform (FFT) analysis. Cryo-TEM image of NLC 1 particle with multi-lamellar structure (a), magnified FFT image (b), inverse FFT image (c), plot profile of inverse FFT (d).

3.4 Thermodynamic Behavior

DSC analysis was performed systematically to understand the crystal polymorphism of the solid component (CP) in each NLC system. CP has been reported to have two different crystalline forms: (1) a metastable α -form with a low melting point and (2) a stable β -form with a high melting point. (Saupe et al., 2005) In a previous study, the primary matrix constituents of SLNs (CP and triglycerides) showed a complex polymorphic behavior with three basic polymorphic forms of crystal α , β' , and β . (Müller et al., 2000) The CP-including SLNs showed that CP content was related to the crystallinity with complex polymorphic matrix or β' -modification. (Chantaburanan et al., 2017; Ruktanonchai et al., 2008)

First, single component was evaluated (**Figure 3-10**), followed by the binary mixture. Only CP exhibited a melting peak ($T_m = 53.53^\circ\text{C}$), indicating a melting peak of β -modification of the crystal, (Müller et al., 2000) whereas CaTG and T80 appeared as pure liquid phases without any melting peaks. Additionally, the binary mixtures of NLC constituents CP:T80 (75:25) and CP:CaTG (50:50) were prepared using the same preparation procedures as for the NLC samples. The results are shown in **Figures 3-11 (a) & (b)**. Both binary systems showed more than two melting peaks, indicating incomplete crystallization of CP a mixing with other components. The melting peaks showed broaden peaks corresponding to the transition of the CP crystal structure rich in

the β -form to the structure including the β' -form or α -form after mixing with T80 or CaTG. Considering a narrow size distribution of NLCs, it is suggested that CP molecules in a NLC particle could take a multiple crystal state.

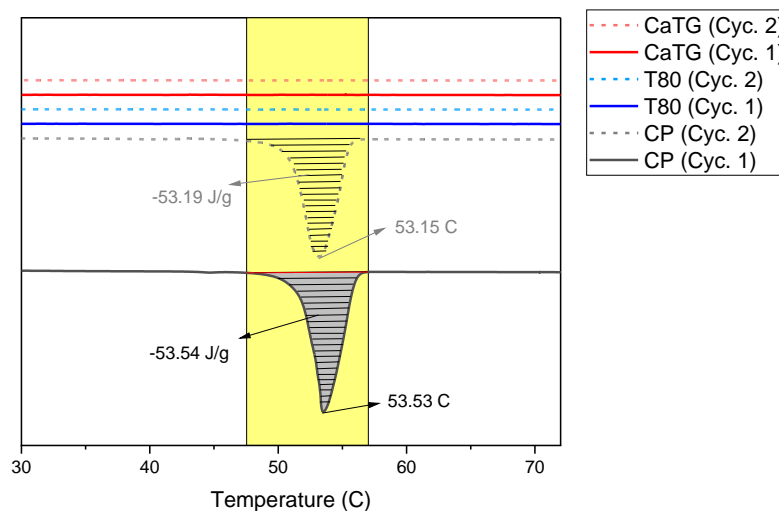


Figure 3- 10 DSC curve of single component

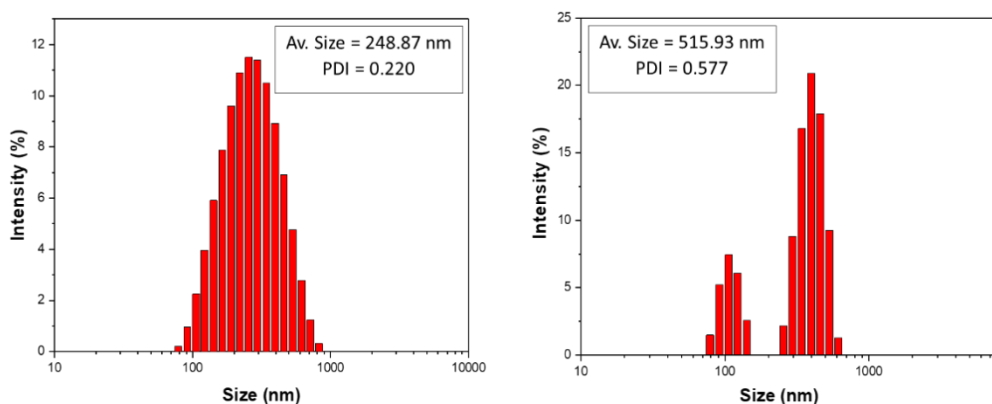


Figure 3- 11 Size distribution of binary mixture, CP:T80 (75:25) (a) and CP:CaTG (50:50) (b)

Additionally, DLS measurements were performed to comprehensively understand the nature of the binary mixtures. The results are shown in **Figures 3-11 (a) & (b)**. The CP:T80 binary mixture demonstrated a moderate particle size distribution (several hundred nanometers) with a small aggregation peak commonly occurring in the lipid nanoparticle system. In contrast, the CP:CaTG system resulted in two peaks with a high PDI (> 0.5), indicating particle heterogeneity. This difference emphasizes the essential role of the surfactant T80, which could be incorporated with CP, with less impact on the

β -form crystallinity. Without the addition of T80, the binary mixture CP:CaTG was separated immediately after the homogenization process ended, and resulting in a highly heterogeneous particles consisting of solid aggregates of CP with mainly β -form crystallinity or some oil droplets consisting of CaTG with β' -modification of CP. These results also supported the core-shell structure of NLCs having a solid CP:T80 matrix at the surface region and a loosely packed CP:CaTG matrix in the core-side region.

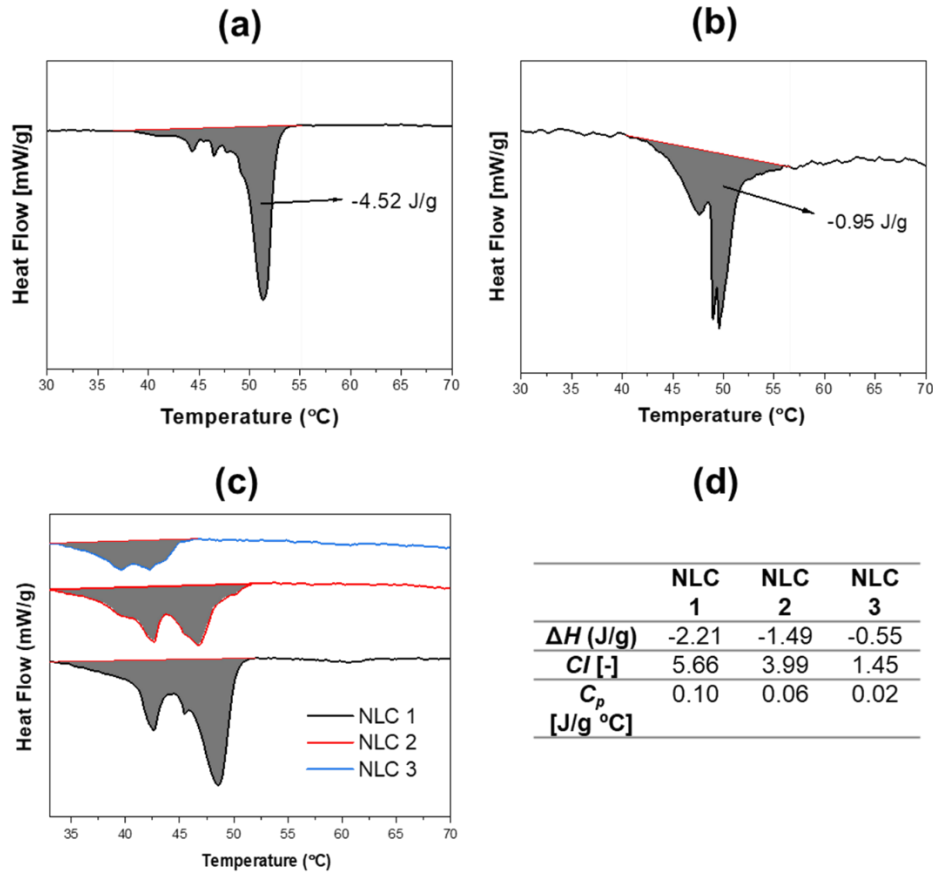


Figure 3- 12 DSC results of CP:T80 (25:75) binary mixture (a); CP:CaTG (50:50) binary mixture (b); DSC result of NLC system (c); Summary of ΔH of each sample (d).

Similar to the binary system, the presence of polymorphic forms of CP in the NLC ternary system was also suggested by the bimodal DSC peaks (**Figure 3-12 (c)**). All NLC samples exhibited broader multi-peaks with lower melting temperatures than T_m of pure CP in β -form ($T_m = 53.53$ °C). Similar results were shown in a previous study; the addition of triglycerides to the CP-matrix disturbed the inner structure of the lipid to form a less ordered structure. Therefore, the melting temperature and enthalpy were decreased.(Chantaburanan et al., 2017) This is consistent with the DPH anisotropy result (**Figure 3-5**) that the liquid lipid decreased the rigidity of NLC. The decrease in the

packing of the crystal structure as a result of the increase in liquid triglycerides in NLC was also supported by the decrease in the transition energy (ΔH), crystallinity index (CI), and specific heat capacity (C_p) (**Figure 3-12 (d)**). This phenomenon has also been reported in other studies, (M. Huang et al., 2017; Li et al., 2022) which indicated that the α and β' -forms are more susceptible to structural transition of NLCs containing high amount of liquid lipids.

3.5 Crystal Behavior

To better understand the transition of the crystal structure of NLCs with respect to lipid composition, XRD analysis was performed. The results are displayed in **Figure 3-13**. The sample showed peaks at different angles ($2-\theta$), indicating the presence of crystal structure. Multiple sharp peaks with greater intensity were observed for NLC 1 than for the other two NLC compositions. In contrast, the intensity of the sharp peaks was significantly reduced in NLC 2 and NLC 3, supporting the hypothesis that the crystal structure was originated from the solidified CP (additional references were provided in **Table 3-1** as the comparison of XRD spectra of pure CP). These results suggested that incorporation of the liquid lipid CaTG in NLC led to a less-ordered crystal structure. Two small peaks at $2-\theta = 8.98$ and 13.52 in sample NLC 1 were not observed in NLC 2 and NLC 3; the difference in peaks might correspond to the multi-lamellarity of the crystal structure in NLC 1, which were not observed in NLC 2 and NLC 3, as shown by the cryo-TEM results. The peak intensity was significantly decreased in the samples NLC 2 and NLC 3, indicating that the multi-lamellar structure could only occur in the CP-enriched NLC. Considering the other peak areas (amorphous area), the higher the concentration of liquid lipid in the NLC system, the more amorphous the structure is formed.

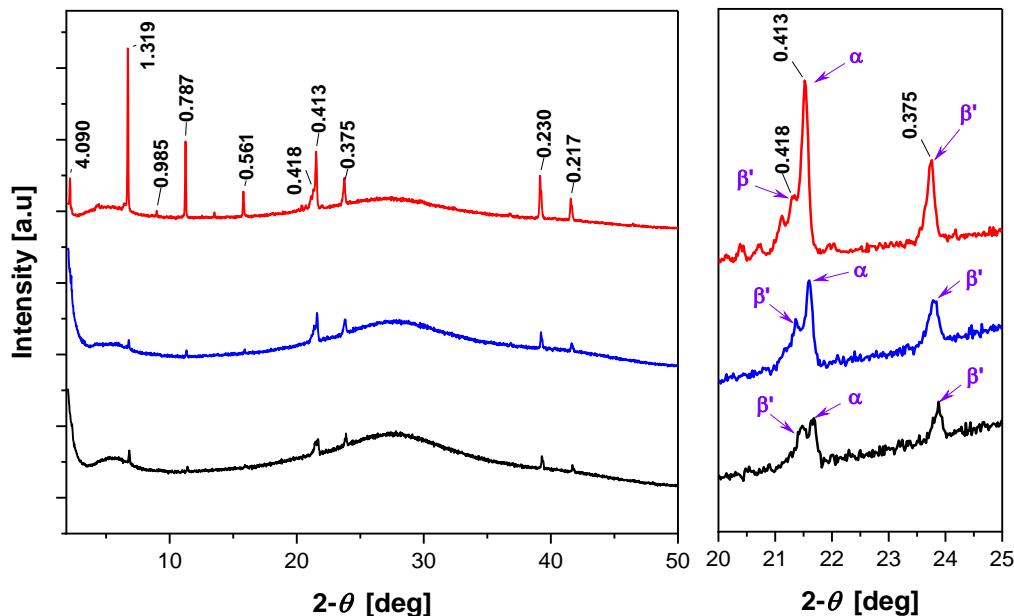


Figure 3- 13 X-Ray Diffraction of different NLC composition, NLC 1 (red); NLC 2 (blue), NLC 3 (black). The label defines the d -spacing in nanometers.

Table 3- 1 Assignment of XRD peaks of CP

2-theta [deg]	NLC Sample [nm]	Cetyl Palmitate		
		source 1 Kim, et al, 2019)	source 2 (Castro et al, 2021) [nm]	source 3 (Pornputtipitak et al., 2019) [nm]
1	2.12	Similar peaks No info.	oor	~4.5
2	6.7		~6.9	~6.7
3	8.98		-	~8.9
4	11.24		~11.2	~11
5	15.8		~16	~13
6	21.32		~21	-
7	21.52		~21.5	~21
8	23.72		~23.5	~23
9	39.14		~39	~38
10	41.56		~42	oor

Further, the XRD peaks matched with the previous reports on crystallinity of CP.(Chantaburanan et al., 2017; Ruktanonchai et al., 2008; Saupe et al., 2005) CP exhibits an orthorhombic sub-cell (β' -modification) in XRD patterns with a spacing of 0.38 and 0.42 nm. The XRD peaks of the NLC samples corresponded to the reference peaks, indicating that NLC contained β' -modification of CP. Furthermore, the peak intensity at 0.375 nm and 0.418 nm decreased with increasing liquid lipid content. In previous study, the peak intensity at d -spacing equal to 0.38 nm and 0.42 nm decreased with increasing

triglycerides content, and it was concluded that the increase in triglycerides in SLN led to a less-ordered structure. The results of NLCs are similar to the previous findings, indicating that increase in liquid lipid could modify the lipid matrix considerably to form a less-ordered structure.

4. Discussion

In the present study, NLC internal structure have been characterized. The result revealed the unique core-shell structure as well as the presence of crystal-like lamellar structure. Some possible mechanisms could be occurred during the core-shell and crystal formation. A more comprehensive explanation would be discussed in this section.

4.1 Properties of Crystal

The detail of crystal-like structures was investigated in cryo-TEM image (**Figure 3-8, 3-9**), DSC (**Figure 3-12**), and XRD results (**Figure 3-13**). As reported in a previous study, the existence of crystals depends on the presence of solid lipids in lipid-based nanoparticles.(Haider et al., 2020; Ruktanonchai et al., 2008)

Based on the FFT analysis of the cryo-TEM images, the average distance between the planes was approximately 4.375 nm (**Figure 3-9**). Although there is a difference between the values due to uncertainties of the electron microscopic determination and XRD measurement, the distance seems to be in reasonable agreement with the XRD peak at $2-\theta = 2.12$ that corresponds to the d -spacing of 4.090 nm (the first peak of NLC 1, **Figure 3-13**). The peaks at $2-\theta = 2.12$ indicates that NLC 1 has a sharper peak corresponding to the β -form, whereas NLC 2 and NLC 3 have broader peaks, corresponding to the polymorphism of CP (α and β' -form). A stack (multi-lamellar) structure with a distance of approximately 4.5 nm has been reported to have a strong relationship with the β -form having a higher melting temperature (T_m) and sharper XRD peak.(Bunjjes et al., 2007) The distance might correspond to the acyl chain of the solid lipid tristearin (C_{18}) used in that study; this findings strengthens that the multi-lamellar structure in NLCs was originated from CP having C_{16} in the acyl chain, and has a fairly good agreement with the distance resulted from cryo-TEM (approximately 4.3 nm).

Furthermore, NLCs showed additional XRD peaks at 0.413 nm, corresponding to the different polymorph (α -modification). (Lavigne et al., 1993; Oehlke et al., 2017) This finding corresponded to the DSC results that NLCs included at least two polymorphism of crystalline CP (α and β' , **Figure 3-12 (c)**) in each particle. The co-existence of different lipid polymorphs was observed dependent on processing factors such as agitation or the presence of an emulsifier. (Rousseau et al., 2005) The multiple polymorphs found in NLCs could be the result of different miscibility of CP with T80 or CaTG, as revealed by the DSC results of the binary compositions (**Figure 3-12 (a) & (b)**). T80 maintains the stable β' -form of the CP crystal; however, CaTG transforms CP crystals to be rich in an unstable α -form. Since T80 is a surfactant that can emulsify the lipid particles, the mixed fraction of T80 and CP may be located on the surface of the particles. This assumption supports the hypothesis of the core-shell structure of NLCs, the consisting of the solid outer core (T80 and CP) and the loosely packed inner core (CaTG and CP).

4.2 Effect of Lipid Composition

According to the results, lipid composition seems to have a significant effect on the core properties of NLC. Therefore, some parameters were selected from the obtained data to better understand the role of the lipid concentration ratio: (i) Anisotropy gap (r_{gap}) is the rigidity difference between $\text{DPH}_{\text{before}}$ and $\text{DPH}_{\text{after}}$. This parameter could represent the existence of the core-shell structure of NLC. The greater the anisotropy gap, the greater the difference in rigidity at the surface and core of the particles; therefore, it indirectly indicates a higher shell fraction of NLCs. (ii) The enthalpy of the transition process (ΔH) is the energy required for the NLC crystal to melt, and it was measured by DSC analysis in our study. This parameter was determined by calculating the transition area of the DSC peak. The higher the ΔH , the higher the number of crystals in the particle; therefore, this parameter could also indicate the solid fraction of the NLC particles. (iii) Crystallinity is the percentage of crystal peak to the total area (crystalline and amorphous) in the XRD results. This parameter directly reflects the number of crystals and increase in the amorphous fraction contributes to the decrease in crystallinity. Hence, this is strongly correlated with the transition enthalpy ΔH .

The effect of the lipid concentration ratio on the selected parameters was further analyzed. Interestingly, a linear correlation was observed between the solid lipid (CP) to

total lipid ratio and the selected parameters when plotted in the graph (**Figure 3-14 (a)**). Although there are only three lipid concentration ratios (solid lipid to total lipid ratio) in our study, the graph could be sufficient to demonstrate the relationship between lipid composition and the observed parameters. In addition, based on different cryo-TEM images of different NLCs, the solid lipid composition influenced not only the above parameters but also the morphology of NLC. As was mentioned in a previous study, solid lipid aggregates formed various crystalline facets at the interface by interacting with the surrounding water, and with the addition of surfactant, lipids at the outer shell formed highly ordered crystalline facets compared to the solid aggregate due to surfactant incorporation (Pink et al., 2019). Hypothetically, these parameters could be controlled by adjusting the solid lipid ratio to obtain the desired NLC properties. For example, for application of topical drug delivery systems, a more rigid carrier can prolong the drug release because it gets deposited on skin surface instead of penetrating through the skin layer; in contrast, the fluid vesicles are preferable for dermal or transdermal diffusion.

4.3 Structure of NLCs

A hypothetical structure was proposed to summarize the influence of the lipid concentration ratio on the NLC properties based on the characterization results (**Figure 3-14 (b)**).

NLC 1 with solid lipid concentration greater than liquid lipid concentration had a spherical core-shell shape, containing multilamellar-like crystal structure (a stacked lamellar/ stripe pattern observed in the cryo-TEM image), and overall high rigidity. On the other hand, NLC 2 ([solid lipid] = [liquid lipid]) and NLC 3 ([solid lipid] < [liquid lipid]) resulted in a faceted structure (irregular spherical structure) with a single-lamellar/ stripe structure, owing to the less rigidity of higher concentration of liquid lipid. NLC 2 and NLC 3 formulations also displayed a core-shell form identical to NLC 1; however, the anisotropy difference between the core and shell was lower than that of NLC 1.

According to a previous study, the NLC internal structure was classified into three types: multiple types, imperfect type, and amorphous type. (Chauhan et al., 2020; Tamjidi et al., 2013; van Tran et al., 2019) The NLC core-shell structure obtained in this study presumably might belong to the multiple types; with some oil compartments inside the core. This result is supported by the DPH_{before} and DPH_{after} results, where the DPH added

during preparation may be located in the oil compartment. However, imperfect crystals, amorphous structure, and oil compartments could not be differentiated in the cryo-TEM images; therefore, the structure of NLC in this study might be either of the multiple type or imperfect type with the shell at the outer phase (or intermediate between multiple and imperfect types).

The core-shell structure of NLCs in this study has a high potential for sustained drug release. Chantaburanan *et al.* reported that hydrophobic drug molecules such as ibuprofen were dissolved in the liquid lipid phase in SLN composed of CP and triglycerides, and such a partition to the inner structure of the lipid matrix with a solid shell slows the ibuprofen release rate.(Chantaburanan et al., 2017) Furthermore, CP dependence of morphological structure implies the ability to control its release rate or stabilities by tuning the lipid composition, which could be useful index for the future studies.

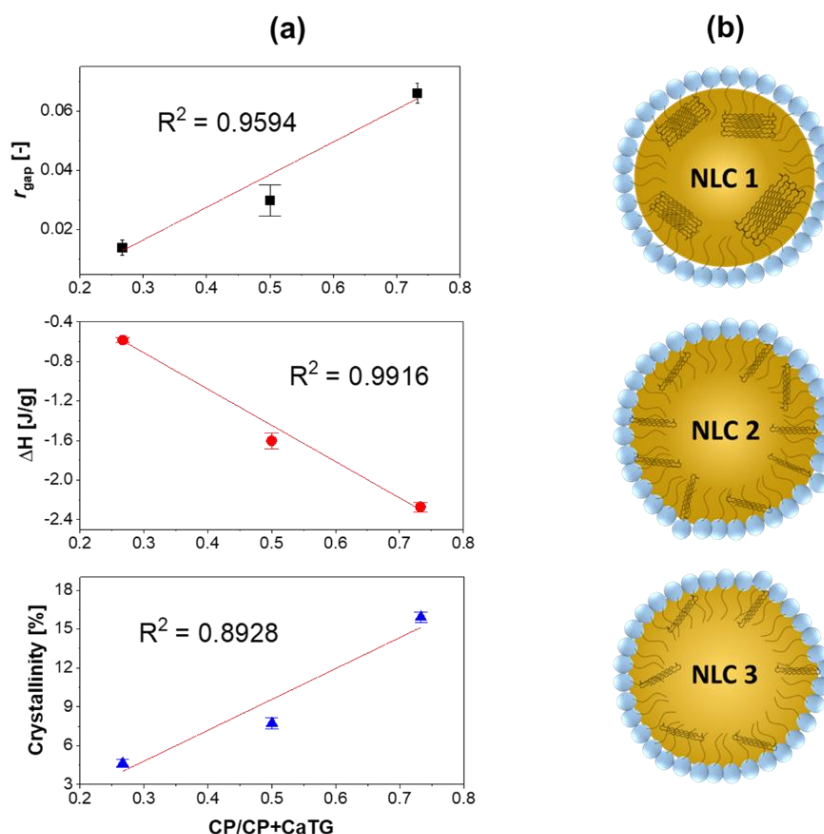


Figure 3- 14 Correlation between the solid lipid to total lipid ratio and the observed parameters (a). Hypothetical structures of NLC with different lipid concentration ratios (b). Error bar represents the standard deviations ($n=3$)

4.4 Long-term Stability of NLC

The present study has excellently demonstrated NLC's superiority in terms of high storage stability; the NLC particles could maintain their size and distribution during six months of storage at refrigerated temperatures (**Figure 3-3**). The high thermo-stability of NLC agrees with other studies that have reported stability for even longer storage duration (Guilherme et al., 2019; Gerhardt et al., 2022). This predominance allows NLCs to be employed as a carrier platform for various targets, particularly thermo-sensitive delivery targets. The storage and distribution of mRNA-based vaccines remains the main challenge. The well-known Pfizer and Moderna COVID-19 vaccines entail delivery and storage at -80 °C and -20 °C, respectively (Uddin & Roni, 2021). Thus, these vaccines are difficult to handle during transportation and challenging in areas with limited resources. Before being administered, the vaccine is thawed and stored in a refrigerator for a limited period of time. Hence, by utilizing the higher thermo-stability feature of NLCs, the product can be stored for a longer time; this feature might also helpful during the distribution and before administration. Although further structural modifications are required to deliver an mRNA vaccine, the high thermo-stability of NLCs could be extremely important in future applications.

5. Strategy of Designing NLCs

NLCs are one of promising delivery platforms for biomolecules. The combination of solid lipid and liquid lipid leads to form a unique properties of lipid matrix that could be essential in the field of drug delivery system, such as the protection of the incorporated drugs from chemical degradation, controlled drug release, improvement of the drug absorption that resulted in a good bioavailability. NLCs have a benefit on its physical stability that demonstrated by the stable particle size and PDI during storage.

In NLC fabrication, some factors need to be considered such as mechanical methodologies and lipid selection/composition, which have effects on the physicochemical properties of NLCs. For instance, a certain condition of ultrasonication can enhance the emulsifying and foaming capacity, and/or reduce the aggregation size which resulted a smaller particle size and long-term stability (Shanshan et al., 2021). Surfactant selection is also essential related to the safety and dispersive stability.

Particularly in the NLC system, the properties of the lipid matrix are highly affected by the lipid composition. Because NLC consists of two different lipids with distinct properties, the resulted lipid matrix and properties as well as the performance of the cargo platforms could be also varied depending on its composition. Feng and coworkers investigated the influence of various oil composition on the transformation, bio accessibility, and intestinal absorption of curcumin in NLCs. The results demonstrated that 20% MCT (liquid oil) has the highest curcumin bioavailability. Their results also implied the importance of lipid composition in the GIT route (Feng et al., 2020).

Based on our previous study, lipid composition plays an essential role in determining the assembly state and the constructed morphology and internal structure, including shape and crystal structure. According to the results of chapter 2, the assembly state of the outer core of NLCs that were resulted by different lipid and surfactant composition could be determined by the results of the fluidity ($1/P$) and polarity (GP_{340}). There are three states of the obtained particles: SLN (solid-lipid nanoparticles), micelles, and oil-in-water emulsions.

In chapter 3, the formation and internal structure of NLCs was studied. The unique core-shell structure was found and become an important feature of NLCs. Additionally, different crystal structure is found to have dependency on the lipid composition. Anisotropy gap, enthalpy difference, and crystallinity were selected as the critical parameters in the NLC internal structure determination.

In the strategy for NLC development, the appropriate selection of the NLC compositions is essential based on the characterization analysis such as the particle size, PDI, fluidity ($1/P$), polarity (GP_{340}), crystallinity and structure. Herein, the design scheme of the preparation of NLCs for DDS is provided as shown in **Figure 3-15**.

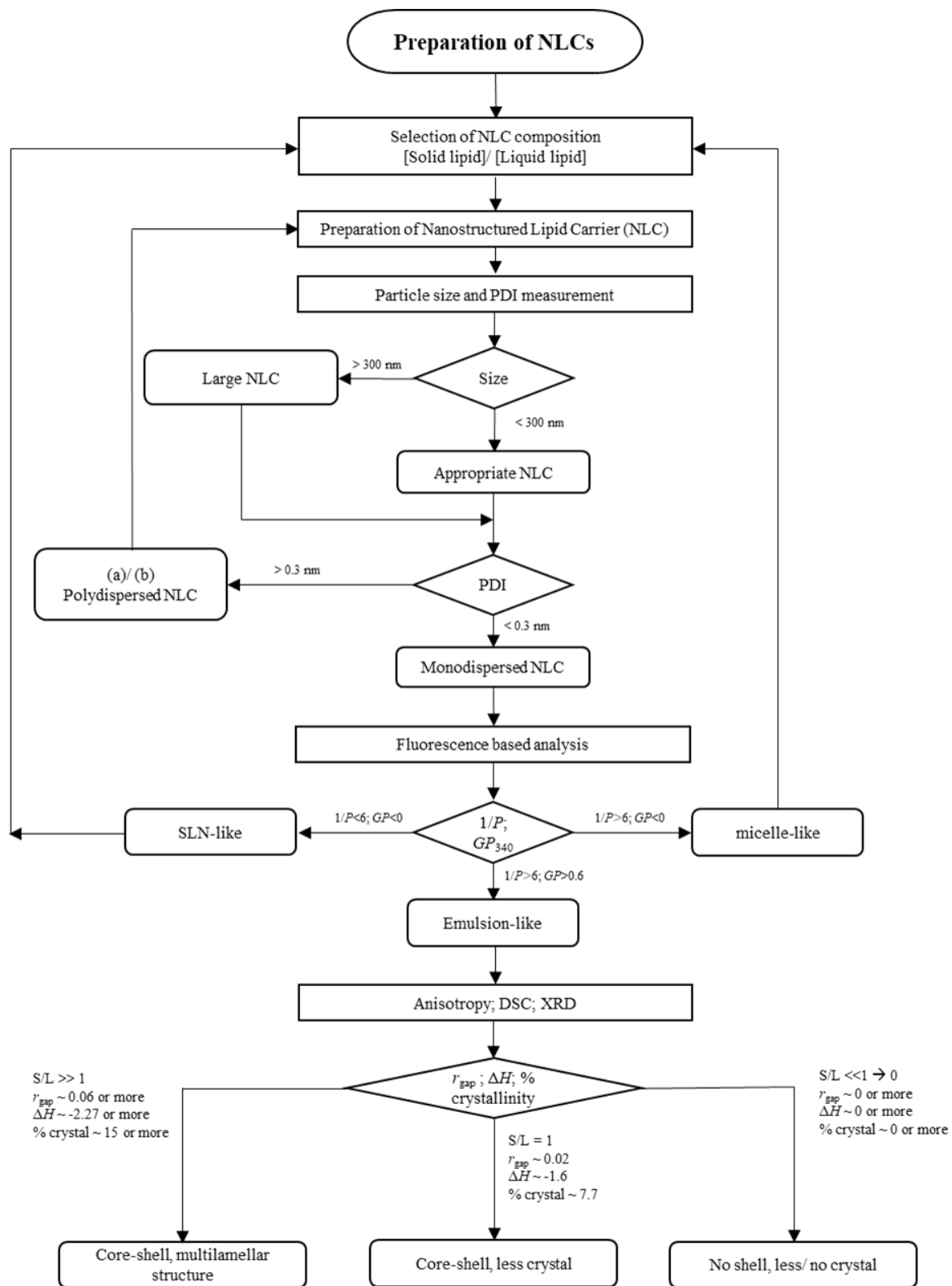


Figure 3- 15 Design scheme for NLCs for Nanocarriers Preparation

6. Summary

Comprehensive molecular and physicochemical characterizations were performed to reveal the internal structure of NLC. Based on particle size and PDI, all NLC formulations were monodispersed solutions with particle size < 230 nm, which is suitable for drug delivery applications. NLCs showed high stability during six months of storage, and this feature can be potentially employed for the future applications. Furthermore, we applied a new methodology of fluorescence anisotropy using DPH to analyze the inner and outer core of NLC's anisotropy. Based on the result, NLC represented a core-shell structure with higher rigidity of the outer core than that of the inner core. The DSC results also revealed this phase heterogeneity, which was derived from different polymorphs of the solid lipid crystals and suggested that the lipid composition could alter the NLC phase. According to the morphological study, NLCs with low solid lipid concentration demonstrated a spherical shape with a faceted structure. Almost all the captured particles had a crystal-like lamellar structure, as confirmed by the XRD peaks. However, the multi-lamellar structure was observed only in the solid lipid-enriched sample. In summary, a linear correlation was seen between the solid lipid concentration to total lipid concentration ratio and the selected parameters (r_{gap} , ΔH , and crystallinity %), indicating that the lipid composition could be altered to adjust these parameters. This study helped to understand how the internal structure and properties of NLC change under various solid and liquid lipid concentrations.

One important finding of this study is the unique core-shell structure of the NLC system and its dependence on the lipid composition; this feature can be applied in designing specific NLC carriers for various products, such as drugs, food, cosmetics, and vaccines. Overall, insight into the detailed NLC internal structure improves our understanding of the microscopic structure and properties of NLC. Based on the characterized scheme of NLCs, the composition of NLCs to encapsulate some biomolecules can be optimized, focusing on the loading performance with its appropriate quality. In the following chapters, the present strategy was applied to the encapsulation of biomolecules into NLCs by selecting polyphenols and tRNA as case studies of small and large biomolecules.

Chapter 4

Characterization of Entrapment Behaviour of Polyphenols in Nanostructured Lipid Carriers and Its Effect on Their Antioxidative Activity

1. Introduction

Antioxidants, as primary or secondary metabolites and as natural or synthetic compounds, are essential in protecting and maintaining human health. As for the mechanisms of their action in inhibiting free radicals, the active antioxidants provide numerous favorable features to various products (Arias et al., 2022; Khalil et al., 2020; Parcheta et al., 2021). In the current decade, the growing interest in antioxidants in food, drugs, and beauty products has been extensively reported (Lv et al., 2022; Tain & Hsu, 2022; Tran et al., 2019; Truong & Jeong, 2022); however, many problems were found to be related to the application of these compounds, such as the degradation caused by the stress condition (pH, light, temperature, and oxidation) (Ioannou et al., 2020; Kawabata et al., 2019; Luana Carvalho de Queiroz et al., 2022; ZAPATA et al., 2022), the quality loss regarding the activity and effectiveness during storage (Ali et al., 2018; Tavares et al., 2020), and the poor water-solubility that leads low bioavailability (Liu et al., 2020; Yang et al., 2020).

One of the promising strategies to overcome those limitations is the utilization of lipid nanocarriers. The hydrophobic environment of nano-size and high stability in the lipid nanocarrier contributes significantly to the antioxidant delivery process, especially for the highly hydrophobic antioxidants (Mitchell et al., 2021). Incorporation of antioxidant compounds into lipid carriers have been reported to have a good performance in some administration routes, such as via skin and oral administration. In the skin application, the lipid nanocarrier could enhance the penetrating abilities of the targeted drug (N. K. Garg et al., 2021; Mendes et al., 2017), while other studies reported an improvement in stability and bioactivity (Netto MPharm & Jose, 2018). Another benefit is the enhancement of solubility of lipophilic antioxidants due to the presence of the lipid. The antioxidants will be wholly distributed throughout the carrier and enhance the

permeation through the skin (Aditya et al., 2013). Additionally, lipid nanocarrier application in oral administrations could improve the *in vivo* performance of highly lipophilic drugs by enhancing the solubility (Khan et al., 2015; Cirri et al., 2018). Some studies also report the advantages of using lipid nanocarriers in medicinal applications, such as enhancing cellular uptake, improving the drug release profile, and maintaining stability (Güney et al., 2014; Vijayakumar et al., 2017).

Among various lipid nanoparticles, the nanostructured lipid carrier (NLC) is one of the most potent vehicles in drug delivery systems. It combines features of its precursors, solid lipid nanoparticles (SLN), and nanoemulsion. By utilizing both solid lipids and liquid lipids as the core components, the structure of the lipid matrix has been reported to have a more flexible condition that could enhance the capacity and protect the target drug simultaneously (R. H. Müller et al., 2002; Haider et al., 2020). NLCs have shown high performance in the antioxidant delivery system, such as increasing bioavailability, stability, and antioxidant capacity (Aditya et al., 2013; S. Khan et al., 2015b; Rodriguez-Ruiz et al., 2018b). Many studies have also been conducted to evaluate the NLC performance in encapsulating some specific antioxidants, such as curcumin (Aditya et al., 2013; Saedi et al., 2018), resveratrol (Soldati et al., 2018), quercetin (Huang et al., 2017; Sun et al., 2014b), astaxanthin (Rodriguez-Ruiz et al., 2018b), and others extracted from natural resources (Azmi et al., 2020; Gonçalves et al., 2021; Saejung et al., 2021). Most of the studies showed a positive result of NLCs in drug delivery performance. However, a more fundamental understanding of how the antioxidant molecules is incorporated with NLC structure, the possible location where the molecules are being entrapped, and their influences on the loading performance and antioxidant activity have never been discussed.

In this chapter, the stability and performance of loading efficiency and antioxidant activity of the polyphenols loaded NLCs were investigated. In the previous study, NLCs consisted of cetyl palmitate (CP) and caprylic triglycerides (CaTG) as the solid and liquid lipid, while for the stabilizer, polysorbate/ Tween 80 (T80) was studied (**Figure 4-1**). The summary of the effect of NLC composition on the phase behavior and self-assembly properties was successfully presented, and the effects of the composition of the lipid constituents and surfactant concentration on the self-assembly properties, phase state, and molecular structure were successfully studied (Izza et al., 2021). According to the results, three samples with the same concentration of T80 (NLC 1, NLC 2, NLC 3) were selected.

Furthermore, three different lipophilic polyphenols (resveratrol, kaempferol, and quercetin) known as strong antioxidant agents, were also studied for their incorporation into the NLC system as the polyphenol-incorporated NLC (Pol-NLC) (**Figure S1**). Through this investigation, the role of NLC structure and composition in the performance of the antioxidant delivery system should be elaborated. Also, the plausible partition of antioxidant molecules incorporated with NLC will be discussed. The obtained result provides valuable information better to understand the role of NLC as an antioxidant carrier.

Figure 4- 1 NLC structure and composition used in this chapter

Furthermore, three different lipophilic polyphenols (resveratrol, kaempferol, and quercetin) known as strong antioxidant agents, were also studied for their incorporation into the NLC system as the polyphenol-incorporated NLC (Pol-NLC) (**Figure 4-2**). Through this investigation, the role of NLC structure and composition in the performance of the antioxidant delivery system should be elaborated. Also, the plausible partition of antioxidant molecules incorporated with NLC will be discussed. The obtained result provides valuable information better to understand the role of NLC as an antioxidant carrier.

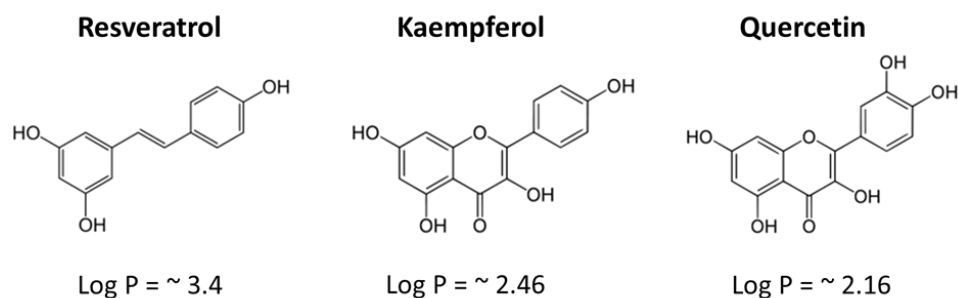


Figure 4- 2 Polyphenol molecules as a drug model were used in this chapter. The Log*P* value is experimentally determined by the partition coefficient of a compound in water and octanol. A negative Log*P* value indicates preferential solubility in water, and a positive value indicates an affinity for octanol. However, in this study, the Log*P* value information refers to the FoodB database (resveratrol ID: *FDB002451*; kaempferol ID: *FDB000633*; quercetin ID: *FDB011904*), which calculated the Log*P* by ChemAxon.

2. Materials and Methods

2.1 Materials

CP was purchased from Tokyo Chemical Industries (Tokyo, Japan), CaTG was purchased from Sigma-Aldrich (St. Louis, MO), and plant-based Tween 80 (T80) was purchased from Fujifilm Wako Pure Chemical Industry (Osaka, Japan). 2,2-Diphenyl-1-picryl-hydrazylhydrate (DPPH) as the free radical agent, and all polyphenols used in this chapter were purchased from Tokyo Chemical Industries (Tokyo, Japan). All other chemicals were purchased from Fujifilm Wako Pure Chemical Industry (Osaka, Japan). All chemicals were used without further purification. Ultrapure water was prepared using Direct-Q® UV3 (Merck Millipore Co., Tokyo, Japan).

2.2 NLC Preparation

The NLC was fabricated using a hot homogenization-ultrasonication method, as reported previously (Guilherme et al., 2019; Izza et al., 2021). Firstly, both lipid components, CP (solid lipid) and CaTG (liquid lipid) were stirred and preheated at 65 °C. At the same time, T80 (surfactant) was prepared separately in a water environment at the same temperature as the lipid component. The total concentration of lipid and surfactant was 100 mM. The detailed information on each sample composition is displayed in **Figure 4-1**. After the solid lipid components were melted and mixed well with the liquid lipid, the solubilized polyphenol (resveratrol, kaempferol, quercetin) in ethanol was added

and stirred again. Then, the T80 solution was added dropwise in the lipid mixture. The stirred-heating process was then continued for 15 minutes before 3 minutes sonication. Power output ultrasound was set by tuning the output dial (no. 4 for this experiment). The polyphenol-incorporated NLC (Pol-NLC) was left for 24 hours at room temperature to stabilize the structure and stored at 4 °C before further analysis. The schematic process of NLC preparation is provided in **Figure 4-3**.

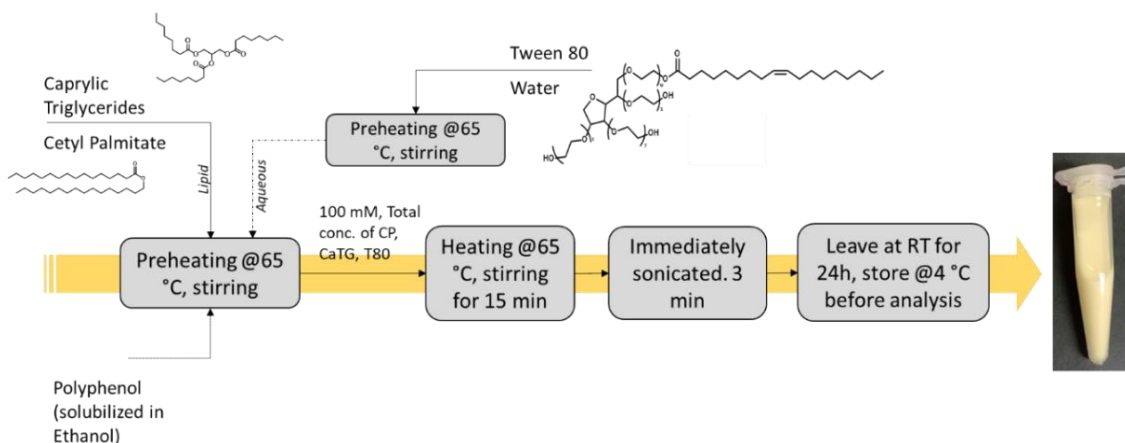


Figure 4- 3 Polyphenol-loaded NLC preparation

2.3 Drug Loading Performance

Prior to analysis, Pol-NLC was centrifuged with an ultra-centrifugation unit (Himac CS100FNX, Hitachi, Japan) at 35000 rpm for one hour to separate the Pol-NLC and untrapped polyphenols (**Figure 4-4**). For the qualitative analysis, 10 µl of the separated Pol-NLC was measured using a confocal Raman microscope (LabRAM HR-800, Horiba Ltd., Kyoto, Japan) with a 532 nm wavelength of exciting laser. Data was accumulated, and the background signals from water were removed to gain the Raman signals. Another signal processing, such as peak searching and smoothing, was conducted with an additional peak analyzer using Origin-Pro 2020 software.

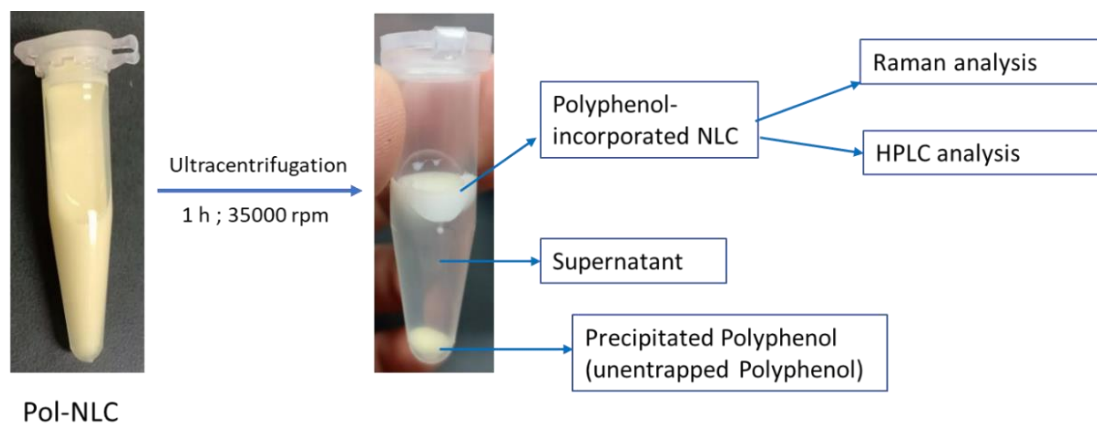


Figure 4- 4 Sample preparation for drug performance analysis (Raman & HPLC analysis)

A high-performance liquid chromatography (HPLC) analysis (Waters 1515 HPLC System, Waters, Milford, MA, USA) equipped with the ODS-3 reverse-phase column (particle diameter: 5 μm , column dimension: 4.6 \times 250 mm) (GL Science Inc., Tokyo, Japan) and UV/Vis detector (Waters 2489, Singapore) was utilized to measure the concentration of the entrapped polyphenols. Before analysis, the centrifugated Pol-NLC was diluted in methanol to dissolve the lipids and the entrapped drugs. The solution was filtered using a cellulose filter (13 mm diameter; 0.22 μm pore size) before being injected into the HPLC apparatus to separate insoluble fractions. The high purity of methanol specified for HPLC was used for the mobile phase at a 1.0 mL/min flow rate. Chromatographic analysis was performed with 25 microliters injection volume at a specific wavelength depending on the maximum UV wavelength of each polyphenol (resveratrol: 305 nm, kaempferol: 365 nm, and quercetin: 364 nm); while the retention time of resveratrol, kaempferol, and quercetin was around 3 min, 6 min, and 4 min, respectively. The concentration of each polyphenol was calculated from the calibration curve (**Figure 4-5**). The entrapment efficiency (EE) was calculated as follows:

$$\% \text{Entrapment Efficiency (EE)} = \frac{\text{Entrapped drug concentration [mM]}}{\text{Initial drug concentration [mM]}} \times 100\% \quad \text{Eq. 4- 1}$$

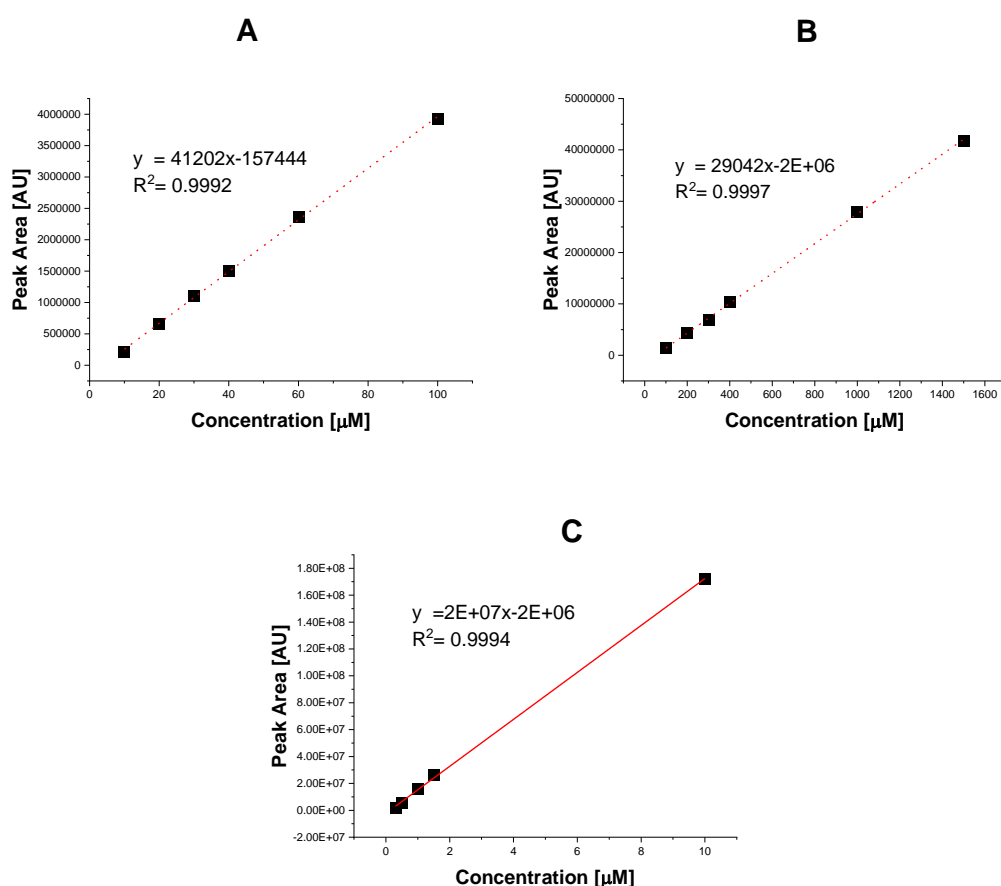


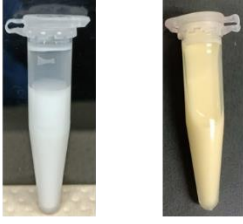
Figure 4- 5 Calibration curve of resveratrol (A); kaempferol (B); quercetin (C). The Peak area is calculated from the assignment peak in HPLC spectra for each compound.

2.4 Antioxidant Activity

The antioxidant activity is expressed by the free radical scavenging ability of Pol-NLC on the DPPH free radical. Firstly, one millimolar of DPPH solution was prepared in ethanol. Then, 50 μ l of this solution was mixed with 1 μ l of Pol-NLC with 949 μ l of water. This mixture was vortexed and incubated in the dark at room temperature (25 °C) for 30 minutes. The absorbance of the mixture was measured using a microplate absorbance spectrophotometer (Bio-Rad, Japan) at 517 nm. The radical scavenging activity was calculated using **Eq. 4-2**.

$$\text{DPPH Radical Scavenging Activity (\%)} = \frac{A_0 - A_1}{A_0} \times 100 \quad \text{Eq. 4- 2}$$

, where A_0 and A_1 are the absorbance of DPPH in the NLC (without polyphenols) and the absorbance of DPPH in Pol-NLC, respectively.



$$\text{Antioxidant Activity (AA) [\%]} = \frac{A_0 - A_1}{A_0} \times 100$$

A_0 = Absorbance of DPPH in blank-NLC
 A_1 = Absorbance of DPPH in Pol-NLC

$$\text{Actual AA} = \frac{[\text{Entrapped}]}{[\text{Initial}]} \times \text{AA [\%]}$$

$$\text{Specific AA [\%/mM]} = \frac{AA_{\text{entrapped}}}{[\text{Entrapped}]}$$

$$AA_{\text{entrapped}} = \frac{AA_{\text{sample}} - AA_{\text{unentrapped}}(1 - [\text{Entrapped}]/[\text{Initial}])}{[\text{Entrapped}]/[\text{Initial}]}$$

$$AA_{\text{unentrapped}} = \frac{AA_{\text{free}}}{[\text{free}]} \times [\text{Unentrapped}]$$

$$\text{Specific AA [\%/mM]} = \frac{1}{[\text{Entrapped}]} \times \frac{AA_{\text{sample}} - AA_{\text{free}} * [\text{Unentrapped}]/[\text{Free}] * (1 - [\text{Entrapped}]/[\text{Initial}])}{[\text{Entrapped}]/[\text{Initial}]}$$

AA_{sample} : Antioxidant activity of the whole Polyphenols in NLC sample

$AA_{\text{entrapped}}$: Antioxidant activity of the entrapped Polyphenols in NLC

$AA_{\text{unentrapped}}$: Antioxidant activity of the unentrapped Polyphenols

AA_{free} : Antioxidant activity of free polyphenols (without NLC)

Figure 4- 6 Definition of Actual AA and Specific AA

2.5 Dynamic Light Scattering

The particle size was analyzed by the dynamic light scattering (DLS) method with Malvern Zetasizer Nano series (Malvern, UK). Before being investigated, the samples were diluted to be 1 mM in ultrapure water and were placed in the measuring-disposable cuvette. The measurement was operated at 25 °C.

3. Results and Discussion

3.1 Particle size distribution and stability

NLCs were successfully prepared with particle sizes ranging between 176-267 nm, as shown in **Figure 4-7 (a)**. Except for resveratrol-incorporated NLC (R-NLC), a slight decrease in particle size could be observed due to decreased solid lipid concentration (NLC 1 to NLC 3). This condition may have occurred due to several reasons, such as the

effect of the solidified CP (solid lipid component) that has an irregular lipid matrix and resulting in larger particle for the sample enriched with CP; or because the original characteristics of CP that has a higher density (volume per unit weight) than CaTG (liquid lipid component). Resveratrol-incorporated NLCs seem to have a larger particle size than the other Pol-NLC and free-NLC. This phenomenon is related to the high hydrophobicity of resveratrol molecules that may cause higher entrapment of resveratrol as well as the particle size. In contrast to SLN, which has only a solid lipid component, NLCs have a smaller particle size due to the dispersion effect of the liquid lipid component (Sakellari et al., 2021; K. W. Wu et al., 2021).

In addition, the size distribution was also analyzed and expressed as polydispersity index (PDI). The lower the PDI value, the more homogeneous the particle size. For DDS application, PDI below 0.3 was reported as acceptable particle size distributions of lipid-based vehicles (Badran, 2014; Danaei et al., 2018). At this PDI value, the dispersion can still be considered as homogeneous in particle size. According to the results (**Figure 4-7 (b)**), all PDI values are less than 0.3, which suggests monodispersion. Although a slight increase could be observed due to liquid lipid addition, the lipid composition seems to have no significant effect on the PDI value.

The stability evaluation was conducted by comparing the fresh and stored samples (two months of storage). In **Figure 4-7 (c)**, the ratios between the parameter of the stored sample and that of the fresh sample are summarized; the sample is not significantly altered after storage if its ratio approaches one. According to the results, the particle size and PDI were not remarkably changed after the storage time. Other studies reported the same stability during storage, resulting in NLC particles being stable even being stored for more than two months (37,42). The use of surfactant played an essential role in particle stability performance (Eh Suk et al., 2020). Inadequate surfactant causes particle coalescence and aggregation, decreasing drug delivery performance (Chauhan et al., 2020; Teeranachaideekul et al., 2007).

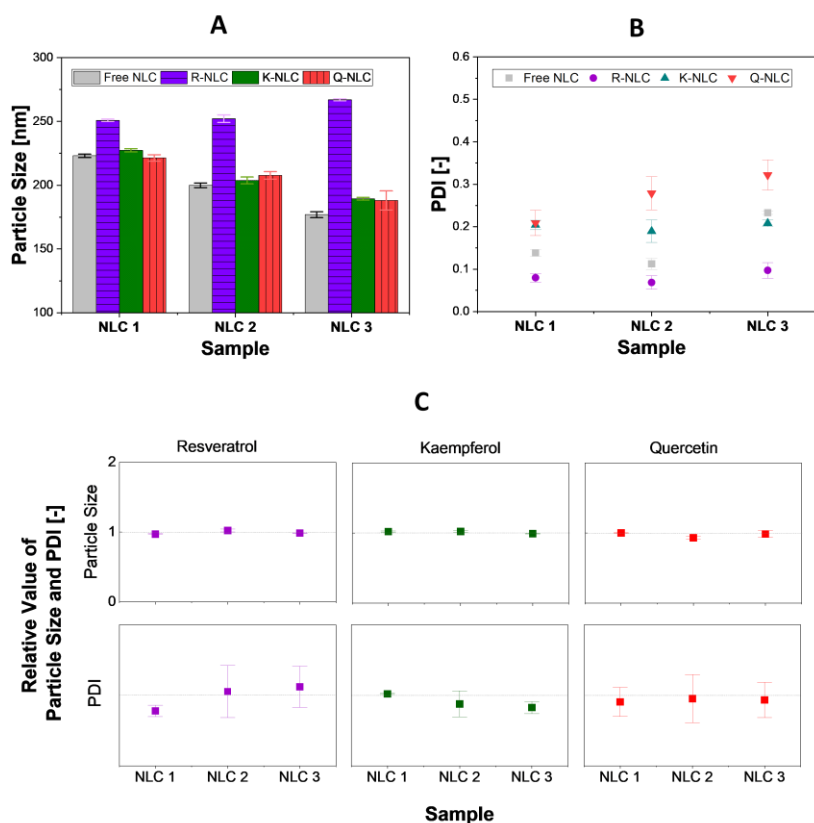


Figure 4- 7 Particle size (A), PDI (B), and stability after 2 months of storage at 4 °C (C). The relative value of particle size and PDI defined as stored NLC sample divided by fresh NLC sample. Error bar represents the standard deviations ($n=3$).

3.2 Drug Loading Performance

Raman spectroscopy was used to analyze qualitatively whether the antioxidant molecules were incorporated with NLCs. Kaempferol-loaded NLC (K-NLC) was selected as the sample representative in this analysis since kaempferol is the intermediate between resveratrol and quercetin in $\text{Log}P$ value, hydrogen bond number, and molecular size. First, the pure kaempferol was tested and compared to the reference spectra from a database (**Figure 4-8**). The result showed identical peaks that ensured the purity of kaempferol. Furthermore, both NLCs with/without kaempferol were investigated, and the results were provided in **Figure 4-9**. The spectra showed relatively great intensity at 2851 cm^{-1} and 2882 cm^{-1} , whose characteristics of the lipid components are assigned to the symmetric and asymmetric vibrational modes of the $-\text{CH}_2-$ group, respectively (Faried et al., 2019; J. Han et al., 2021).

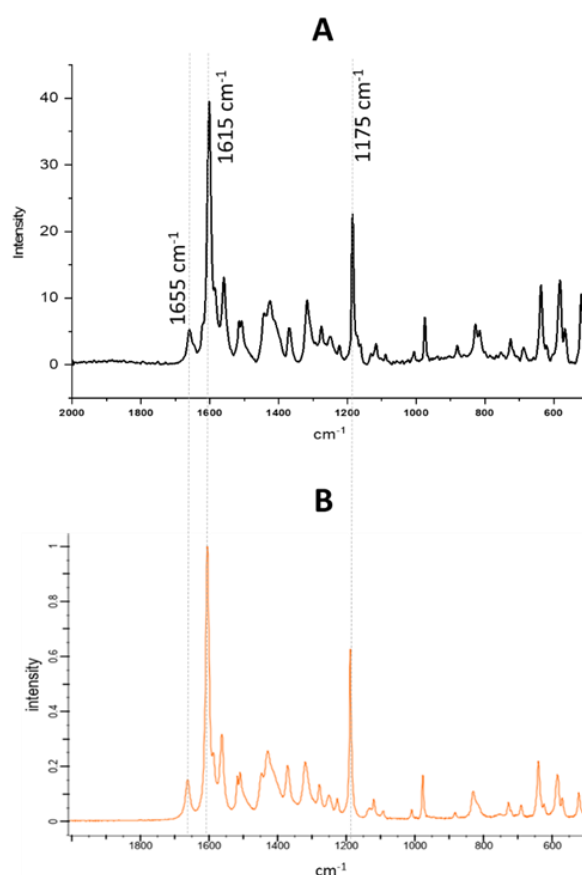


Figure 4- 8 Raman spectra of Kaempferol in this study (A); Kaempferol from Spectra Base (John Wiley & Sons, Inc. SpectraBase) (B)

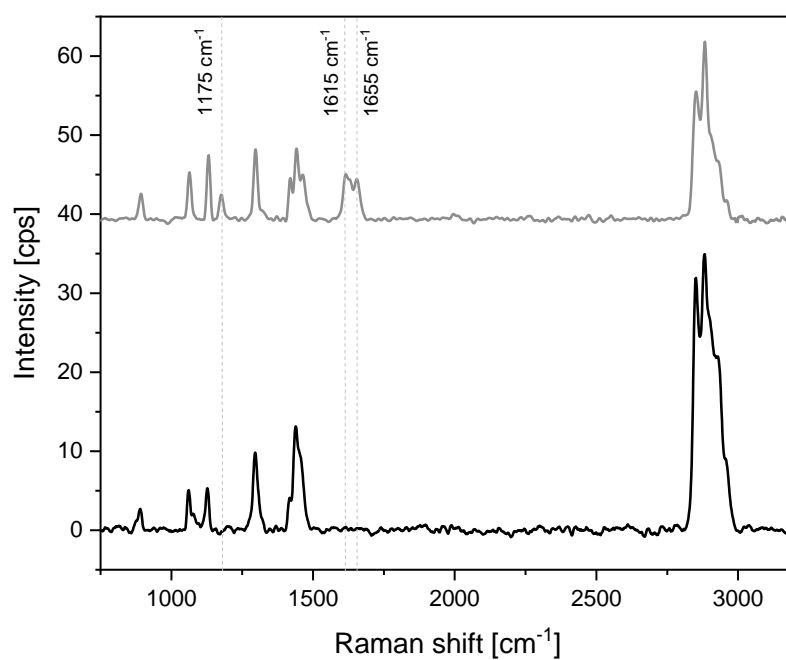


Figure 4- 9 Raman spectrum of Blank-NLC (black) and K-NLC (gray)

The other highlighted peaks are at 1175 cm^{-1} , 1615 cm^{-1} and 1655 cm^{-1} , which can be found only in K-NLC. The peak at $\sim 1600\text{ cm}^{-1}$ corresponds to the $\text{C}=\text{C}_{\text{str}}$ aromatic ring found in the polyphenols observed here. These peaks have also been reported as the characteristics of phenolics compound as the most antioxidant resources (Huguenin et al., 2015; Pompeu et al., 2018). Compared to the pure NLC (**Figure 4-8**), those peaks in K-NLC match the three highest peaks from the pure NLC. With the presence of those phenolic-peak characteristics, incorporation of the antioxidant molecules into the NLC was proven.

The performance of drug loading was evaluated by how much the drug can be entrapped into the NLC system. The entrapment efficiency of each polyphenol was determined by using HPLC analysis with the procedure mentioned above. Prior to the primary analysis, a trial was conducted with eight millimolar resveratrol to determine the initial concentration of the polyphenols (**Figure 4-10**). The result showed that the NLC could entrap $\sim 60\%$ of the initial concentration. Therefore, a five millimolar initial concentration was used for further samples.

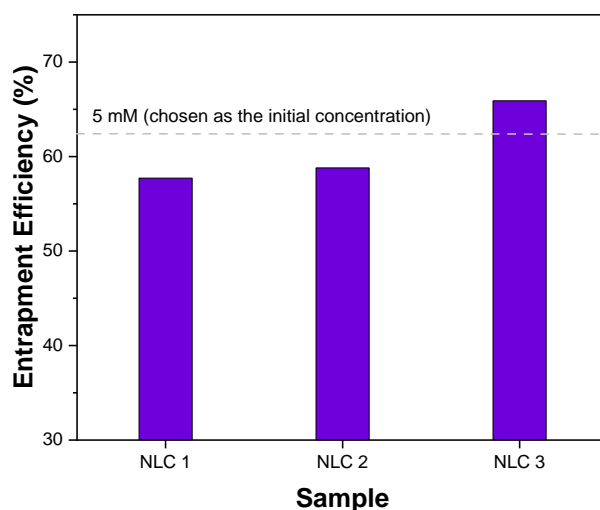


Figure 4- 10 Entrapment efficiency evaluation of resveratrol in NLC with 8 mM initial concentration.

The entrapment efficiency of the NLC is shown in **Figure 4-11**. The result indicated that the NLC could load resveratrol more than the other polyphenols, followed by kaempferol and quercetin. The hydrophobicity of each polyphenol might be the main factor to explain this phenomenon. According to the Log *P* value (**Figure 4-2**), resveratrol

is the most hydrophobic molecule showing lower solubility in an aqueous environment; thus, it can probably penetrate to the deeper location (more hydrophobic environment) of NLCs. The higher entrapment efficiency could also correspond to the solubility of each polyphenol in the lipids and the interior structure of NLCs (Imran et al., 2020).

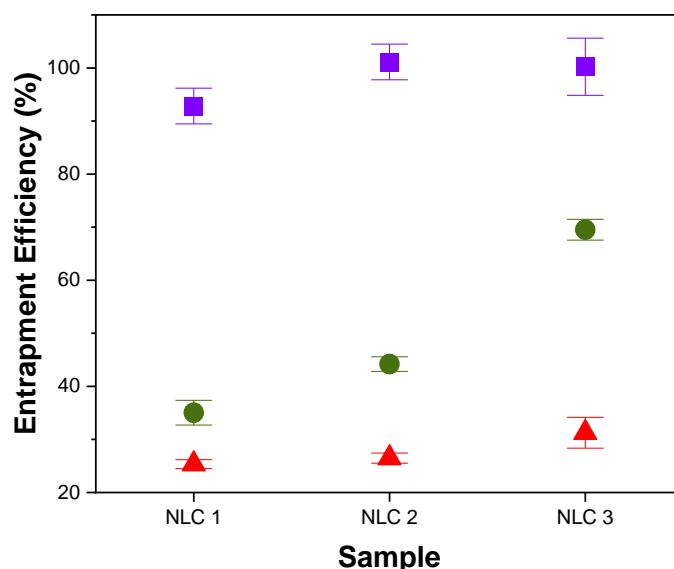


Figure 4- 11 Entrapment Efficiency of Pol-NLC. Resveratrol (purple square); Kaempferol (green sphere); Quercetin (red triangle). The initial concentration of Polyphenol in all samples was 5 mM. Error bar represents the standard deviations ($n=3$).

Furthermore, data in **Figure 4-11** demonstrated that the different compositions of the lipid constituents did not significantly affect the entrapment efficiency of resveratrol and quercetin. In contrast, the addition of liquid lipid could increase the EE of the kaempferol. Since the initial concentration of polyphenols is five millimolar, resveratrol could be loaded even until 100% in the NLC. The amount of the loaded resveratrol could also be higher when its initial concentration is higher, especially in the sample with a higher liquid lipid concentration (NLC 3), as shown in **Figure 4-10**. In addition, quercetin, having the most OH-groups in the molecule, becomes the most hydrophilic compared to kaempferol and resveratrol. Quercetin molecules might be located at the outer shell (interphase) of the NLC and could not penetrate into hydrophobic space at a deeper location. As a result, the quercetin was less entrapped than other phenolics, so the lipid composition did not significantly affect the entrapment efficiency of quercetin.

On the other hand, lipid composition seemed to have a significant effect on the kaempferol loading. The entrapment efficiency increases with the increase of liquid lipid concentration in the NLC system. Regarding its hydrophobicity, kaempferol is the intermediate between resveratrol and quercetin; therefore, the entrapped amount of kaempferol was less than that of resveratrol penetrating a deeper location (hydrophobic environment) than quercetin. By adding more liquid lipid concentration to the NLC, the fluidity inside the core increases (Izza et al., 2021), making it easier to penetrate the deeper location (J. Han et al., 2017). NLC 1 with a higher concentration of CP might have a crystal structure that comes from solidified CP. This crystal-solidified CP might interact with surfactant molecules at the interface. As previously reported, lipids at the interface may form crystalline facets that are more ordered than solid aggregate due to surfactant incorporation (Pink et al., 2019). Therefore, highly packed lipid conditions may inhibit the penetration or incorporation of polyphenol molecules. The result that NLC 3 has higher entrapment efficacy agrees with some previous studies that increasing liquid lipid concentration can enhance the loading performance of NLC (Bhatt et al., 2021; Uprit et al., 2013).

3.3 Antioxidant Activity

The antioxidant activity of Pol-NLC should be expressed as the result of Eq. 2. However, the untrapped polyphenols that might interfere the data were not being separated in the measurement. Therefore, the actual antioxidant activity was calculated in advance by considering the entrapped and untrapped polyphenol, as shown in **Figure 4-6**. The percentage of antioxidant activity generated per unit concentration of each entrapped polyphenol is defined as the specific antioxidant activity. Both the actual and specific antioxidant activity are shown in **Figure 4-12**.

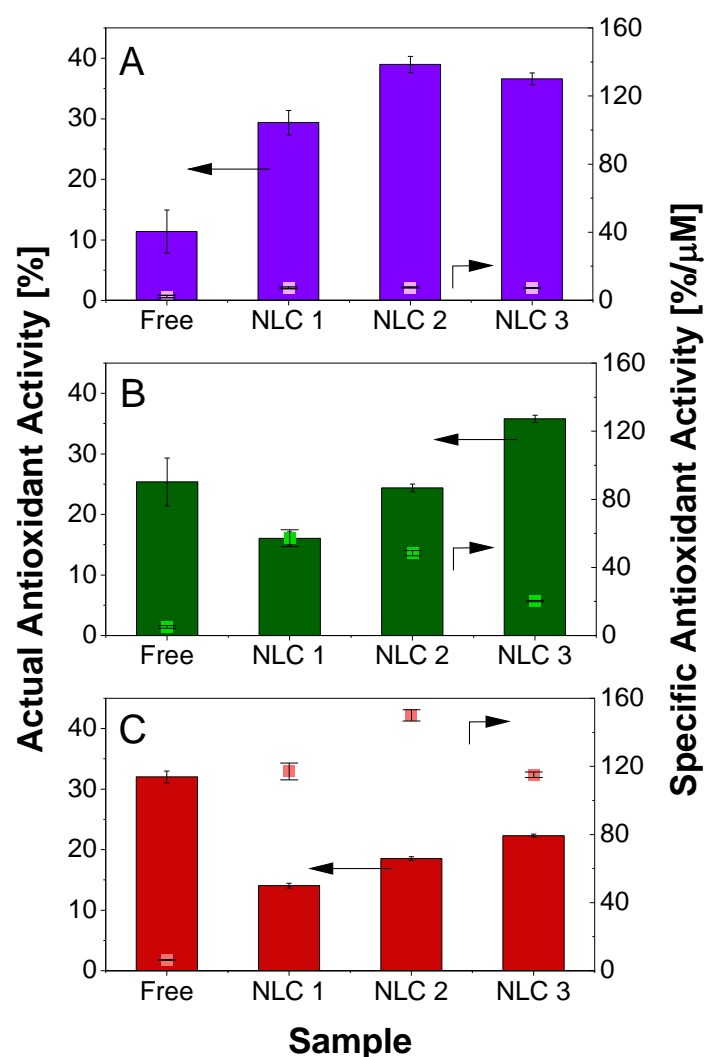


Figure 4- 12 Antioxidant Activity of Pol-NLC. Resveratrol (A); Kaempferol (B); Quercetin (C). Error bar represents the standard deviations ($n=3$).

In the case of R-NLC, the actual antioxidant activity of entrapped resveratrol is higher than that of the free-resveratrol, while for K-NLC and Q-NLC, the opposite situation has occurred. This result indicates that the entrapped polyphenols are the most critical factor that affect the actual antioxidant activity. In the R-NLC, NLC can load almost 100% of resveratrol, whereas K-NLC and Q-NLC can only trap ~35%-70% and less than 30%, respectively (**Figure 4-11**). The higher amount of entrapped resveratrol was causing the higher actual antioxidant activity.

The specific antioxidant activity was evaluated to make a more comprehensive analysis. This term describes the antioxidant activity per unit concentration of the

entrapped polyphenols. Surprisingly, the result shows that all the NLC formulations could improve the specific antioxidant activity compared to the free polyphenols. Some factors could be responsible for this advantage including the water-oil interface and lipid environment being considered as the active site of antioxidant reaction (Budilarto & Kamal-Eldin, 2015; Mardani-Ghahfarokhi & Farhoosh, 2020; Tian et al., 2022), where radicals might be trapped and scavenged according to their location and concentration. Therefore, with the presence of the NLC, the antioxidant reaction was more facilitated not only by the hydrogen donor mechanism but also by physically stable conditions for the reaction. From the viewpoint of polyphenols, these might be more protected against the stress condition by the NLC during the process of antioxidant reaction. Those circumstances might be the primary impact on increasing the specific antioxidant activity.

Contrary to the actual antioxidant activity, Q-NLC has the highest specific activity, followed by K-NLC and R-NLC, suggesting that the number of hydroxyl groups significantly influences the antioxidant activity. With the hydrogen donor as the main mechanism for radical scavenging, the more -OH group of polyphenols could directly increase the antioxidant activity (Lin et al., 2014). Otherwise, the location of the entrapped quercetin might influence the interaction with radicals when the reaction occurs. As mentioned above, due to the lower hydrophobicity of quercetin, it might be located at the outer shell or interface of NLC. This condition supports easing its interaction with the DPPH radical agent, which may be trapped at the same location. It is possible that the NLC structure would be changed by polyphenols incorporation. As reported in the previous study, the addition of polyphenol molecules can change the physicochemical properties of the local environment, such as micro fluidity and polarity of the lipid vesicles (liposomes) that can form a nano-ordered environment (bilayer membrane structure) (J. Han et al., 2017, 2021). Therefore, together with the locations of polyphenols, the arrangements of molecules in the NLC might be the factor affecting the antioxidant activities.

4. Conclusion

In summary, a schematic figure of the phenomenon in this chapter was provided in **Figure 4-13**. This figure reveals that resveratrol could be the most effective molecule

encapsulated in NLC, followed by kaempferol and quercetin. The hydrophobicity of polyphenols could be the most influential on the entrapment efficiency of each polyphenol, and further on the actual antioxidant activity. On the other hand, even though quercetin was the least encapsulated in the NLC, it has the highest specific antioxidant activity and could be the most efficient antioxidant agent compared to resveratrol and kaempferol, especially when incorporated with NLCs. Even though the entrapped location of polyphenols might be the main factor of antioxidant activity performance, the fact that entrapment efficiency of kaempferol differs by the NLC composition indicated that the structure of NLC as a result of lipid composition might also affect the loading performance. Regarding the design of polyphenol-incorporated NLCs, the result from this chapter might be very useful to determine the drug amount and lipid composition by considering the activity of the targeted drug-incorporated NLC. Therefore, the use of the drug could be optimized, and the formulation of drug-incorporated nanocarriers would become more efficient. Finally, all data demonstrated that polyphenol incorporation in the NLC results in a better performance of the specific antioxidant activity, and NLCs could be potentially used as an antioxidant delivery system.

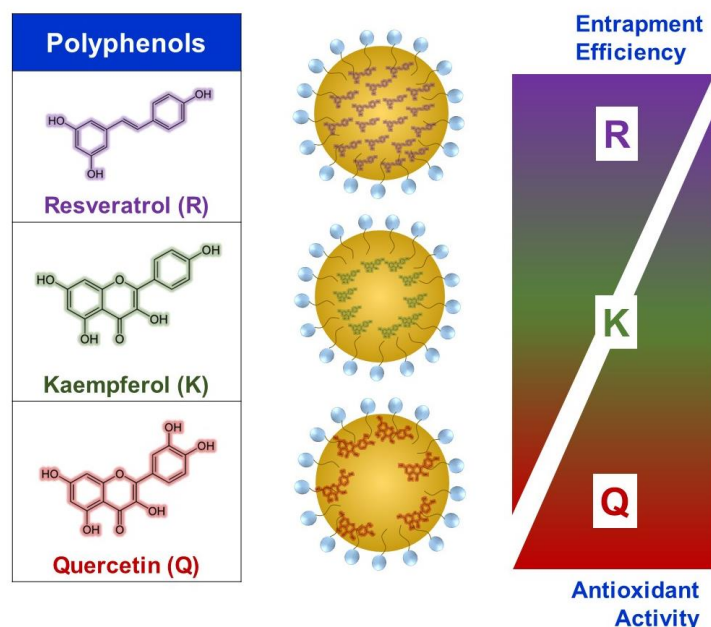


Figure 4- 13 Schematic Illustration of this chapter

Chapter 5

Investigation of tRNA Conformation During NLCs Fabrication

1. Introduction

The recent advances in nanotechnology exhibited potential for more precision medication. For example, the utilization of lipid nanoparticles (LNPs) for the designated delivery of drugs and other therapeutic molecules can expand bioavailability and pharmacokinetics properties. In fact, the intrinsic nature of hydrophilicity, large size, and poor membrane permeability of nucleic acids obstructed the development of nucleic acid-based therapeutics (Stoddard et al., 2018). LNPs can be a strong alternative to viral-intervened nucleic acid delivery platform, with a wide application, such as RNA interference (RNAi) therapy or RNA-based vaccines through intracellular delivery, respectively, of short interfering RNA (siRNA) or messenger RNA (mRNA) (Xue et al., 2015).

As corona virus disease 2019 (COVID-19) has spread worldwide, many researchers are attempting to develop efficacious vaccines against the virus. The low stability of RNA vaccines is the most critical issue. In addition, RNA cannot easily cross a cell membrane to enter target cells upon injection due to its size, negative charge, and hydrophilicity. Therefore, RNA formulations are aimed to overcome these drawback of RNA molecules, especially to stabilize and protect RNA molecules from degradation. One such way is the uses LNPs as the delivery system (Hou et al., 2021; Pilkington et al., 2021; Schoenmaker et al., 2021).

NLCs, one of the most promising LNPs, denoted as a hybrid formulation in between liquid emulsion and SLN that historically created for the delivery of lipophilic drug molecules. The existence of solid lipid in the lipid core, with a liquid lipid from a triglyceride make the highly hydrophobic core that preferable for lipophilic molecules. The mixture lipid of the core generates a semi-crystalline lipid matrix that exhibits a high dispersion stability relative to liquid emulsion and SLNs, it has advantages in manufacturability by controlling the fraction of the solid lipid component.

Due to the high hydrophobicity of the lipid core, NLC particles are not well adapted for delivery platform of nucleic acid-based product. Therefore, the loading of biomacromolecules such as siRNA or mRNA occurs through the association with their outer shell either by chemical modifications or by incorporation of cationic lipids that generates electrostatic interactions with negatively charged target (del Pozo-Rodríguez et al., 2007; H. R. Kim et al., 2008; Resnier et al., 2014).

In this chapter, the incorporation of cationic lipid (dioleoyl-3-trimethylammonium propane; DOTAP) into NLC was evaluated to encapsulate tRNA as a model of RNA-based therapy. Additionally, the investigation of tRNA conformation during the fabrication process will also be performed by using circular dichroism (CD) analysis. The obtained result is expected to have a significant contribution in the development of a high stability NLC-based platform for RNA therapy, or vaccines.

2. Material and Methods

2.1 Materials

CP and CaTG were purchased from Sigma-Aldrich (St. Louis, MO), polysorbate 80 from plant (T80) was purchased from Fujifilm Wako Pure Chemical Industry (Osaka, Japan). Molecular structures and physical properties of CP, CaTG, and T80 are shown in **Fig. 2-1 (Chapter 2)**. Dioleoyl-3-trimethylammonium propane (DOTAP) was purchased from Coatsome-NOF Cooperation, US. Ribonucleic acid, transfer (tRNA) originating from wheat germ as an RNA model was purchase from Sigma Aldrich (St. Louis, MO). All chemicals were used without further purification. Ultrapure water was prepared using Direct-Q® UV3 (Merck Millipore Co., Tokyo, Japan).

2.2 DOTAP-modified NLC Preparation

The NLC was fabricated using a hot homogenization-ultrasonication method as was previously described in chapter 2 and 3. Some modification was applied in this chapter. DOTAP and tRNA solution was prepared with the concentration of 2 mM and 25.44 μ M, respectively. This solution was added to mixed-melted lipid of CP and CaTG. Afterward, the preheated aqueous T80 was added dropwise to the lipid mixture. The final concentration of DOTAP and tRNA were 1 mM and 12.72 μ M, respectively; while the

total concentration of CP, CaTG, and T80 was 20 mM. The composition of NLC 1 and NLC 3 referred to the chapter 3 and 4. The schematic diagram of tRNA-DOTAP-NLC preparation is provided in **Figure 5-1**.

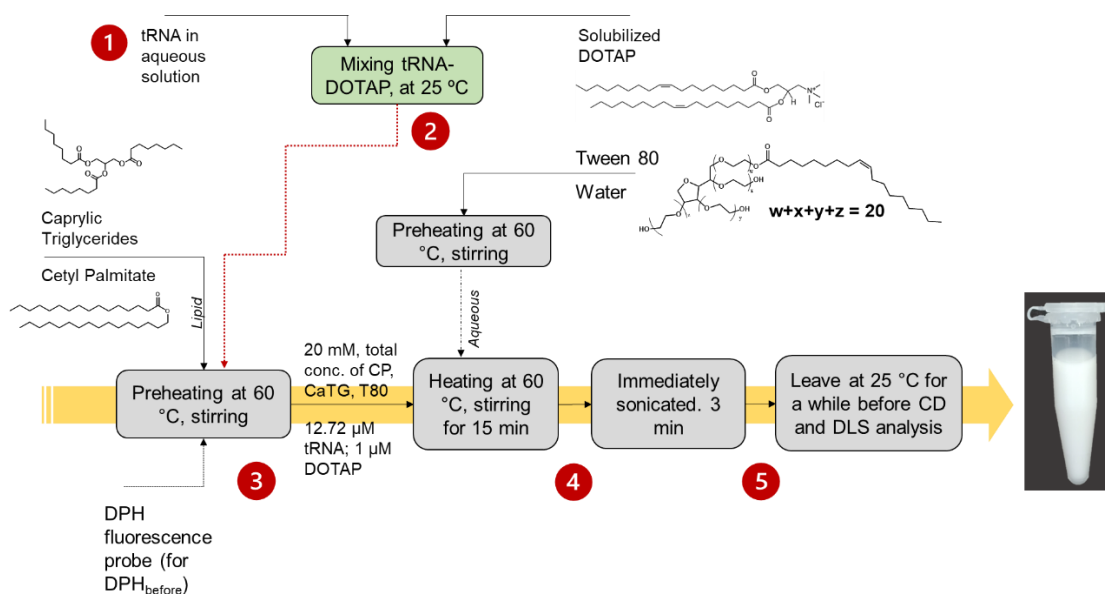


Figure 5- 1 Schematic Diagram of NLC-DOTAP-tRNA fabrication

The following is the information of the NLC-DOTAP-tRNA preparation stage:

- | | |
|---------|---|
| Stage 1 | = tRNA solution |
| Stage 2 | = tRNA-DOTAP mixture |
| Stage 3 | = CP-CaTG-tRNA-DOTAP |
| Stage 4 | = CP-CaTG-T80-tRNA-DOTAP (heating) |
| Stage 5 | = CP-CaTG-T80-tRNA-DOTAP (heating and sonicating) |

2.3 Particle Size, PDI and Zeta Potential

Particle size, PDI, and zeta potential was conducted by the dynamic light scattering (DLS) method with Malvern Zetasizer Nano series (Malvern, UK). Before being investigated, the samples were diluted to be 1 mM of the total NLC constituents (CP, CaTG, T80) in ultrapure water and were placed in the measuring-disposable folded capillary cuvette. The measurement was operated at 25 °C.

2.4 Circular Dichroism (CD) Analysis

The conformational changes in tRNA in the absence or presence of DOTAP-NLC were evaluated by a spectropolarimeter (J-820 SFU, JASCO, Tokyo, Japan). The CD spectrum was recorded from 300 to 200 nm using a quartz cell (0.1 cm pathlength), where scan speed was 100 nm/min and slit width was 1 nm. Three scanned data were accumulated, and then background signals (obtained from buffer or vesicle suspension) were removed to gain spectrum data. The total concentration of tRNA in CD scanning analysis was 4 μ M. The measurements were conducted using ultrapure water as the solvent.

2.5 Entrapment Efficiency

NLC-DOTAP-tRNA was centrifuged at 35000 rpm for 1 hour with ultracentrifugation unit (Himac CS100FNX, Hitachi, Japan) before analysis. As tRNA is soluble in water, the untrapped tRNA can be collected with the supernatant. Thereafter, the supernatant was filtered using ultrafiltration unit (20 kDa) to separate the remaining lipid. The untrapped tRNA concentration was measured by UV-Vis Spectroscopy. A calibration curve was prepared to calculate the concentration of the untrapped tRNA. Finally, the entrapment efficiency could be calculated with the Eq. 5-1.

$$\% \text{Entrapment Efficiency (EE)} = \frac{[\text{Initial tRNA}] - [\text{untrapped tRNA}]}{[\text{Initial drug}]} \times 100\% \quad \text{Eq. 5-1}$$

3. Result and Discussion

3.1 Basic Nano-properties of NLC-DOTAP-tRNA

Particle size, PDI, and zeta potential of DOTAP-NLC-tRNA were investigated. The hydrodynamic diameter (particle size), PDI, and zeta potential (ZP) obtained from this study were summarized in the **Figure 5-2**. According to the result, we could see that particle size of DOTAP modified NLC systems with or without tRNA have less than 300 nm particle size except for NLC 1 with tRNA (**Figure 5-2 A**). On the other hand, the PDI show that all the samples' indices are less than 0.3, which is considerably as a monodispersed suspension. In NLC 1, the particle size is 1159 nm which is significantly higher than the system without tRNA, as well as compared to NLC 3. The large,

monodispersed particle, it can be implied that the presence of tRNA was impact to the high lipid component and resulting in a much larger particle. Based on the NLC 3, the addition of DOTAP and tRNA has no significant effect to the particle size and PDI. Also, compared to the previous study in chapter 2-4, the particle size of NLC-DOTAP-tRNA of NLC 3 is identical.

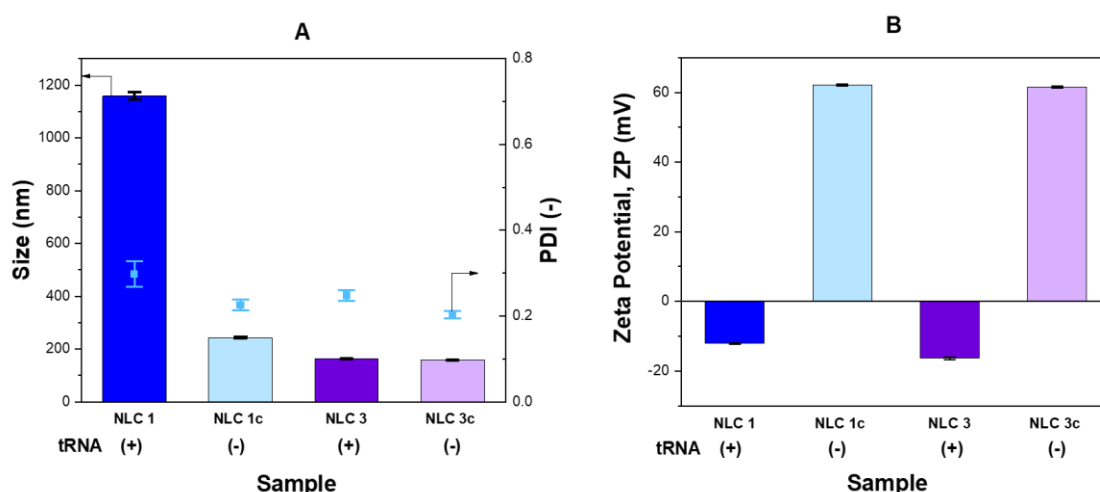


Figure 5- 2 DLS result of NLC-DOTAP-tRNA. Particle size and PDI (A); Zeta Potential (B). *Light blue and light purple* colour are the control sample without tRNA. Error bar represents the standard deviations ($n=3$)

Both NLC 1 and NLC 3 have a negatively charged of particles when it is added by tRNA that are shown in **Figure 5-2 B**. Compared to the original properties of NLC without DOTAP modification and tRNA (**Figure 2-2 B, Chapter 2**), ZP = -12 and ZP = -16 for NLC 1 and 3, respectively; both DOTAP modified NLC1 and NLC3 with tRNA have negative ZP values. There are two possibilities. One is due to the nature of the lipid components having the dissociation of fatty acid carboxylic, or carbonyl functional group (Ginés et al., 2017; Nahak et al., 2016). The other possibility is the existence of tRNA, as it consists of negative phosphates on their backbones. Even though there might be interact with the DOTAP, there is still possibility of free tRNA existing that could contribute to the negative surface charge of particles. The NLC-DOTAP without tRNA exhibit a high positively charged particle, which most probably generated by the DOTAP in the system since T80 is a non-ionic surfactant. Therefore, free bulk-tRNA might have absorbed to the positively charged NLCs and which results in the negative ZP values.

3.2 Step-by-step Evaluation of NLC-DOTAP-tRNA in Their Formulation Process

To comprehensively understand the structural formation of NLC-DOTAP-tRNA resulting by the operating procedures during the preparation, a step-by-step evaluation of size, PDI, and zeta potential was conducted through the 5 stages as defined in **Figure 5-1**. By this evaluation, a more detailed understanding of the factors affecting the nanoparticle properties during the fabrication could be potentially achieved. The result of step-by-step evaluation can be found in **Figure 5-3**.

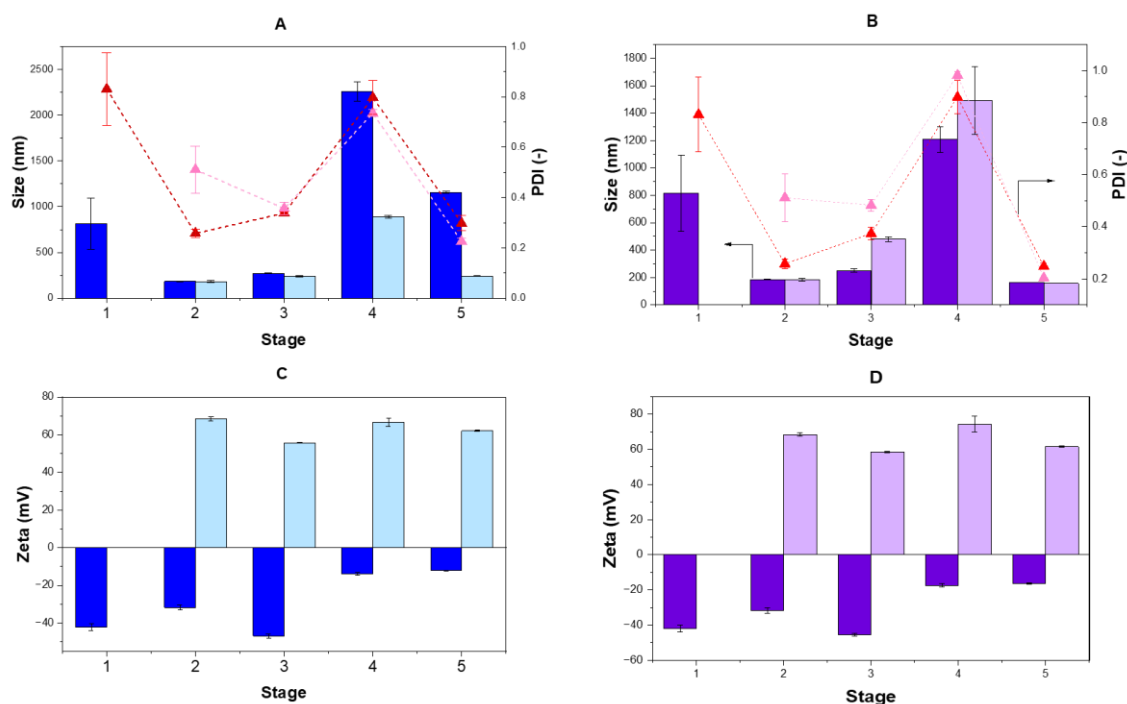


Figure 5- 3 DLS Analysis result of step-by-step evaluation of NLC-DOTAP-tRNA during fabrication. Particle size and PDI of NLC 1 (A) and NLC 3 (B); Zeta potential of NLC 1 (C) and NLC 3 (D). Light colour is the control sample without tRNA. Error bar represents the standard deviations (n=3)

According to particle size and PDI, the trend is identical between NLC 1 (**Figure 5-3 A**) and NLC 3 (**Figure 5-3 B**). There is only one significant difference size in stage 4 and 5, where the addition of T80, heating, and sonicating was applied. Sequentially from the first stage, a large molecule of tRNA was initially observed. The large and heterogenic molecules were found may be caused by the randomly folded tRNA. At the second stage, the mixed state of tRNA and DOTAP, both NLCs showed smaller particle size. Since DOTAP has positive charge, it may electrically interact with the negatively charged phosphate on tRNA. The strong interaction between tRNA and DOTAP unfold tRNA structure, therefore, the particle size of the DOTAP-tRNA assemblies is small.

When the DOTAP-tRNA solution were added to the melted CP and CaTG mixture under stirred-heated condition (stage 3), the particle size and PDI did not significantly changed, unless the increase of control sample of NLC 3. Thereafter, both size and PDI increased for both NLC 1 and NLC 3 at the stage 4, when T80 added to the mixture. This result means that the lipids and tRNA formed loosely binding large assemblies after the addition of T80. Because T80 has hydrophilic head group and hydrophobic tail, it stands to be located on lipid-water interphase. The particle size of samples with tRNA is relatively high, so the interaction between the T80 and tRNA-lipid assemblies might form heterogenic aggregations.

Finally, the last step is the sonication process to make the particles homogenic (stage 5). At this stage, a different behavior of NLC 1 and NLC 3 was found. In NLC 3, the particle size decreases significantly as well as the PDI, that implies the monodispersed particle. This final NLC3-DOTAP-tRNA is typically same as NLC compared to the previous study. On the other hand, the NLC1-DOTAP-tRNA still have a large particle size around 1000 nm compared to the NLC1-DOTAP which has similar size and PDI with general NLC. This might occur because of the presence has a particular effect on the highly solid lipid NLC (NLC 1). The interaction between CP-T80 and tRNA at the surface resulted in a tight formation that more difficult to disrupt by ultrasonication.

The zeta potential demonstrated a similar behavior of NLC 1 and NLC 3, as can be seen in **Figure 5-3 C & D**. A highly positive ZP was exhibited by all the control samples that was the result of the presence of the DOTAP as catanionic lipid in NLC system. In contrast, all the samples with tRNA showed negatively charge because of the nature of tRNA that is consisted by phosphates. A markable decrease of ZP negativity was captured from stage 3 to 4, where T80 was added. The decrease might be caused by the neutral charge of T80 which has a dominant effect on ZP because its location at the particle surface.

3.3 tRNA conformation during NLC-DOTAP-tRNA fabrication

The conformation of tRNA was observed by analyzing the circular-dichroism (CD) spectra. tRNA has conformation of α -form double helix that has negative peak at 208 nm and positive peak at around 265 nm. These peaks generally decreased together with its denaturation caused by the stress conditions. Therefore, the conformation of

tRNA during the DOTAP-NLC fabrication could be investigated. CD spectra of tRNA are shown in **Figure 5-4**. The summary of the result according to the CD spectra, a negative peak around 208 nm and positive peak around 265 nm are appeared, confirmed the existence of tRNA in each sample.

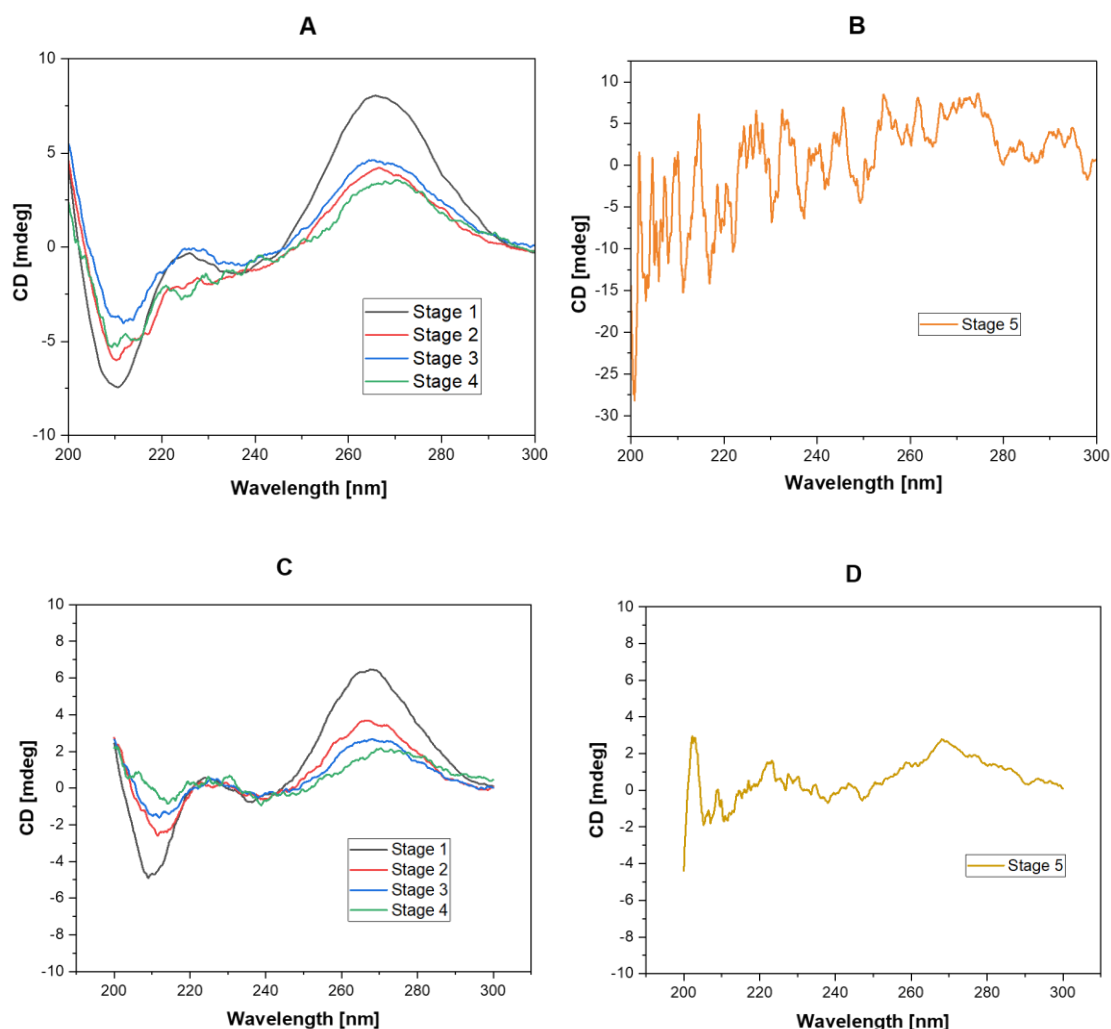


Figure 5- 4 CD Spectra of tRNA during NLC-DOTAP-tRNA fabrication. NLC 1, stage 1-4 (A); stage 5 (B); NLC 3, stage 1-4 (C); stage 5 (D).

A decrease in the intensity of CD ellipticity (θ) is observed after the addition of DOTAP in stage 2 (**Figure 5-4 A & C**). This result agrees with a previous study of Suga et al (2011), they reported that tRNA was denatured in the presence of the cationic liposomes. It could be explained that the electrostatic interaction of RNA and DOTAP occurred, and by the presence of cationic lipid, the melting temperature of tRNA was increased in proportion to the surface charge density of liposomes. This result indicated that the cationic liposomes denatured tRNA and then the denatured tRNA was stabilized

on the liposomes (Suga et al., 2011). Therefore, the current results explain the denature of tRNA structure occurred during the NLC formation with cationic lipid. In NLC 1, we could even see the peak at any wavelength unless the noisy peak at stage 5 that indicates the most of tRNA denatured in formation of NLC1. Likewise, even though a sloping peak could be observed, the peak of NLC 3 in stage 5 hardly represent as the conformation of double helix structure.

3.4 Entrapment Efficiency

The loading performance of the nanocarrier was determined by how much the targeted molecules can be entrapped, generally expressed by entrapment efficiency. In this study, the entrapment efficiency was measured by analyzing the concentrations of untrapped tRNA in the supernatant just after the NLC-DOTAP-tRNA had been ultracentrifuged. After that, the entrapment efficiency was calculated with **Equation 5-1**. A calibration curve of tRNA absorbance at 260 nm of wavelengths was made before calculating the untrapped tRNA (**Figure 5-5 A**). The entrapment efficiency of NLC-DOTAP-tRNA is provided in **Figure 5-5 B**.

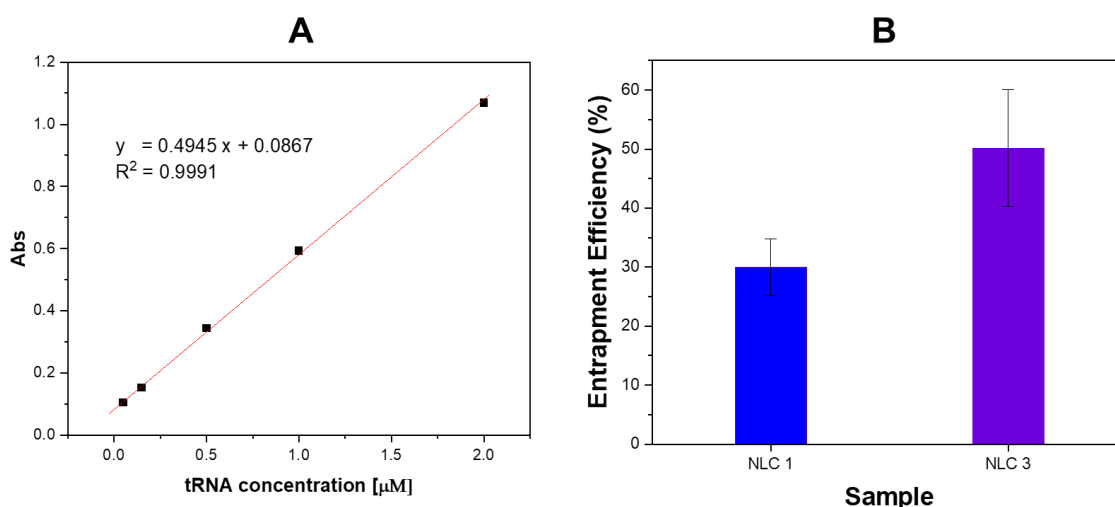


Figure 5- 5 Calibration curve of tRNA at 260 nm (A); Entrapment efficiency of DOTAP-NLC-tRNA (B). Error bar represents the standard deviations ($n=3$)

The result of entrapment efficiency indicated that DOTAP-modified NLC can load such biomolecules as tRNA. NLC 3 exhibits higher entrapment efficiency than NLC 1. Based on the previous study, NLC 3 formed less crystal structure than that of NLC 1. As a result, NLC3 can accommodate more material in its lipid matrix than NLC1. Also, CaTG as the liquid lipid has a highly hydrophobic nature that can be more interacted with

DOTAP tails. NLC 3 has higher liquid lipid concentration, therefore, the more DOTAP-tRNA could be entrapped in its structure.

3.5 Plausible structure formation of NLC-DOTAP-tRNA during preparation

Based on the step-by-step investigation about NLC-DOTAP-tRNA nanoparticle-properties and tRNA conformation during the fabrication, the plausible formation of NLC-DOTAP-tRNA during the fabrication process is proposed as illustrated in **Figure 5-6 A & B**. Sequentially, at the first stage, the tRNA is folded, some of them changed to unfolded just after the mixing process with DOTAP. In this second stage, the particle size was decreased. Thereafter, no significant change observed when the mixed DOTAP-tRNA added the melted CP and CaTG under heating. When the aqueous T80 was added to the mixture at stage 4, the particle size increased. As was mentioned, this might be because the particle is started to form heterogenic aggregation; whereas tRNA could possibly located inside the large aggregate or for some reasons interact with the lipid on the surface of the aggregates. A decrease in ZP were observed for both data, corresponding to the neutral charge of T80 that can reduces the negativity of the surface charge.

From stage 5, a different behavior of the particle size was captured. In NLC 3, the particle size was significantly decreased after sonication as the normal effect of sonication process as the homogenizer. However, in the NLC 1, the sample with tRNA still has a large particle size, even though the control sample (without tRNA) has similar size with that of NLC3. This can be because there is a specific interaction between tRNA and CP or CP-T80 that might cause a very strong binding and could not be separated using ultrasonication. As reported previously, the CP and T80 might has specific interaction resulting crystal lamellar-like structure on the surface and tightened the interaction with tRNA on the surface. Another possibility is that solid lipid (CP), expelled out the complex of tRNA and DOTAP around near surface due to the lamellarity, and resulted particles formed the large size of particles with heterogeneity in size (high PDI). This logic is consisting to the hypothesis that NLC3 with high liquid lipid has more high entrapment efficiency presumably due to the fluid accommodation space inside the particle to encapsulate the tRNA and DOTAP complex.

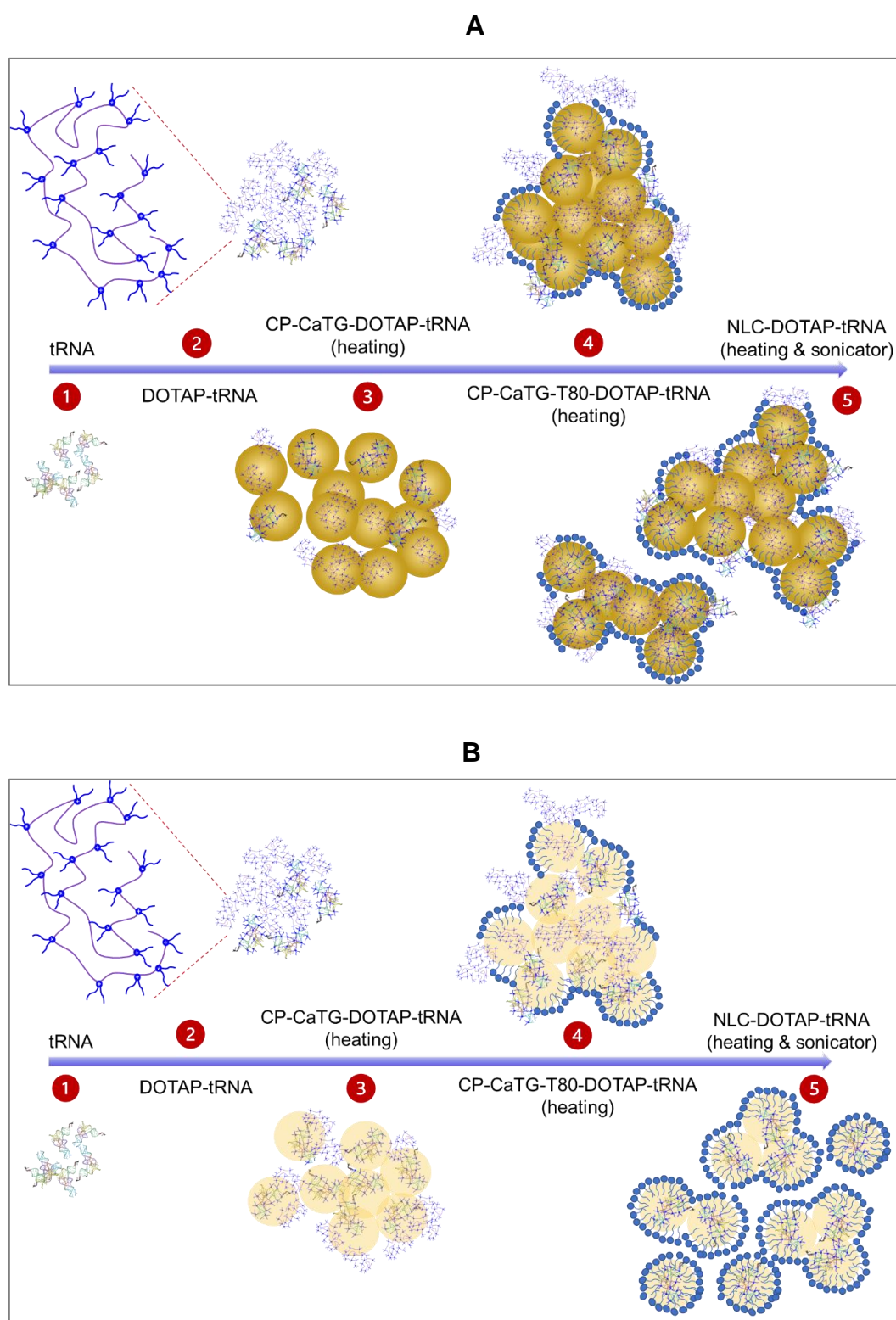


Figure 5- 6 Illustration of the plausible formation of NLC-DOTAP-tRNA during fabrication; NLC 1 (A), NLC 3 (B)

4. Summary

The investigation of the conformation of tRNA encapsulated in DOTAP-modified NLC has been performed in this chapter. It was found that compared to NLC in the previous chapters, NLC 1 has larger particle size with existence of DOTAP-modified tRNA; while in NLC 3, the final product has a similar property with the previous chapters, as well as the zeta potential. Based on CD spectra, both of NLC 1 and NLC 3 resulted in a denatured tRNA at the final state (stage 5). Also, according to the experiment to detect the entrapment efficiency of tRNA, NLC 3 has a higher entrapment efficiency. At final stage, a summary of the plausible formation of NLC-DOTAP-tRNA have been provided. This information of the formation of particles during preparation and the step-by-step properties investigation could be valuable for the future application of NLC for encapsulating bio-based molecules such as nucleic acid, RNA, DNA, and others for therapeutic applications.

Chapter 6

General Conclusion

Fundamental characteristics of lipid nanocarrier, including NLCs plays an essential role in the drug delivery system. In this study, a thorough characterization of physicochemical properties and internal structure of the NLC was performed. Based on the characterized properties of the NLCs, a method to encapsulate such biomolecules (i.e., polyphenols and RNA) was established, focusing on their loading performance and behaviors. The findings obtained are expected to be applied in optimizing the design and formulation of NLC as a drug carrier.

In chapter 2, the physicochemical properties and self-assembly state of NLCs have been systematically characterized based on the fluidity ($1/P$) and polarity (GP_{340}). A ternary diagram of the aqueous solution mixing three lipids (cetyl-palmitate (CP: solid), caprylic triglyceride (CaTG: liquid), and Tween 80(T80)) was clarified based on the properties to summarize the possible structures formed at different compositions of NLC, showing the formation of four possible NLCs, such as micelles, O/W emulsions, solid-lipid nanoparticles, and their intermediate states. The formation of CP/CaTG/T80 assemblies is dominated by O/W emulsion-like characteristics, which were strongly affected by the presence of liquid lipid. Based on the ternary diagram, T80 was the most influential component in the NLC system. Finally, the ternary diagram provides new information about the assembly state of NLC constituents that could become an important reference for developing high-performance NLCs.

In chapter 3, a molecular and physicochemical characterizations of the NLC core region were performed. A modified method of conventional fluorescence-based analysis was newly developed to investigate the anisotropy of inner and outer cores of different NLCs. The obtained results show that NLC represented a unique core-shell structure with higher rigidity of the outer core than that of the inner core. Further internal characterizations revealed that NLC could have a polymorphism crystal lamellar structure depending on the lipid composition. According to the results, the ratio of solid lipid to total lipid concentration has a linear correlation with some observed parameters (r_{gap} , ΔH ,

and crystallinity %), implying that those parameters could be controlled by adjusting the lipid composition. These parameters can be used to predict the existence of the shell, rigid state fraction, and crystals in the NLC structure. The above findings improve the understanding of the microscopic structure and properties of NLC core and could be applied in designing a specific NLC carrier for various products and administration.

The above studies clarify the effect of lipid composition on the molecular and physicochemical properties of NLCs. Based on the obtained characteristics, a method to encapsulate some biomolecules was proposed based on the loading performance with its appropriate quality, by selecting polyphenols and tRNA as case studies of small and large biomolecules.

In chapter 4, NLC was designed for a drug delivery system (DDS) for some polyphenol molecules. Three different polyphenols with different lipophilicity were employed as targeted loading drugs in NLC, then investigation of particle stability, drug loading performance, and antioxidant activity of polyphenols incorporated NLCs were performed. The results indicated that the hydrophobicity of polyphenols could be the most influential on the entrapment efficiency of each polyphenol and further on the actual antioxidant activity. The particle size and distribution were suitable for DDS applications, and all the samples demonstrated good stability after 2 months of storage. Based on Raman spectroscopy analysis, polyphenols were successfully encapsulated in NLCs. Quantitative high-performance liquid chromatography analysis indicated that NLCs could load resveratrol more than kaempferol and quercetin. In addition, NLCs have successfully improved all the antioxidant activity per unit concentration of polyphenol (specific antioxidant activity) compared to the free polyphenols. Quercetin-incorporated NLCs showed the highest specific antioxidant activity. This result is the opposite of entrapment efficiency and actual antioxidant activity, most likely influenced by the location of entrapped polyphenol molecules. As it was performed, NLCs are highly recommended to be applied as an antioxidant delivery system.

In chapter 5, the evaluation of NLC performance in loading RNA-based products is conducted. tRNA was selected as a product model and 1,2-dioleoyl-3-trimethylammonium-propane (DOTAP) was employed as a supporting lipid to improve its loading performance in NLCs. The effect of lipid composition be investigated by

analyzing the circular dichroism (CD) spectroscopic analysis. The conformation of tRNA was evaluated with CD spectroscopy by varying the timing of the tRNA addition of precursor solution of NLC. It was found that the DOTAP-modified NLC could entrap the tRNA and the structure of tRNA could be denatured during loading. The NLC with high amount of liquid lipid represented higher loading efficacy and well-dispersed small particle size, while the one with high amount of solid lipid showed large heterogenic particle properties with low encapsulation efficiency. Based on the investigation, the effects of NLC composition to the final particle size and entrapment efficiency were clarified in loading the RNA molecules.

Suggestion for Future Works

1. Modification of the lipid component in regard of properties for specific administration route

As was mentioned, the fundamental properties of drug carriers are essential in determining the success of drug delivery. It can determine the drug release profile and safety of the drug molecules during the delivery process. In the previous study (Chapter 2 and 3), the characteristics of NLC and the behavior related to its composition has been studied. Based on the result, it is possible to formulate a particular NLC properties that might be suitable for a specific purpose regarding a specific administration pathway. To establish a wider understanding of NLC characteristics and behaviors, additional investigation of some lipid candidates is required to be observed. The nature of the lipid constituent might demonstrate different behaviors regarding the interaction to another lipid constituent or the surfactant resulting in a different property and structure of NLC.

Some parameters can be considered in selecting the candidate of the lipid constituent for NLC. For example, it is physiologically acceptable, biodegradable, non-toxic and safe. Other than that, more specific property such as type and structure of lipid that might affect the characteristics of NLC. Also, the solubility of the targeted delivery molecules or the partition coefficient in the lipid candidate must be concerned more as it will affect the loading performance and efficiency.

2. Extended applications of NLC as a carrier platform for natural resources-based product

In the recent years, the separation of bioactive materials from natural resource has been widely studied with numerous extraction and isolation methods. The extracted bioactive product can be utilized as drugs, additives for functional foods, cosmetics, *etc.*, depending on their active ingredients. Despite many advantages of bioactive ingredients in maintaining human health, the therapeutic use is often limited by its poor stability against environmental conditions such as light, oxygen, and temperature. Also, human biological condition such as pH and the presence of enzymes are included in the main

factors affecting stability of active ingredients. Those limitations related to the stability resulting in compromised bioactivity, bio-accessibility, and bioavailability, which hampers the therapeutic application of the therapeutic agents. In this regard, NLC is proposed as one of promising strategies which offer some special advantages, such as high drug loading, long-term stability, sustained release, biodegradable, and most importantly can increase the local deposition of the drug.

This research is expected to demonstrate new technology for developing drug delivery systems for encapsulating natural resources active compounds. Therefore, the results can be useful for pharmaceutical industry to develop technologies to design a drug delivery system, which could also be transferred to other industries that potentially uses a natural ingredient, such as food, cosmetics or skin care industries.

Nomenclatures

T_m	=	Melting temperature	°C
M_w	=	Molecular weight	g/ mol
P	=	Fluorescence polarization of probe in NLC system	[-]
GP_{340}	=	General polarization calculating at exciting light at 340 nm	[-]
G	=	Correction factor	[-]
$\text{Log } P$	=	Octanol-water partition coefficient	[-]
PDI	=	Polydispersity index	[-]
ζ	=	Zeta potential	[mV]
r	=	Fluorescence anisotropy	[-]
ΔH	=	Transition energy	[J/g]
CI	=	Crystallinity index	[-]
C_p	=	Heat capacity	[J/g °C]
$2-\theta$	=	Angles in XRD analysis	[Deg]
EE	=	Entrapment efficiency	[%]
AA	=	Antioxidant activity	[%]

List of Abbreviations

CD	=	Circular Dichroism
<i>CI</i>	=	Crystallinity Index
COVID	=	Coronavirus Disease
DDS	=	Drug Delivery System
DLS	=	Dynamic Light Scattering
DMPC	=	1,2-dimyristoyl-sn-glycero-3-phosphocholine
DOPC	=	1,2-dioleoyl-sn-glycero-3-phosphocholine
DOTAP	=	1,2-dioleoyl-3-trimethylammonium-propane
DPH	=	1,6-Diphenyl-1,3,5-hexatriene
DPPH	=	2,2-Diphenyl-1-picrylhydrazylradical
DSC	=	Differential Scanning Calorimetry
EE	=	Entrapment Efficiency
FFT	=	Fast Fourier Transformation
<i>GP</i>	=	General Polarization
HPLC	=	High-Performance Liquid Chromatography
LE	=	Liquid Emulsion
LNP	=	Lipid Nanoparticles
NLC	=	Nanostructured Lipid Carrier
PDI	=	Polydispersity Index
RNA	=	Ribonucleic Acid
SLN	=	Solid Lipid Nanoparticles
T80	=	Tween 80
TEM	=	Transmission Electron Microscopy
XRD	=	X-Ray Diffraction

References

- Aburai, K., Hatanaka, K., Takano, S., Fujii, S., & Sakurai, K. Characterizing an siRNA-containing lipid-nanoparticle prepared by a microfluidic reactor: Small-angle x-ray scattering and cryotransmission electron microscopic studies. *Langmuir*, **2020**, 36(42), 12545–12554.
- Aditya, N. P., Shim, M., Lee, I., Lee, Y., Im, M. H., & Ko, S. Curcumin and genistein coloaded nanostructured lipid carriers: In vitro digestion and antiproliferative cancer activity. *Journal of Agricultural and Food Chemistry*, **2013**, 61(8), 1878–1883.
- Ali, A., Chong, C. H., Mah, S. H., Abdullah, L. C., Choong, T. S. Y., & Chua, B. L. Impact of storage conditions on the stability of predominant phenolic constituents and antioxidant activity of dried piper betle extracts. *Molecules*, **2018**, 23(2), 1–15.
- Alsaad, A. A. A., Hussien, A. A., & Gareeb, M. M. Solid lipid nanoparticles (SLN) as a novel drug delivery system: A theoretical review. *Systematic Reviews in Pharmacy*, **2020**, 11(5), 259–273.
- Arias, A., Feijoo, G., & Moreira, M. T. Exploring the potential of antioxidants from fruits and vegetables and strategies for their recovery. *Innovative Food Science & Emerging Technologies*, **2022**, 77, 102974.
- Azmi, N. A. N., Hasham, R., Ariffin, F. D., Elgharbawy, A. A. M., & Salleh, H. M. Characterization, stability assessment, antioxidant evaluation and cell proliferation activity of virgin coconut oil-based nanostructured lipid carrier loaded with Ficus deltoidea extract. *Cosmetics*, **2020**, 7(4), 1–15.
- Badran, M. Formulation and in vitro evaluation of flufenamic acid loaded deformable liposomes for improved skin delivery. *Digest Journal of Nanomaterials and Biostructures*, **2014**, 9(1), 83–91.
- Barthlott, W., Mail, M., & Neinhuis, C. Superhydrophobic hierarchically structured surfaces in biology: Evolution, structural principles and biomimetic applications. *Philosophical Transactions of the Royal Society A: Mathematical, Physical and Engineering Sciences*, **2016**, 374, 20160191 .
- Barthlott, Wilhelm, Mail, M., Bhushan, B., & Koch, K. Plant surfaces: Structures and functions for biomimetic innovations. *Nano-Micro Letters*, **2017**, 9(2), 1–40.
- Bashiri, S., Ghanbarzadeh, B., Ayaseh, A., Dehghannya, J., Ehsani, A., & Ozyurt, H. Essential oil-loaded nanostructured lipid carriers: The effects of liquid lipid type on the physicochemical properties in beverage models. *Food Bioscience*, **2020**, 35, 100526.
- Bhatt, S., Sharma, J. B., Kamboj, R., Kumar, M., Saini, V., & Mandge, S. Design and optimization of febuxostat-loaded nano lipid carriers using full factorial design. *Turkish Journal of Pharmaceutical Sciences*, **2021**, 18(1), 61–67.
- Bnyan, R., Khan, I., Ehtezazi, T., Saleem, I., Gordon, S., O'Neill, F., & Roberts, M. Surfactant effects on lipid-based vesicles properties. *Journal of Pharmaceutical Sciences*, **2018**, 107(5), 1237–1246.

- Bompard, J., Rosso, A., Brizuela, L., Mebarek, S., Blum, L. J., Trunfio-Sfarghiu, A. M., Lollo, G., Granjon, T., Girard-Egrot, A., & Maniti, O. Membrane fluidity as a new means to selectively target cancer cells with fusogenic lipid carriers. *Langmuir*, **2020**, 36(19), 5134–5144.
- Budilarto, E. S., & Kamal-Eldin, A. The supramolecular chemistry of lipid oxidation and antioxidation in bulk oils. *European Journal of Lipid Science and Technology*, **2015**, 117, 1095–1137.
- Bui, T. T., Suga, K., Kuhl, T. L., & Umakoshi, H. Melting-temperature-dependent interactions of ergosterol with unsaturated and saturated lipids in model membranes. *Langmuir*, **2019**, 35(32), 10640–10647.
- Bui, T. T., Suga, K., & Umakoshi, H. Ergosterol-induced ordered phase in ternary lipid mixture systems of unsaturated and saturated phospholipid membranes. *Journal of Physical Chemistry B*, **2019**, 123(29), 6161–6168.
- Bunjes, H., Steiniger, F., & Richter, W. Visualizing the structure of triglyceride nanoparticles in different crystal modifications. *Langmuir*, **2007**, 23(7), 4005–4011.
- Carvajal-Vidal, P., González-Pizarro, R., Araya, C., Espina, M., Halbaut, L., Gómez de Aranda, I., García, M. L., & Calpena, A. C. Nanostructured lipid carriers loaded with Halobetasol propionate for topical treatment of inflammation: Development, characterization, biopharmaceutical behavior and therapeutic efficacy of gel dosage forms. *International Journal of Pharmaceutics*, **2020**, 585, 119480.
- Castro, S. R., Ribeiro, L. N. M., Breitzkreitz, M. C., Guilherme, V. A., Rodrigues da Silva, G. H., Mitsutake, H., Alcântara, A. C. S., Yokaichiya, F., Franco, M. K. K. D., Clemens, D., Kent, B., Lancellotti, M., de Araújo, D. R., & de Paula, E. A pre-formulation study of tetracaine loaded in optimized nanostructured lipid carriers. *Scientific Reports*, **2021**, 11(1), 21463.
- Chantaburanan, T., Teeranachaideekul, V., Chantasart, D., Jintapattanakit, A., & Junyaprasert, V. B. Effect of binary solid lipid matrix of wax and triglyceride on lipid crystallinity, drug-lipid interaction and drug release of ibuprofen-loaded solid lipid nanoparticles (SLN) for dermal delivery. *Journal of Colloid and Interface Science*, **2017**, 504, 247–256.
- Chauhan, I., Yasir, M., Verma, M., & Singh, A. P. Nanostructured lipid carriers: A groundbreaking approach for transdermal drug delivery. *Advanced Pharmaceutical Bulletin*, **2020**, 10(2), 150–165.
- Cirri, M., Maestrini, L., Maestrelli, F., Mennini, N., Mura, P., Ghelardini, C., & di Cesare Mannelli, L. Design, characterization and in vivo evaluation of nanostructured lipid carriers (NLC) as a new drug delivery system for hydrochlorothiazide oral administration in pediatric therapy. *Drug delivery*, **2018**, 25(1), 1910–1921.
- Cizmar, P., & Yuana, Y. Detection and characterization of extracellular vesicles by transmission and cryo-transmission electron microscopy. *Methods in molecular biology (Clifton, N.J.)*, **2017**, 1660, 221–232.
- Danaei, M., Dehghankhold, M., Ataei, S., Hasanzadeh Davarani, F., Javanmard, R., Dokhani, A., Khorasani, S., & Mozafari, M. R. Impact of particle size and

- polydispersity index on the clinical applications of lipidic nanocarrier systems. *Pharmaceutics*, **2018**, 10(2), 1–17.
- De Granada-Flor, A., Sousa, C., Filipe, H. A. L., Santos, M. S. C. S., & De Almeida, R. F. M. Quercetin dual interaction at the membrane level. *Chemical Communications*, **2019**, 55(12), 1750–1753.
- del Pozo-Rodríguez, A., Delgado, D., Solinís, M. A., Gascón, A. R., & Pedraz, J. L. Solid lipid nanoparticles: Formulation factors affecting cell transfection capacity. *International Journal of Pharmaceutics*, **2007**, 339(1), 261–268.
- Desai, P. P., Date, A. A., & Patravale, V. B. Overcoming poor oral bioavailability using nanoparticle formulations - Opportunities and limitations. *Drug Discovery Today: Technologies*, **2012**, 9(2), 1740–6749.
- Eh Suk, V. R., Mohd. Latif, F., Teo, Y. Y., & Misran, M. Development of nanostructured lipid carrier (NLC) assisted with polysorbate nonionic surfactants as a carrier for l-ascorbic acid and Gold Tri.E 30. *Journal of Food Science and Technology*, **2020**, 57(9), 3259–3266.
- Eygeris, Y., Patel, S., Jozic, A., Sahay, G., & Sahay, G. Deconvoluting Lipid Nanoparticle Structure for Messenger RNA Delivery. *Nano Letters*, **2020**, 20(6), 4543–4549.
- Faried, M., Suga, K., Okamoto, Y., Shameli, K., Miyake, M., & Umakoshi, H. Membrane surface-enhanced raman spectroscopy for cholesterol-modified lipid systems: effect of gold nanoparticle size. *ACS Omega*, **2019**, 4(9), 13687–13695.
- Feng, J., Huang, M., Chai, Z., Li, C., Huang, W., Cui, L., & Li, Y. The influence of oil composition on the transformation, bioaccessibility, and intestinal absorption of curcumin in nanostructured lipid carriers. *Food and Function*, **2020**, 11(6), 5223–5239.
- Garg, J., Pathania, K., Sah, S. P., & Pawar, S. v. Nanostructured lipid carriers: a promising drug carrier for targeting brain tumours. *Future Journal of Pharmaceutical Sciences*, **2022**, 8(1), 1–31.
- Garg, N. K., Tandel, N., Bhadada, S. K., & Tyagi, R. K. Nanostructured lipid carrier-mediated transdermal delivery of aceclofenac hydrogel present an effective therapeutic approach for inflammatory diseases. *Frontiers in Pharmacology*, **2021**, 12, 1–18.
- Gaur, P. K., Mishra, S., Bajpai, M., & Mishra, A. Enhanced oral bioavailability of Efavirenz by solid lipid nanoparticles: In vitro drug release and pharmacokinetics studies. *BioMed Research International*, **2014**, 2014, 1–9.
- Gerhardt, A., Voigt, E., Archer, M., Reed, S., Larson, E., van Hoeven, N., Kramer, R., Fox, C., & Casper, C. A flexible, thermostable nanostructured lipid carrier platform for RNA vaccine delivery. *Molecular Therapy - Methods and Clinical Development*, **2022**, 25, 205–214.
- Ginés, L., Mandal, S., Ashek-I-Ahmed, Cheng, C. L., Sow, M., & Williams, O. A. Positive zeta potential of nanodiamonds. *Nanoscale*, **2017**, 9(34), 12549–12555.
- Gonçalves, C., Ramalho, M. J., Silva, R., Silva, V., Marques-Oliveira, R., Silva, A. C., Pereira, M. C., & Loureiro, J. A. Lipid nanoparticles containing mixtures of

- antioxidants to improve skin care and cancer prevention. *Pharmaceutics*, **2021**, *13*(12), 1–17.
- Guilherme, V. A., Ribeiro, L. N. M., Alcântara, A. C. S., Castro, S. R., Rodrigues da Silva, G. H., da Silva, C. G., Breitzkreitz, M. C., Clemente-Napimoga, J., Macedo, C. G., Abdalla, H. B., Bonfante, R., Cereda, C. M. S., & de Paula, E. Improved efficacy of naproxen-loaded NLC for temporomandibular joint administration. *Scientific reports*, **2019**, *9*(1), 11160.
- Güney, G., Kutlu, H. M., & Genç, L. Preparation and characterization of ascorbic acid loaded solid lipid nanoparticles and investigation of their apoptotic effects. *Colloids and Surfaces B: Biointerfaces*, **2014**, *121*, 270–280.
- Haider, M., Abidin, S. M., Kamal, L., & Orive, G. Nanostructured lipid carriers for delivery of chemotherapeutics: A review. *Pharmaceutics*, **2020**, *12*(3), 1–26.
- Han, F., Yin, R., Che, X., Yuan, J., Cui, Y., Yin, H., & Li, S. Nanostructured lipid carriers (NLC) based topical gel of flurbiprofen: Design, characterization and in vivo evaluation. *International Journal of Pharmaceutics*, **2012**, *439*(1–2), 349–357.
- Han, J., Amau, M., Okamoto, Y., Suga, K., & Umakoshi, H. Investigation of Quercetin interaction behaviors with lipid bilayers: Toward understanding its antioxidative effect within biomembrane. *Journal of Bioscience and Bioengineering*, **2021**, *132*(1), 49–55.
- Han, J., Suga, K., Hayashi, K., Okamoto, Y., & Umakoshi, H. Multi-level characterization of the membrane properties of resveratrol-incorporated liposomes. *Journal of Physical Chemistry B*, **2017**, *121*(16), 4091–4098.
- Harris, F. M., Best, K. B., & Bell, J. D. Use of laurdan fluorescence intensity and polarization to distinguish between changes in membrane fluidity and phospholipid order. *Biochimica et Biophysica Acta - Biomembranes*, **2002**, *1565*(1), 123–128.
- Hayashi, K., Shimanouchi, T., Kato, K., Miyazaki, T., Nakamura, A., & Umakoshi, H. Span 80 vesicles have a more fluid, flexible and wet surface than phospholipid liposomes. *Colloids and Surfaces B: Biointerfaces*, **2011**, *87*(1), 28–35.
- Hoeller, S., Sperger, A., & Valenta, C. Lecithin based nanoemulsions: A comparative study of the influence of non-ionic surfactants and the cationic phytosphingosine on physicochemical behaviour and skin permeation. *International Journal of Pharmaceutics*, **2009**, *370*(1–2), 181–186.
- Honary, S., & Zahir, F. Effect of zeta potential on the properties of nano-drug delivery systems - A review (Part 2). *Tropical Journal of Pharmaceutical Research*, **2013**, *12*(2), 265–273.
- Hou, X., Zaks, T., Langer, R., & Dong, Y. Lipid nanoparticles for mRNA delivery. *Nature Reviews Materials*, **2021**, *6*(12), 1078–1094.
- Houacine, C., Adams, D., & Singh, K. K. Impact of liquid lipid on development and stability of trimyristin nanostructured lipid carriers for oral delivery of resveratrol. *Journal of Molecular Liquids*, **2020**, *316*, 113734.
- How, C. W., Abdullah, R., & Abbasalipourkabir, R. Physicochemical properties of nanostructured lipid carriers as colloidal carrier system stabilized with polysorbate 20 and polysorbate 80. *African Journal of Biotechnology*, **2011**, *10*(9), 1684–1689.

- Huang, J., Wang, Q., Li, T., Xia, N., & Xia, Q. Nanostructured lipid carrier (NLC) as a strategy for encapsulation of quercetin and linseed oil: Preparation and in vitro characterization studies. *Journal of Food Engineering*, **2017**, 215, 1–12.
- Huang, M., Su, E., Zheng, F., & Tan, C. Encapsulation of flavonoids in liposomal delivery systems: The case of quercetin, kaempferol and luteolin. *Food and Function*, **2017**, 8(9), 3198–3208.
- Huguenin, J., Hamady, S. O. S., & Bourson, P. Monitoring deprotonation of gallic acid by Raman spectroscopy. *Journal of Raman Spectroscopy*, **2015**, 46(11), 1062–1066.
- Imran, M., Iqbal, M. K., Imtiyaz, K., Saleem, S., Mittal, S., Rizvi, M. M. A., Ali, J., & Baboota, S. Topical nanostructured lipid carrier gel of quercetin and resveratrol: Formulation, optimization, in vitro and ex vivo study for the treatment of skin cancer. *International Journal of Pharmaceutics*, **2020**, 587, 119705.
- Ioannou, I., Chekir, L., & Ghoul, M. Effect of heat treatment and light exposure on the antioxidant activity of flavonoids. *Processes*, **2020**, 8(9), 1–17.
- Iwasaki, F., Luginbühl, S., Suga, K., Walde, P., & Umakoshi, H. Fluorescent probe study of aot vesicle membranes and their alteration upon addition of aniline or the aniline dimer p-aminodiphenylamine (PADPA). *Langmuir*, **2017**, 33(8), 1984–1994.
- Izza, N., Suga, K., Okamoto, Y., Watanabe, N., Bui, T. T., Wibisono, Y., Fadila, C. R., & Umakoshi, H. Systematic characterization of nanostructured lipid carriers from cetyl palmitate/caprylic triglyceride/tween 80 mixtures in an aqueous environment. *Langmuir*, **2021**, 37(14), 4284–4293.
- Jores, K., Mehnert, W., Drechsler, M., Bunjes, H., Johann, C., & Mäder, K. Investigations on the structure of solid lipid nanoparticles (SLN) and oil-loaded solid lipid nanoparticles by photon correlation spectroscopy, field-flow fractionation and transmission electron microscopy. *Journal of Controlled Release*, **2004**, 95(2), 217–227.
- Joshi, M., & Patravale, V. Nanostructured lipid carrier (NLC) based gel of celecoxib. *International Journal of Pharmaceutics*, **2008**, 346(1), 124–132.
- Kawabata, K., Takato, A., Oshima, S., Akimoto, S., Inagaki, M., & Nishi, H. Protective effect of selected antioxidants on naproxen photodegradation in aqueous media. *Antioxidants*, **2019**, 8(10), 1–11.
- Kelidari, H. R., Saeedi, M., Akbari, J., Morteza-semnani, K., Valizadeh, H., Maniruzzaman, M., Farmoudeh, A., & Nokhodchi, A. Development and optimisation of spironolactone nanoparticles for enhanced dissolution rates and stability. *AAPS PharmSciTech*, **2017**, 18(5), 1469–1474.
- Khalil, I., Yehye, W. A., Etxeberria, A. E., Alhadi, A. A., Dezfooli, S. M., Julkapli, N. B. M., Basirun, W. J., & Seyfoddin, A. Nanoantioxidants: Recent trends in antioxidant delivery applications. *Antioxidants*, **2020**, 9(1), 1–30.
- Khan, N., Shah, F. A., Rana, I., Ansari, M. M., Din, F. ud, Rizvi, S. Z. H., Aman, W., Lee, G.-Y., Lee, E.-S., Kim, J.-K., & Zeb, A. Nanostructured lipid carriers-mediated brain delivery of carbamazepine for improved in vivo anticonvulsant and anxiolytic activity. *International Journal of Pharmaceutics*, **2020**, 577, 119033.

- Khan, S., Baboota, S., Ali, J., Khan, S., Narang, R. S., & Narang, J. K. (a). Nanostructured lipid carriers: An emerging platform for improving oral bioavailability of lipophilic drugs. *International Journal of Pharmaceutical Investigation*, **2015**, 5(4), 182–191.
- Khan, S., Baboota, S., Ali, J., Khan, S., Narang, R. S., & Narang, J. K. (b). Nanostructured lipid carriers: An emerging platform for improving oral bioavailability of lipophilic drugs. *International Journal of Pharmaceutical Investigation*, **2015**, 5(4), 182–191.
- Khosa, A., Reddi, S., & Saha, R. N. Nanostructured lipid carriers for site-specific drug delivery. *Biomedicine and Pharmacotherapy*, **2018**, 103, 598-613.
- Kim, H. R., Kim, I. K., Bae, K. H., Lee, S. H., Lee, Y., & Park, T. G. Cationic solid lipid nanoparticles reconstituted from low density lipoprotein components for delivery of siRNA. *Molecular Pharmaceutics*, **2008**, 5(4), 622–631.
- Kim, M. H., Kim, K. T., Sohn, S. Y., Lee, J. Y., Lee, C. H., Yang, H., Lee, B. K., Lee, K. W., & Kim, D. D. Formulation and evaluation of nanostructured lipid carriers (NLCs) of 20(s)-protopanaxadiol (PPD) by box-behnken design. *International Journal of Nanomedicine*, **2019**, 14, 8509–8520.
- Kumar, R. Lipid-based nanoparticles for drug-delivery systems. In *Nanocarriers for Drug Delivery: Nanoscience and Nanotechnology in Drug Delivery*, **2018**, 249–284.
- Lavigne, F., Bourgaux, C., Ollivon, M. Phase transitions of saturated triglycerides. *Journal de Physics IV*, **1993**, 03, 137-140.
- Li, C., Liu, D., Huang, M., Huang, W., Li, Y., & Feng, J. Interfacial engineering strategy to improve the stabilizing effect of curcumin-loaded nanostructured lipid carriers. *Food Hydrocolloids*, **2022**, 127, 107552.
- Liakopoulou, A., Mourelatou, E., & Hatziantoniou, S. Exploitation of traditional healing properties, using the nanotechnology's advantages: The case of curcumin. *Toxicology Reports*, **2021**, 8, 1143–1155.
- Lin, C. H., Chen, C. H., Lin, Z. C., & Fang, J. Y. Recent advances in oral delivery of drugs and bioactive natural products using solid lipid nanoparticles as the carriers. *Journal of Food and Drug Analysis*, **2017**, 25(2), 219-234.
- Lin, C., Zhu, C., Hu, M., Wu, A., Zerendawa, B., & Suolangqimei, K. Structure-activity relationships of antioxidant activity in vitro about flavonoids isolated from pyrethrum tatsienense. *Journal of Intercultural Ethnopharmacology*, **2014**, 3(3), 123-127.
- Liu, M., Liu, Y., Ge, Y., Zhong, Z., Wang, Z., Wu, T., Zhao, X., & Zu, Y. Solubility, antioxidation, and oral bioavailability improvement of mangiferin microparticles prepared using the supercritical antisolvent method. *Pharmaceutics*, **2020**, 12(2), 1–15.
- Luana Carvalho de Queiroz, J., Medeiros, I., Costa Trajano, A., Piuvezam, G., Clara de França Nunes, A., Souza Passos, T., & Heloneida de Araújo Morais, A. Encapsulation techniques perfect the antioxidant action of carotenoids: a systematic review of how this effect is promoted. *Food Chemistry*, **2022**, 385, 132593.

- Lv, R., Dong, Y., Bao, Z., Zhang, S., Lin, S., & Sun, N. Advances in the activity evaluation and cellular regulation pathways of food-derived antioxidant peptides. *Trends in Food Science & Technology*, **2022**, 122(1), 171–186.
- Ma, Y., Benda, A., Kwiatek, J., Owen, D. M., & Gaus, K. Time-resolved laurdan fluorescence reveals insights into membrane viscosity and hydration levels. *Biophysical Journal*, **2018**, 115(8), 1498–1508.
- Mach, M., Kowalska, M., Olechowska, K., Hąc-Wydro, K., & Wydro, P. The influence of cationic lipid - 1-palmitoyl-2-oleoyl-sn-glycero-3-ethylphosphocholine - on model lipid membranes. *Biochimica et Biophysica Acta - Biomembranes*, **2020**, 1862(2), 183088.
- Mardani-Ghahfarokhi, A., & Farhoosh, R. Antioxidant activity and mechanism of inhibitory action of gentisic and α -resorcylic acids. *Scientific Reports*, **2020**, 10(1), 1–11.
- Mendes, M., Nunes, S. C. C., Sousa, J. J., Pais, A. A. C. C., & Vitorino, C. Expanding transdermal delivery with lipid nanoparticles: A new drug-in-NLC-in-adhesive design. *Molecular Pharmaceutics*, **2017**, 14(6), 2099–2115.
- Moldovan, M. L., Ionut, I., Bogdan, C. Cosmetic products containing natural based emollients for restoring impaired skin barrier: formulation and in vivo evaluation. *Farmacia*, **2016**, 69(1), 129–134.
- Mitchell, M. J., Billingsley, M. M., Haley, R. M., Wechsler, M. E., Peppas, N. A., & Langer, R. Engineering precision nanoparticles for drug delivery. *Nature Reviews Drug Discovery*, **2021**, 20(2), 101–124.
- Müller, R. H., Radtke, M., & Wissing, S. A. (a). Solid lipid nanoparticles (SLN) and nanostructured lipid carriers (NLC) in cosmetic and dermatological preparations. *Advanced Drug Delivery Reviews*, **2002**, 54, 131–155.
- Müller, R. H., Radtke, M., & Wissing, S. A. (b). Nanostructured lipid matrices for improved microencapsulation of drugs. *International Journal of Pharmaceutics*, **2002**, 242(1–2), 121–128.
- Müller, Rainer H, Mäder, K., & Gohla, S. Solid lipid nanoparticles (SLN) for controlled drug delivery – a review of the state of the art. *European Journal of Pharmaceutics and Biopharmaceutics*, **2000**, 50(1), 161–177.
- Nahak, P., Karmakar, G., Chettri, P., Roy, B., Guha, P., Besra, S. E., Soren, A., Bykov, A. G., Akentiev, A. V., Noskov, B. A., & Panda, A. K. (a). Influence of lipid core material on physicochemical characteristics of an ursolic acid-loaded nanostructured lipid carrier: An attempt to enhance anticancer activity. *Langmuir*, **2016**, 32(38), 9816–9825.
- Naseri, N., Valizadeh, H., & Zakeri-Milani, P. Solid lipid nanoparticles and nanostructured lipid carriers: Structure preparation and application. *Advanced Pharmaceutical Bulletin*, **2015**, 5(3), 305–313.
- Netto MPharm, G., & Jose, J. Development, characterization, and evaluation of sunscreen cream containing solid lipid nanoparticles of silymarin. *Journal of Cosmetic Dermatology*, **2018**, 17(6), 1073–1083.

- Nielsen, C. K., Kjems, J., Mygind, T., Snabe, T., Meyer, R. L., Effects of Tween 80 on Growth and Biofilm Formation in Laboratory Media. *Frontiers in Microbiology*, **2016**, 7, 1878.
- Oehlke, K., Behnsnlian, D., Mayer-Miebach, E., Weidler, P. G., & Greiner, R. Edible solid lipid nanoparticles (SLN) as carrier system for antioxidants of different lipophilicity. *PloS one*, **2017**, 12(2), e0171662–e0171662.
- Onuki, Y., Morishita, M., Chiba, Y., Tokiwa, S., & Takayama, K. Docosahexaenoic acid and eicosapentaenoic acid induce changes in the physical properties of a lipid bilayer model membrane. *Chemical and Pharmaceutical Bulletin*, **2006**, 54(1), 68–71.
- Parasassi, T., & Gratton, E. Membrane lipid domains and dynamics as detected by Laurdan fluorescence. *Journal of Fluorescence*, **1995**, 5(1), 59–69.
- Parcheta, M., Świsłocka, R., Orzechowska, S., Akimowicz, M., Choińska, R., & Lewandowski, W. Recent developments in effective antioxidants: The structure and antioxidant properties. *Materials*, **2021**, 14(8), 1–24.
- Pilkington, E. H., Suys, E. J. A., Trevaskis, N. L., Wheatley, A. K., Zukancic, D., Algarni, A., Al-Wassiti, H., Davis, T. P., Pouton, C. W., Kent, S. J., & Truong, N. P. From influenza to COVID-19: Lipid nanoparticle mRNA vaccines at the frontiers of infectious diseases. *Acta Biomaterialia*, **2021**, 131, 16–40.
- Pindiprolu, S. K. S. S., Kumar, C. S. P., Kumar Golla, V. S., Likitha, P., K, S. C., Esub Basha, S. K., & Ramachandra, R. K. Pulmonary delivery of nanostructured lipid carriers for effective repurposing of salinomycin as an antiviral agent. *Medical Hypotheses*, **2020**, 143, 109858.
- Pink, D. L., Loruthai, O., Ziolk, R. M., Wasutrasawat, P., Terry, A. E., Lawrence, M. J., & Lorenz, C. D. On the structure of solid lipid nanoparticles. *Small*, **2019**, 15(45), 1–10.
- Pompeu, D. R., Larondelle, Y., Rogez, H., Abbas, O., Pierna, J. A. F., & Baeten, V. Characterization and discrimination of phenolic compounds using Fourier transform Raman spectroscopy and chemometric tools. *Biotechnology, Agronomy and Society and Environment*, **2018**, 22(1), 13–28.
- Poojari, C., Wilkosz, N., Lira, R. B., Dimova, R., Jurkiewicz, P., Petka, R., Kepczynski, M., & Róg, T. Behavior of the DPH fluorescence probe in membranes perturbed by drugs. *Chemistry and Physics of Lipids*, **2019**, 223, 104784.
- Pornputtapitak, W., Pantakitcharoenkul, J., Teeranachaideekul, V., Sinthiptharakoon, K., Sapcharoenkun, C., & Meemuk, B. Effect of oil content on physiochemical characteristics of γ -oryzanol-loaded nanostructured lipid carriers. *Journal of Oleo Science*, **2019**, 68(8), 699–707.
- Rabe, M., Kerth, A., Blume, A., & Garidel, P. Albumin displacement at the air–water interface by Tween (Polysorbate) surfactants. *European Biophysics Journal*, **2020**, 49(7), 533–547.
- Resnier, P., LeQuinio, P., Lautram, N., André, E., Gaillard, C., Bastiat, G., Benoit, J.-P., & Passirani, C. Efficient in vitro gene therapy with PEG siRNA lipid nanocapsules

- for passive targeting strategy in melanoma. *Biotechnology Journal*, **2014**, 9(11), 1389–1401.
- Richard, C., Cassel, S., & Blanzat, M. Vesicular systems for dermal and transdermal drug delivery. *RSC Advances*, **2020**, 11(1), 442–451.
- Rodriguez-Ruiz, V., Salatti-Dorado, J. Á., Barzegari, A., Nicolas-Boluda, A., Houaoui, A., Caballo, C., Caballero-Casero, N., Sicilia, D., Venegas, J. B., Pauthe, E., Omid, Y., Letourneur, D., Rubio, S., Gueguen, V., & Pavon-Djavid, G. Astaxanthin-loaded nanostructured lipid carriers for preservation of antioxidant activity. *Molecules*, **2018**, 23(10), 1–12.
- Rousseau, D., Hodge, S. M., Nickerson, M. T., & Paulson, A. T. Regulating the β' → β polymorphic transition in food fats. *Journal of the American Oil Chemists' Society*, **2005**, 82(1), 7–12.
- Ruktanonchai, U., Limpakdee, S., Meejoo, S., Sakulkhu, U., Bunyapraphatsara, N., Junyaprasert, V., & Puttipipatkachorn, S. The effect of cetyl palmitate crystallinity on physical properties of gamma-oryzanol encapsulated in solid lipid nanoparticles. *Nanotechnology*, **2008**, 19(9), 095701.
- Saedi, A., Rostamizadeh, K., Parsa, M., Dalali, N., & Ahmadi, N. Preparation and characterization of nanostructured lipid carriers as drug delivery system: Influence of liquid lipid types on loading and cytotoxicity. *Chemistry and Physics of Lipids*, **2018**, 216, 65–72.
- Saejung, T., Don-In, J., & Chimsook, T. Preparation of ethanolic butterfly pea extract using microwave assisted extraction and loaded nanostructured lipid carriers: Evaluation of antioxidant potential for stabilization of fish oil. *Key Engineering Materials*, **2021**, 873, 1–5.
- Saji, V. S. Wax-based artificial superhydrophobic surfaces and coatings. *Colloids and Surfaces A: Physicochemical and Engineering Aspects*, **2020**, 602, 125132.
- Sakellari, G. I., Zafeiri, I., Batchelor, H., & Spyropoulos, F. Formulation design, production and characterisation of solid lipid nanoparticles (SLN) and nanostructured lipid carriers (NLC) for the encapsulation of a model hydrophobic active. *Food Hydrocolloids for Health*, **2021**, 1, 100024.
- Salminen, H., Gömmel, C., Leuenberger, B. H., & Weiss, J. Influence of encapsulated functional lipids on crystal structure and chemical stability in solid lipid nanoparticles: Towards bioactive-based design of delivery systems. *Food Chemistry*, **2016**, 190, 928–937.
- Salvi, V. R., & Pawar, P. Nanostructured lipid carriers (NLC) system: A novel drug targeting carrier. *Journal of Drug Delivery Science and Technology*, **2019**, 51, 255–267.
- Sánchez-López, E., Espina, M., Doktorovova, S., Souto, E. B., & García, M. L. Lipid nanoparticles (SLN, NLC): Overcoming the anatomical and physiological barriers of the eye – Part II - Ocular drug-loaded lipid nanoparticles. *European Journal of Pharmaceutics and Biopharmaceutics*, **2017**, 110, 58–69.
- Saupe, A., Wissing, S. A., Lenk, A., Schmidt, C., & Müller, R. H. Solid lipid nanoparticles (SLN) and nanostructured lipid carriers (NLC) -- structural

- investigations on two different carrier systems. *Bio-medical materials and engineering*, **2005**, 15(5), 393–402.
- Schlupp, P., Blaschke, T., Kramer, K. D., Hölte, H. D., Mehnert, W., & Schäfer-Korting, M. Drug release and skin penetration from solid lipid nanoparticles and a base cream: A systematic approach from a comparison of three glucocorticoids. *Skin Pharmacology and Physiology*, **2011**, 24(4), 199–209.
- Schoenmaker, L., Witzigmann, D., Kulkarni, J. A., Verbeke, R., Kersten, G., Jiskoot, W., & Crommelin, D. J. A. mRNA-lipid nanoparticle COVID-19 vaccines: Structure and stability. *International Journal of Pharmaceutics*, **2021**, 601, 120586.
- Sen Gupta, A. Role of particle size, shape, and stiffness in design of intravascular drug delivery systems: Insights from computations, experiments, and nature. *Wiley Interdisciplinary Reviews: Nanomedicine and Nanobiotechnology*, **2016**, 8(2), 255–270.
- Shah, A., Aftab, S., Nisar, J., Ashiq, M. N., & Iftikhar, F. J. Nanocarriers for targeted drug delivery. *Journal of Drug Delivery Science and Technology*. **2021**, 62, 102426.
- Shaker, S., Gardouh, A., & Ghorab, M. Factors affecting liposomes particle size prepared by ethanol injection method. *Research in Pharmaceutical Sciences*, **2017**, 12(5), 346–352.
- Shanshan, W., Meigui, H., Chunyang, L., Zhi, C., Li, C., Wuyang, H., Ying, L., & Jin, F. Fabrication of ovalbumin-burdock polysaccharide complexes as interfacial stabilizers for nanostructured lipid carriers: Effects of high-intensity ultrasound treatment. *Food Hydrocolloids*, **2021**, 111, 106407.
- Soldati, P. P., Polonini, H. C., Paes, C. Q., Restrepob, J. A. S., Creczynski-Pasa, T. B., Chaves, M. G. A. M., Brandão, M. A. F., Pittella, F., & Raposo, N. R. B. Controlled release of resveratrol from lipid nanoparticles improves antioxidant effect. *IFAC-Papers On-Line*, **2018**, 51(27), 16–21.
- Stoddard, B. L., Khvorova, A., Corey, D. R., Dynan, W. S., & Fox, K. R. Editorial: Nucleic Acids Research and Nucleic Acid Therapeutics. *Nucleic Acids Research*, **2018**, 46(4), 1563–1564.
- Stott, B. M., Vu, M. P., McLemore, C. O., Lund, M. S., Gibbons, E., Brueseke, T. J., Wilson-Ashworth, H. A., & Bell, J. D. Use of fluorescence to determine the effects of cholesterol on lipid behavior in sphingomyelin liposomes and erythrocyte membranes. *Journal of Lipid Research*, **2008**, 49(6), 1202–1215.
- Suga, K., Kitagawa, K., Taguchi, S., Okamoto, Y., & Umakoshi, H. Evaluation of molecular ordering in bicelle bilayer membranes based on induced circular dichroism spectra. *Langmuir: the ACS journal of surfaces and colloids*, **2020**, 36(12), 3242–3250.
- Suga, K., Kondo, D., Otsuka, Y., Okamoto, Y., & Umakoshi, H. (a). Characterization of aqueous oleic acid/oleate dispersions by fluorescent probes and raman spectroscopy. *Langmuir*, **2016**, 32(30), 7606–7612.
- Suga, K., Otsuka, Y., Okamoto, Y., & Umakoshi, H. (a). Gel-phase-like ordered membrane properties observed in dispersed oleic acid/1-oleoylglycerol self-

- assemblies: systematic characterization using raman spectroscopy and a laurdan fluorescent probe. *Langmuir*, **2018**, 34(5), 2081–2088.
- Suga, K., Tanabe, T., Tomita, H., Shimanouchi, T., & Umakoshi, H. Conformational change of single-stranded RNAs induced by liposome binding. *Nucleic Acids Research*, **2011**, 39(20), 8891–8900.
- Suga, K., & Umakoshi, H. Detection of nanosized ordered domains in DOPC/DPPC and DOPC/CH binary lipid mixture systems of large unilamellar vesicles using a TEMPO quenching method. *Langmuir*, **2013**, 29(15), 4830–4838.
- Suga, K., Yokoi, T., Kondo, D., Hayashi, K., Morita, S., Okamoto, Y., Shimanouchi, T., & Umakoshi, H. Systematical characterization of phase behaviors and membrane properties of fatty acid/ didecyldimethylammonium bromide vesicles. *Langmuir*, **2014**, 30(43), 12721–12728.
- Sun, M., Nie, S., Pan, X., Zhang, R., Fan, Z., & Wang, S. (a). Quercetin-nanostructured lipid carriers: Characteristics and anti-breast cancer activities in vitro. *Colloids and Surfaces B: Biointerfaces*, **2014**, 113, 15–24.
- Taguchi, S., Suga, K., Hayashi, K., Okamoto, Y., Jung, H.-S., Nakamura, H., & Umakoshi, H. Systematic characterization of DMPC/DHPC self-assemblies and their phase behaviors in aqueous solution. *Colloids and Interfaces*, **2018**, 2(4), 73.
- Tain, Y., & Hsu, C. Oxidative stress-induced hypertension of developmental origins : preventive aspects of antioxidant therapy. *Antioxidants*, **2022**, 11(511), 1–20.
- Tamjidi, F., Shahedi, M., Varshosaz, J., & Nasirpour, A. Nanostructured lipid carriers (NLC): A potential delivery system for bioactive food molecules. *Innovative Food Science and Emerging Technologies*, **2013**, 19, 29–43.
- Tavares, I. M. de C., Sumere, B. R., Gómez-Alonso, S., Gomes, E., Hermosín-Gutiérrez, I., Da-Silva, R., & Lago-Vanzela, E. S. Storage stability of the phenolic compounds, color and antioxidant activity of jambolan juice powder obtained by foam mat drying. *Food research international*, **2020**, 128, 108750.
- Teeranachaideekul, V., Müller, R. H., & Junyaprasert, V. B. Encapsulation of ascorbyl palmitate in nanostructured lipid carriers (NLC)-Effects of formulation parameters on physicochemical stability. *International Journal of Pharmaceutics*, **2007**, 340(1–2), 198–206.
- Tenchov, R., Bird, R., Curtze, A. E., & Zhou, Q. Lipid nanoparticles from liposomes to mrna vaccine delivery, a landscape of research diversity and advancement. *ACS Nano*, **2021**, 15(11), 16982–17015.
- Terada, T., Kulkarni, J. A., Huynh, A., Chen, S., van der Meel, R., Tam, Y. Y. C., & Cullis, P. R. Characterization of lipid nanoparticles containing ionizable cationic lipids using design-of-experiments approach. *Langmuir*, **2021**, 37, 1120–1128.
- Tian, L., Zhang, S., Yi, J., Zhu, Z., Cui, L., Decker, E. A., & McClements, D. J. Factors impacting the antioxidant/prooxidant activity of tea polyphenols on lipids and proteins in oil-in-water emulsions. *Lwt*, **2022**, 156, 113024.
- Tran, V. Van, Loi, T., Moon, J., & Lee, Y. Core-shell materials, lipid particles and nanoemulsions, for delivery of active antioxidants in cosmetics applications:

- challenges and development strategies. *Chemical Engineering Journal*, **2019**, 368, 88–114.
- Tronino, D., Offerta, A., Ostacolo, C., Russo, R., de Caro, C., Calignano, A., Puglia, C., & Blasi, P. Nanoparticles prolong N-palmitoylethanolamide anti-inflammatory and analgesic effects in vivo. *Colloids and Surfaces B: Biointerfaces*, **2016**, 141, 311–317.
- Truong, V. L., & Jeong, W. S. Antioxidant and anti-inflammatory roles of tea polyphenols in inflammatory bowel diseases. *Food Science and Human Wellness*, **2022**, 11(3), 502–511.
- Uddin, M. N., & Roni, M. A. Challenges of storage and stability of mRNA-based Covid-19 vaccines. *Vaccines*, **2021**, 9(9), 1–9.
- Uebbing, L., Ziller, A., Siewert, C., Schroer, M. A., Blanchet, C. E., Svergun, D. I., Ramishetti, S., Peer, D., Sahin, U., Haas, H., & Langguth, P. Investigation of pH-responsiveness inside lipid nanoparticles for parenteral mRNA application using small-angle X-ray scattering. *Langmuir*, **2020**, 36(44), 13331–13341.
- Üner, M., & Yener, G. Importance of solid lipid nanoparticles (SLN) in various administration routes and future perspectives. *International Journal of Nanomedicine*, **2007**, 2 (3), 289–300.
- Uprit, S., Kumar Sahu, R., Roy, A., & Pare, A. Preparation and characterization of minoxidil loaded nanostructured lipid carrier gel for effective treatment of alopecia. *Saudi Pharmaceutical Journal*, **2013**, 21(4), 379–385.
- van Tran, V., Loi Nguyen, T., Moon, J. Y., & Lee, Y. C. Core-shell materials, lipid particles and nanoemulsions, for delivery of active antioxidants in cosmetics applications: challenges and development strategies. *Chemical Engineering Journal*, **2019**, 368, 88–114.
- Vijayakumar, A., Baskaran, R., Jang, Y. S., Oh, S. H., & Yoo, B. K. Quercetin-loaded solid lipid nanoparticle dispersion with improved physicochemical properties and cellular uptake. *AAPS PharmSciTech*, **2017**, 18(3), 875–883.
- Watanabe, N., Goto, Y., Suga, K., Nyholm, T. K. M., Slotte, J. P., & Umakoshi, H. (a). Solvatochromic modeling of laurdan for multiple polarity analysis of dihydrosphingomyelin bilayer. *Biophysical Journal*, **2019**, 116(5), 874–883.
- Watanabe, N., Suga, K., Slotte, J. P., Nyholm, T. K. M., & Umakoshi, H. Lipid-surrounding water molecules probed by time-resolved emission spectra of laurdan. *Langmuir*, **2019**, 35. 6762–6770.
- Wu, K. W., Sweeney, C., Dudhipala, N., Lakhani, P., Chaurasiya, N. D., Tekwani, B. L., & Majumdar, S. Primaquine loaded solid lipid nanoparticles (SLN), nanostructured lipid carriers (NLC), and nanoemulsion (NE): effect of lipid matrix and surfactant on drug entrapment, in vitro release, and ex vivo hemolysis. *AAPS pharmscitech*, **2021**, 22(7), 1–12.
- Wu, Y., Song, X., Kebebe, D., Li, X., Xue, Z., Li, J., Du, S., Pi, J., & Liu, Z. Brain targeting of Baicalin and Salvianolic acid B combination by OX26 functionalized nanostructured lipid carriers. *International Journal of Pharmaceutics*, **2019**, 571, 118754.

- Xue, H. Y., Guo, P., Wen, W.-C., & Wong, H. L. Lipid-based nanocarriers for rna delivery. *Current Pharmaceutical Design*, **2015**, *21*, 3140-3147.
- Yang, B., Dong, Y., Wang, F., & Zhang, Y. Nanoformulations to enhance the bioavailability and physiological functions of polyphenols. *Molecules*, **2020**, *25*(20), 1–36.
- Zapata, J. E., Sepúlveda, C. T., & Alvarez, A. C. Kinetics of the thermal degradation of phenolic compounds from achiote leaves (*Bixa orellana* L.) and its effect on the antioxidant activity. *Food Science and Technology*, **2022**, *42*, 1–8.
- Zhai, J., Fong, C., Tran, N., & J. Drummond, C. Non-lamellar lyotropic liquid crystalline lipid nanoparticles for the next generation of nanomedicine. *ACS Nano*, **2019**, *13*(6), 6178–6206.
- Zhao, C., Zhang, J., Hu, H., Qiao, M., Chen, D., Zhao, X., & Yang, C. Design of lactoferrin modified lipid nano-carriers for efficient brain-targeted delivery of nimodipine. *Materials Science and Engineering: C*, **2018**, *92*, 1031–1040.
- Zhao, J., Piao, X., Shi, X., Si, A., Zhang, Y., & Feng, N. Podophyllotoxin-loaded nanostructured lipid carriers for skin targeting: In vitro and in vivo studies. *Molecules*, **2016**, *21*(11), 1549.
- Zhao, S., Yang, X., Garamus, V. M., Handge, U. A., Bérengère, L., Zhao, L., Salamon, G., Willumeit, R., Zou, A., & Fan, S. Mixture of nonionic/ionic surfactants for the formulation of nanostructured lipid carriers: Effects on physical properties. *Langmuir*, **2014**, *30*(23), 6920–6928.
- Zheng, M., Falkeborg, M., Zheng, Y., Yang, T., & Xu, X. Formulation and characterization of nanostructured lipid carriers containing a mixed lipids core. *Colloids and Surfaces A: Physicochemical and Engineering Aspects*, **2013**, *430*, 76–84.
- Zhou, X., Zhang, X., Ye, Y., Zhang, T., Wang, H., Ma, Z., & Wu, B. Nanostructured lipid carriers used for oral delivery of oridonin: An effect of ligand modification on absorption. *International Journal of Pharmaceutics*, **2015**, *479*(2), 391–398.

List of Publications

[Papers]

1. Ni'matul Izza, Keishi Suga, Yukihiro Okamoto, Nozomi Watanabe, Tham Thi Bui, Yusuf Wibisono, Cut Rifda Fadila, Hiroshi Umakoshi. Systematic Characterization of Nanostructured Lipid Carriers from Cetyl Palmitate / Caprylic Triglyceride / Tween 80 Mixtures in an Aqueous Environment. *Langmuir*, **37**, 4284-4293 (2021). <https://doi.org/10.1021/acs.langmuir.1c00270>.
2. Ni'matul Izza, Nozomi Watanabe, Yukihiro Okamoto, Keishi Suga, Yusuf Wibisono, Naoko Kajimura, Kaoru Mitsuoka, Hiroshi Umakoshi. Dependence of Core-Shell Structure on Lipid Composition of Nanostructured Lipid Carriers: Implications for Drug Carrier Design. *ACS Applied Nano Material*, in press (2022). <https://doi.org/10.1021/acsanm.2c02214>.
3. Ni'matul Izza, Nozomi Watanabe, Yukihiro Okamoto, Yusuf Wibisono, Hiroshi Umakoshi. Characterization of Entrapment Behavior of Polyphenols in Nanostructured Lipid Carriers and Its Effect on Their Antioxidative Activity. *Journal of Bioscience and Bioengineering*, in press (2022). <https://doi.org/10.1016/j.jbiosc.2022.06.009>

[Related Papers]

1. Ni'matul Izza, Nani Sumarni, Niken Dieni Pramesi, Ucha Aditya Mahardi, Shinta Rosalia Dewi. Extraction of Phenolic Compounds from *Coleus amboinicus* Leaves by Microwave-assisted Extraction: Optimization of the Operating Condition. *Int. J. on Adv. Sci., Eng. and Information Tech.*, **12(3)**, in press (2022).
2. Yusuf Wibisono, Eka Mustika Diniardi, Dikianur Alvianto, Bambang Dwi Argo, Mochamad Bagus Hermanto, Shinta Rosalia Dewi, Ni'matul Izza, Angky Wahyu Putranto, Saiful Saiful. Cacao Pod Husk Extract Phenolic Nanopowder-Impregnated Cellulose Acetate Matrix for Biofouling Control in Membranes. *Membranes*, **11(10)**, Article No. 748 (13 pages) (2021).
3. Yusuf Wibisono, Restu Vitri Astuti, Gunomo Djoyowasito, Angky Wahyu Putranto, Ni'matul Izza, Dikianur Alvianto. Assessment of Point-of-Use Membrane-Based Drinking Water Appliance for Local Community. *Journal of Engineering Science & Technology Review*, **14(5)**, 1-7 (2021).
4. Panggulu Ahmad R Utoro, Agung Sukoyo, Sandra Sandra, Ni'matul Izza, Shinta Rosalia Dewi, Yusuf Wibisono. High-Throughput Microfiltration Membranes with Natural Biofouling Reducer Agent for Food Processing. *Processes*, **7**, Article No. 1 (14 pages) (2019).

[Articles/ Reviews]

1. Nozomi Watanabe, Ni'matul Izza, Hiroshi Umakoshi, Science of Self-Organization of Lipids (*in Japanese*), *Annual Report of Research Center for Ultra-High Voltage Electron Microscopy (CUHVEM)*, Osaka Univ., *in press* (2022).

[International Conference/ Symposium]

1. Ni'matul Izza, Nozomi Watanabe, Yukihiro Okamoto, Hiroshi Umakoshi. Core Structure Characterization of Nanostructured Lipid Carrier (NLC) Constituted by Cetyl Palmitate/ Caprylic Triglycerides/ Tween 80, *International Conference on Nanomaterials and Biomaterials (ICNB)*, Japan (Virtual), 2021. (Oral presenter)
2. Ni'matul Izza, Nozomi Watanabe, Yukihiro Okamoto, Yusuf Wibisono, Hiroshi Umakoshi. Molecular and Physicochemical Properties of Nanostructured Lipid Carriers (NLC) Constituted by Cetyl Palmitate/ Caprylic Triglycerides/ Tween 80. *International Virtual Symposium on Chemistry, Chemistry Beyond Borders (CBB)*, Indonesia (Virtual), 2021. (Oral presenter)
3. Ni'matul Izza, Dewi Trisnantini. The Optimization of Ultrasonic-Assisted Extraction of Antioxidant Compounds from Butterfly Pea Flower (*Clitoria ternatea* L.) by Using Response Surface Methodology. *11th International Conference on Global Resource Conservation*, Indonesia (Virtual), 2020. (Oral Presenter)
4. Ni'matul Izza, Shinta Rosalia Dewi, Ashried Setyanda, Agung Sukoyo, Panggulu Utoro, Dimas Firmanda Al Riza, Yusuf Wibisono. Microwave-Assisted Extraction of Phenolic Compounds from *Moringa oleifera* Seed as Anti-Biofouling Agents in Membrane Processes. *International Mechanical and Industrial Engineering Conference (IMIEC)*, Indonesia, 2018. (Oral Presenter)

Acknowledgements

The author is deeply grateful to Prof. Dr. Hiroshi Umakoshi (Division of Chemical Engineering, Graduate School of Engineering Science, Osaka University) for his insightful comments, guidance, and warm encouragement throughout this work. The author is thankful to Prof. Dr. Nobuyuki Matsubayashi, Prof. Dr. Shinji Sakai (Division of Chemical Engineering, Graduate School of Engineering Science, Osaka University), and Dr. Yusuf Wibisono (Bioprocess Engineering Study Program, Universitas Brawijaya) for the number of valuable comments and suggestions during the completion of this thesis. The author also would like to express the greatest appreciation to Assist. Prof. Dr. Nozomi Watanabe (Division of Chemical Engineering, Graduate School of Engineering Science, Osaka University) and Assoc. Prof. Dr. Keishi Suga (Department of Chemical Engineering, Graduate School of Engineering, Tohoku University) for their valuable comments, guidance, and helpful advice. The author would like to express her gratitude to Assoc. Prof. Dr. Yukihiro Okamoto (Division of Chemical Engineering, Graduate School of Engineering Science, Osaka University) for his enormous encouragements on this research. The author would like to offer one's special thanks to Ms. Keiko Fukumoto for her kind support during this work.

The author is thankful to Prof. Dr. Y. Okano, Prof. Dr. M. Nakano, Prof. Dr. T. Hirai, Prof. Dr. N. Nishiyama, Prof. Dr. Tomoo Mizugaki, and all the staff of Division of Chemical Engineering, Graduate School of Engineering Science, Osaka University for their kind cooperation during this research.

The author wishes to thank Prof. Dr. K. Mitsuoka, Dr. N. Kajimura (Research Center for Ultra-High Voltage Electron Microscopy, Osaka University) for their cooperative collaboration during this work. The author also thanks Prof. Dr. T. Kuhl (University of California, Davis) for her insightful comments.

The author is particularly grateful for the assistance given by C. R. Fadila. Special thanks are given to following colleagues for their experimental collaboration: K. Tanimura, K. Kitagawa, Y. Murata, Y. Goto, Kojima, B. T. Tham, M. Faried, M.S. Chern, H. Takase, N. Ikushima, R. Ueno, D. Matsui, S. Furuno, R. Murazawa, A. Ajaikumar, W. Wakileh, T. Ozawa, Y. Suzaki, A. Suzuta, K. Hamaguchi, S. Watase, N. Ito, S. Sogabe, J. Nakamura, Y. Nagamura, Y. Niwa, R. Xuehui, T. Samwang, L. Weiyu, P. Soontornapaluk, Z. Nicholella, M. Watanabe, N. Kadonishi, N. Fukuda, Y. Fujiyama, L. Junghu, and all members of the Bio-inspired Chemical Engineering (B-ICE) Laboratory.

The author would like to express deepest appreciation to her family who have taken good care of her during study. A deepest love for her husband, Achmad Yazid Ichsan, who always encouraged to pursue her dreams and supported in the ups and downs during PhD. The author is extremely grateful for her children, Chalya Shafiya and Achmad Ibrahim Alfanouva, for their smile and spirit they give every single day. The author would like to express her deepest gratitude to her parents, Masjidi A. S and Nur Ahadah, and siblings, Nur Fauziyah and Fathan Fahmi for their endless prayer, love, and support during her study in Japan.

The author gratefully acknowledged the financial support of this work by the scholarship of the Japanese Government (MEXT) Scholarship, and Japan International Agency (JICA).